Master Thesis, Department of Geosciences

Diagenesis and reservoir quality of deeply buried Permian sandstones in the Central Graben

A mineralogical, petrographical and petrophysical approach

Zeeshan Mohabbat

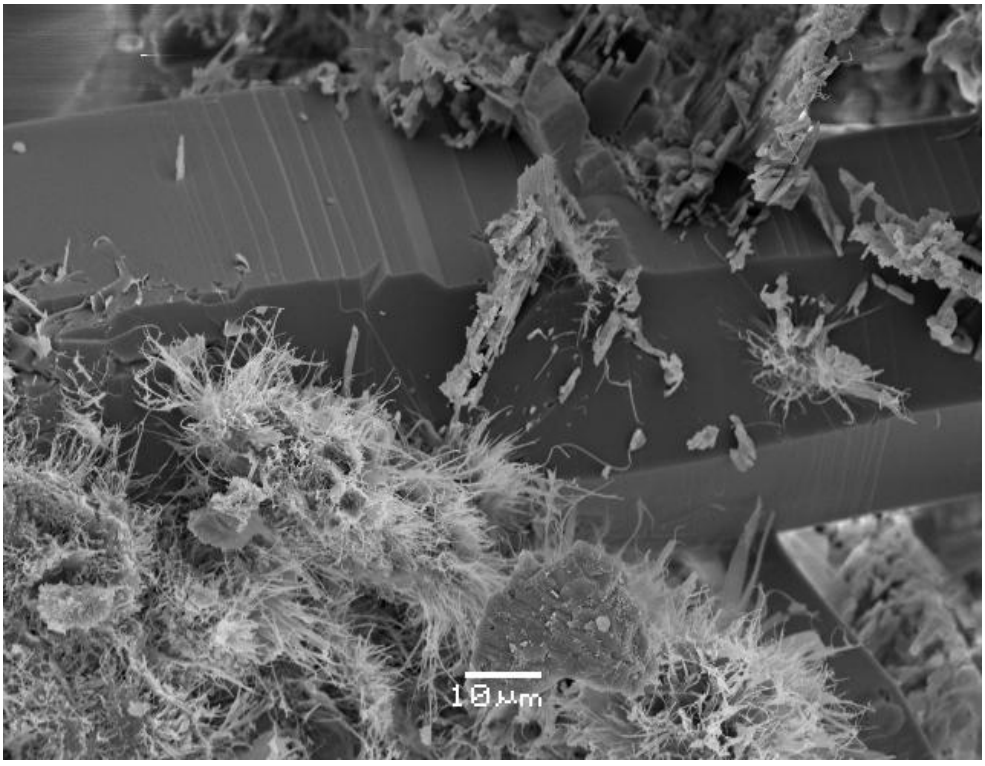

UNIVERSITY OF OSLO

FACULTY OF MATHEMATICS AND NATURAL SCIENCES

Diagenesis and reservoir quality of deeply buried Permian sandstones in the Central Graben

A mineralogical, petrographical and petrophysical approach

Zeeshan Mohabbat

Master Thesis in Geosciences

Discipline: PEGG

Department of Geosciences

Faculty of Mathematics and Natural Sciences

University of Oslo

01.06.2012

ACKNOWLEDGEMENTS

I feel instigated from within to extend my steadfast thanks to ALMIGHTY ALLAH whose magnanimous and chivalrous blessings enabled me to perceive and purse my ambitions and objectives. Special praises to Prophet Muhammad PBUH, who is bellwether for humanity as a whole.

I feel great honor in expressing my avid gratifications to my supervisor Jens Jahren, under whose dynamic supervision, auspicious and considerate guidance, encouragement and altruistic attitude, I was able to accomplish work presented in this dissertation.

I also extend my special thanks to Phd Student Tom Erik Maast for his esteemed guidance, suggestions, discussion and professional support throughout my thesis work. I also thank to Berit Løken Berg for always being supportive and helpful in my SEM studies. Without her help I believe my project was incomplete.

Thanks to Danial Farvardini and Azeem Hussain for all fruitful discussions through the entire length of this thesis. We will always be great friends.

Special thanks to Ahmad Salman, Waqas Ahmad, Ali Mustafa Khan Niazi, Muhammad Waqas Javed, Muhammad Jamil, Attiq-ur-Rehman, Tausif Ahmad and Aftab Javed for their support and confidence in me, and for the help during the course of this thesis.

In the end my whole hearted and incessant gratitude to my loving parents, my brothers and my sisters, who always appreciated, encouraged, and helped me during my eighteen years of studies.

Zeeshan Mohabbat

01.06.2012

ABSTRACT

The study deals with the diagenesis and reservoir quality prediction of deeply buried Rotliegend sandstone from Northern Permian Basin (NPB) in the Central Graben. Cored intervals from two wells (1/3-5 and 2/10-2) have been investigated by petrographical and petrophysical analysis.

Quartz cementation is the main process destroying porosity in deeply buried quartz rich sandstone reservoirs of the North Sea. Quartz cement precipitation takes place as syntaxial overgrowths, which starts at temperatures above 70^{o}C-80^{o}C. The Rotliegend sandstone is buried at the depth below 4km. As quartz cementation follows a time/temperature integral, all the pore spaces are expected to be filled with quartz cement in Rotliegend sandstone. Porosity preserving mechanisms such as grain coatings and hydrocarbon emplacement may preserve porosity at greater depths. In deeply buried sandstone reservoirs of the North Sea, grain coatings are most important porosity preserving mechanism covering the detrital grain surfaces and giving no surface area available for quartz cementation.

All above mentioned porosity preserving mechanisms have been investigated, but detailed petrographic analysis confirms that only illite coating has been found most frequently covering the detrital grain surfaces and effectively inhibiting quartz cementation. Although illite coating has preserved porosity but on the other hand, it has severely damaged the permeability of Rotliegend sandstone. Quartz cementation has negligible effect on porosity loss. The pore-filling authigenic kaolinite and carbonate cements have mainly caused the porosity reduction. The presence of unaltered kaolinite together with K-feldspar at this depth suggests that the process of illitization of kaolinite is still going on.

Samples from well 2/10-2 contain very high intergranular volume (IGV) values and less affected from mechanical compaction, indicating that early carbonate cement have helped preserving high IGV, whereas, samples from well 1/3-5 are more mechanically compacted representing relatively low IGV values.

TABLE OF CONTENTS

Chapter 1
INTRODUCTION

1.1 Introduction

This project is a part of collaboration between University of Oslo and DNO (Det Norske Oljeselskap). The aim of the thesis is to increase the understanding of reservoir quality prediction of deeply buried Permian sandstones in Norwegian sector of the Central Graben.

The reservoir quality of sandstones at any buried depth is controlled by (1) the initial depositional porosity and permeability, (2) the extent of both mechanical and chemical compaction, and (3) type and amount of pore-filling cement (Worden and Morad 2009). Mechanical compaction causes the porosity reduction until chemical compaction starts. At depths greater than 2.5 km, quartz cementation is considered the main porosity reducing process in reservoir rocks (Paxton et al. 2002). Cementation is strongly controlled by temperature and kinetics. A good understanding of the factors controlling the cementation exists in deeply burried reservoirs (>4 km), since normal quartz cementation would lead to limited reservoir properties at similar depths. Reservoir quality in the deeply buried sandstone therefore depends on factors preventing or delaying the quartz cementation. These factors include the grain coatings like chlorite and micro-quartz (Bjorlykke and Jahren 2010).

1.2 Purpose and methods

The main objective of this thesis is to characterize the reservoir quality of deeply burried (>4 km) Rotliegend sandstones in Northern Permian Basin from the cored reservoir interval in wells 1/3-5 and 2/10-2. This study also includes the investigation of diagenetic clay coating and its distribution in Rotliegend sandstones, and assesses the influence on reservoir quality.

This has been done by using two methods:

i. Well correlation and petrophysical evaluation
ii. Mineralogical and petrographic analysis
    - Optical microscopy
    - Scanning electron microscopy

1.3 Study area

The study area is located in Central Graben within the North Sea in blocks 1/3 and 2/10. Block 1/3 is a part of Hidra high. The structure is located in Northern Permian Basin on the east side of Central Graben. Block 2/10 is a part of Grensen spur. The block, being the southernmost in Norwegian North Sea sector, borders both UK and Danish sector lines (NPD, 2012).

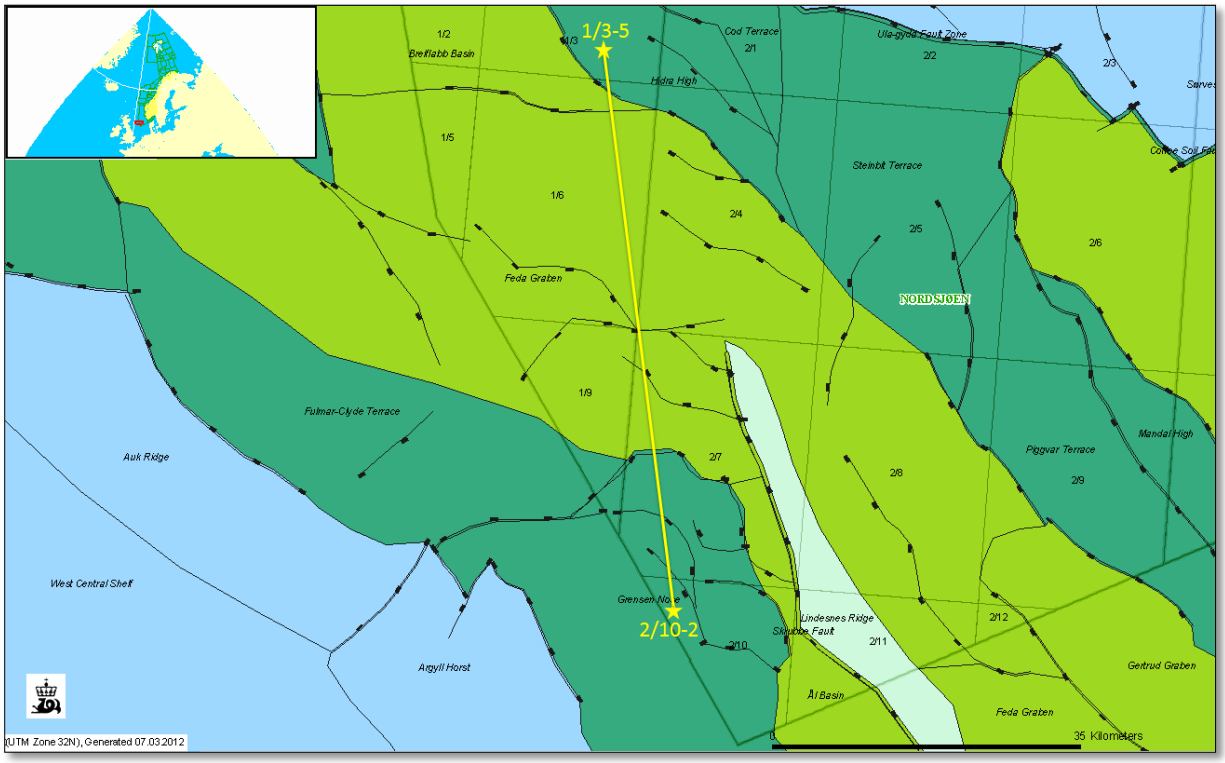

Figure 1.1 Structural map of study area. Yellow stars indicate the well locations (Modified from NPD 2012).

Chapter 2
GEOLOGICAL FRAMEWORK

2.1 Introduction

The chapter deals with the structural evolution and stratigraphic settings of the Central Graben that is located in middle and southern part of North Sea (Figure 2.1).

The term "Norwegian Central Trough" was first introduced by Rønnevik et al. (1975). In Norway, the Central Trough is the official nomenclature although "Central Graben" is more accepted (Gowers et al. 1993).

The present structural configuration of the North Sea is mainly the result of rifting events that occurred from Late Jurassic to Early Cretaceous (Figure 2.1). The extension history of the North Sea rift system started in Devonian times (Zanella and Coward 2003). The tectonic events like Permo-Triassic and Late Jurassic-Early Cretaceous rifting phases, thermal cooling and subsidence contributed in making the present North Sea sedimentary basin (Ravnås et al. 2000).

2.2 Structural setting

The North Sea is a triple rift system having Viking Graben, the Moray Firth Basins and the Central Graben as its three arms. The Central Graben is more symmetrical in character as compared to the Viking Graben and the Moray Firth Basins which are asymmetrical (Zanella and Coward 2003).

The structural history of the North Sea has gone through a very complex evolution through time with failed rifting systems, episodes of subsidence and uplift, inversions and several intra plate rifting (Figure 2.2).

The collision between Gondwana and Laurussia in Late Visean of the Early Carboniferous times resulted in the Variscan Orogeny which post-dates the Pre-Cambrian and the Caledonian orogenies (Glennie and Underhill 1998). These two megacontinents were both migrating northwards with different rates of movement; hence the southerly located Gondwana caught up and collided with Laurussia. The southern and central parts of the North Sea areas were in a foreland basinal setting in front of the northward moving Variscan fold-and-thrust system with the final closure of the Rheic Ocean in Late Carboniferous times.

According to Glennie and Underhill (1998) the basin development related to post Variscan times in the North Sea can be divided into six major events, namely;

1) Permo-Triassic postorogenic rifting,
2) Late Triassic-Jurassic opening of western Tethys,
3) Middle Jurassic doming of the North Sea,
4) Development of the triple junction North Sea failed rift system,
5) Creation of the Atlantic Ocean, and
6) Cretaceous-Early Tertiary closure of the Tethys Ocean and the creation of the Alpine fold chain.

The Northern Permian Basin (NPB) and the Southern Permian Basin (SPB) (figure 2.3), in north Western Europe were developed during Permian. These east westerly aligned basins were separated by the Mid North Sea High (MNSH)-Ringkøbing-Fyn High (RFH) (e.g. Glennie et al. 2003; Brekke et al. 2001). In connection to these Permian basins, one tectonic process occurred in the earliest Permian times is the east to west oriented transtensional reactivation of north west to south easterly aligned lines of weakness (Glennie and Underhill 1998). These lines were originated from the underlying tornquist lineaments which affected the later events and resulted in the volcanism of Lower Rotliegend, the collapse of the Variscan highlands and subsidence of the NPB and SPB (Glennie 1998). In the future, the NPB and its associated sediments would become part of the central graben system.

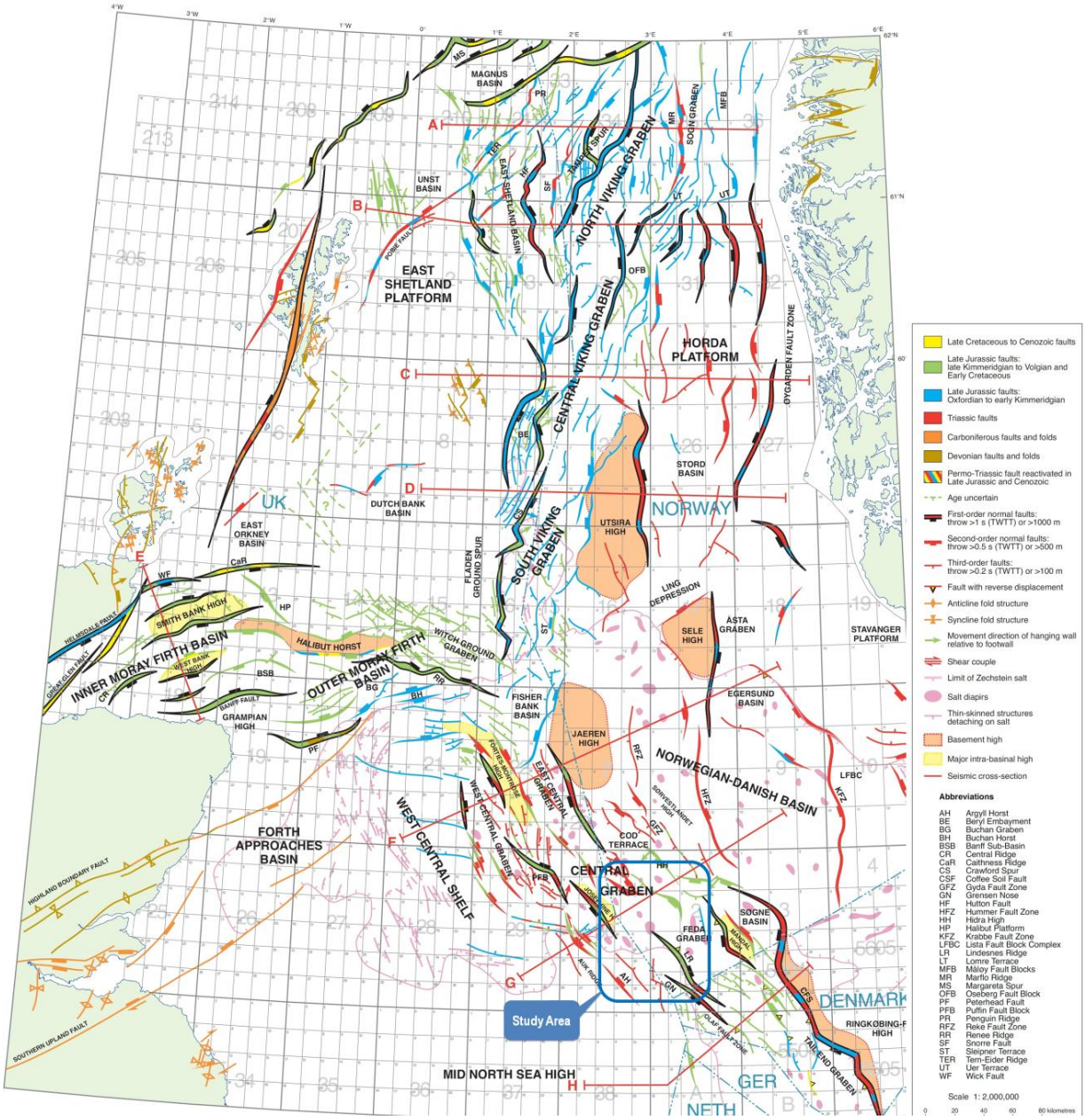

Figure 2.1 Regional structural map of North Sea. The study area is marked in blue box (modified after Zanella and Coward 2003).

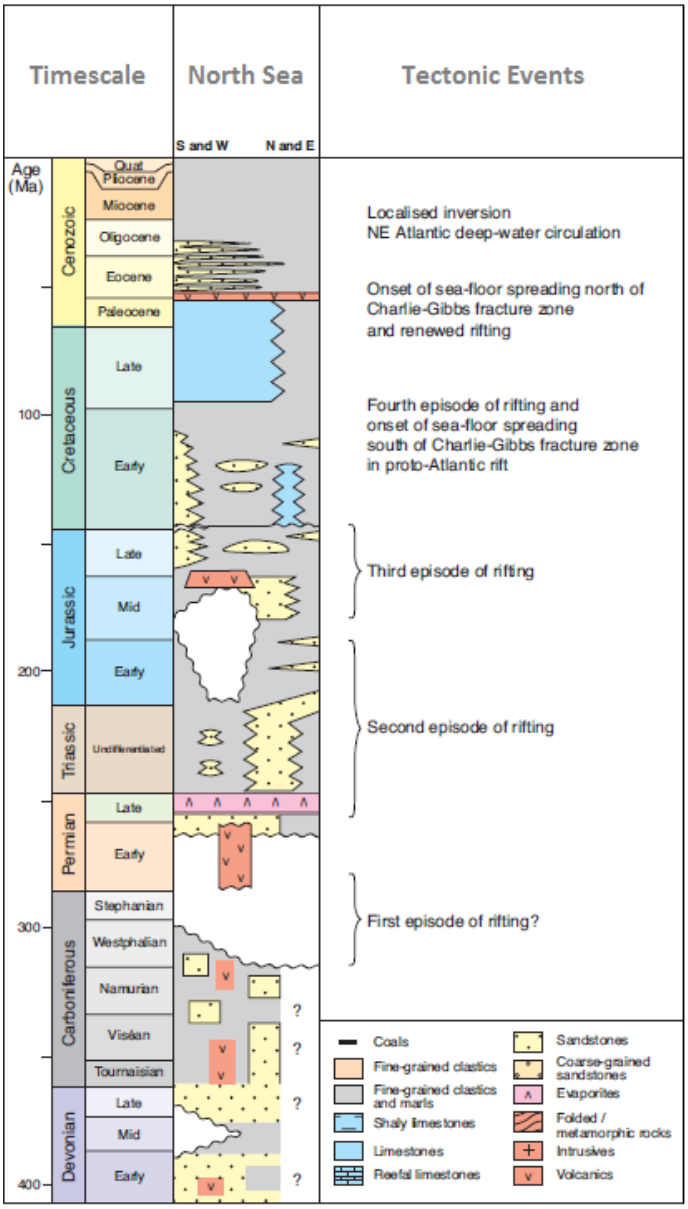

Figure 2.2, Tectonostratigraphic chart of the North Sea (modified after Zanella and Coward 2003).

Permian, Early Triassic and Middle Late Jurassic periods of rifting produced the central graben. The variations and direction of the Triassic extension in the central and northern North Sea are uncertain.

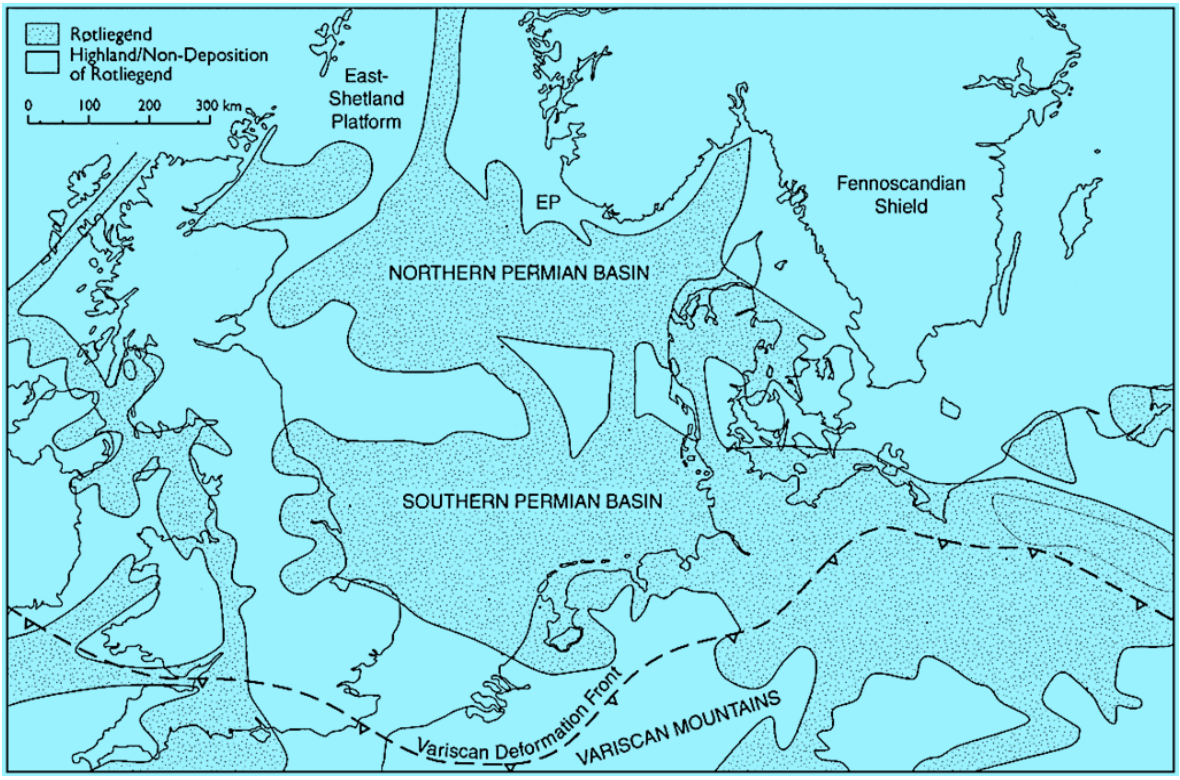

Figure 2.3 Outline of the Northern and Southern Permian Basins (Stemmerik et al. 2000).

2.2.1 Late Jurassic rifting

The major extension phase during Late Jurassic time lead to the formation of the Viking Graben, the Moray Firth Basins and the Central Graben triple junction rift system in the North Sea (Zanella and Coward 2003). Extension along this triple rift system is defined by different authors in different ways.

According to vector-triangle model of Errat et al. (1999), the extension in these three rifts took place in two phases. The vector diagram (Figure 2.4) shows that in first phase (Callovian to Early Kimmeridgian), major extension took place along the Viking Graben, and in the second phase (Early Kimmeridgian to Volgian), major extension took place along the Central Graben.

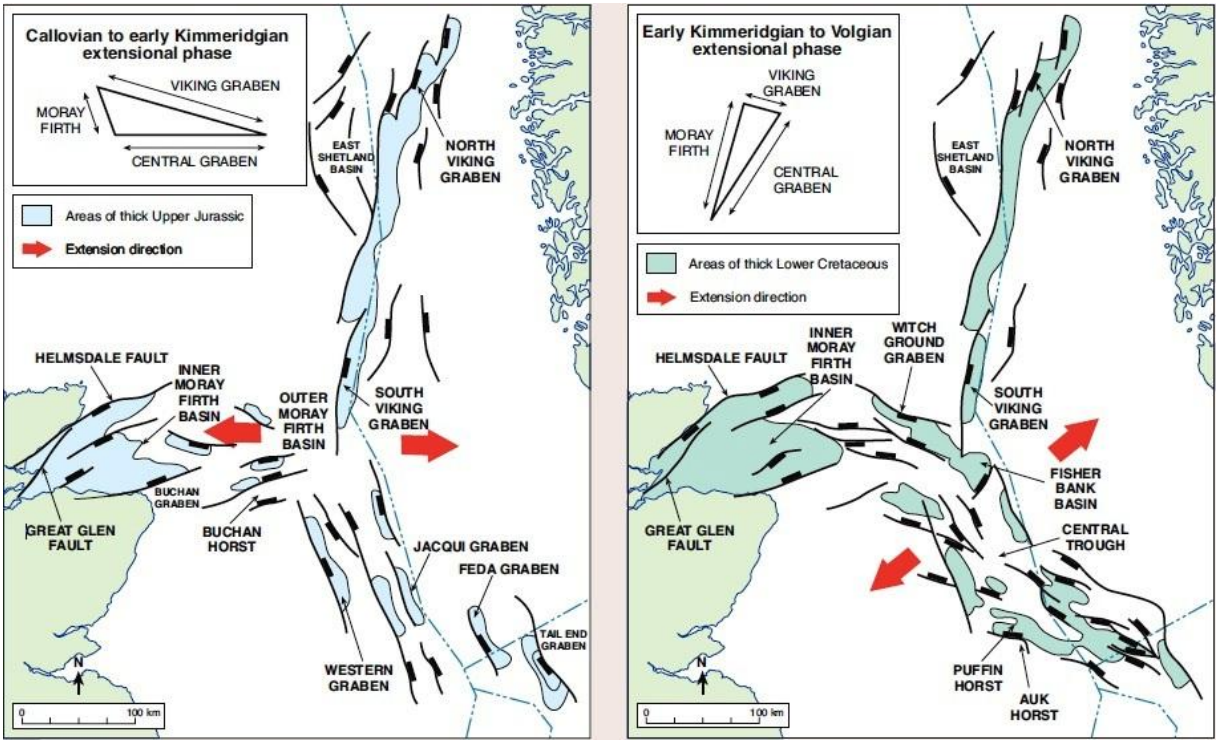

Figure 2.4 'Two-phase' model for the orthogonal opening of the North Sea rift (Errat et al. 1999).

2.3 Stratigraphic framework

The last plate tectonic package of Pangea and the future beginning of rifting with in the supercontinent influenced the Permian period extending from the Asselian (299Ma) to the Changhsingian (251Ma). An early period of magmatism with subsequent widespread erosion (Saalian unconformity (Figure 2.6)) and later by the development of shallow marine environments in low latitudes (15°N) are the characteristic features of this time span of Earth's history (Brekke et al. 2001).

Due to the greater depths of the formation, the Rotliegend facies distribution in Northern Permian Basin (NPB) is not well known. However, based on the data that is available today, generally the NPB is probably consisting of the same sedimentary facies as the well-studied Southern Permian Basin (SPB) (Glennie 1998), namely Wiessliegend, fluvial, aeolian and sabkha facies. The Wiessliegend is identified as colorless and structure less sand in poorly preserved aeolian beds from the Southern Permain Basin. The correlation of the Auk and Fraserburg Formation (Northern Permain Basin) with the Leman and Silverpit Formations (Southern Permain Basin) exist on the basis of similarities in facies distribution(Glennie 1998). The Auk Formation is mainly massive aeolian sandstone and the Fraserburgh

Formation is interpreted as shales. In UK Shell/Esso well 21/11-1 the Fraserburgh shales are interpreted as dune bordered sabkha contains dolomitic, micaceous, and anhydritic sandstones with adhesion ripple marks (Deegan and Scull 1977).

2.3.1 Stratigraphic setting

The Central Graben and the specified study area within this graben is mainly related to the Northern Permian Basin, hence the Southern Permian Basin will not be discussed any further. Glennie et al. (2003) is recommended for further reading on the SPB.

The Permian sequence of the North Permian Basin was greatly influenced by extreme climatic conditions and deposited as desert sandstones or as evaporates and carbonates. The sequence has been divided into two lithostratigraphic divisions named as Rotliegend and Zechstein Groups. Rotliegend Group is further subdivided into different Units such as Lower Rotliegend, Upper Rotliegend 1, Altmark Unconformity and Upper Rotliegend 2 (Glennie et al. 2003). Figure 2.6 shows a lithostratigraphic chart including all of the above mentioned Permian Groups and Units.

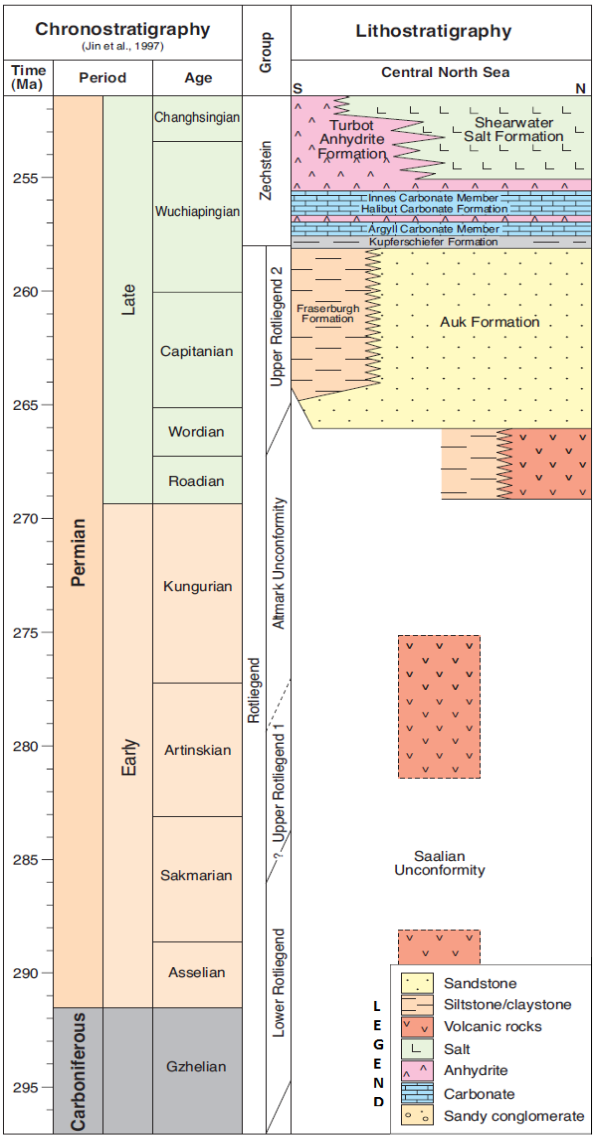

Figure 2.6 Permian stratigraphic chart (Modified after Glennie et al. 2003).

The global boundary between these two groups is now set to the beginning of Roadian stage (269 Ma) (Glennie et al. 2003); however, in Europe, the Rotliegend and Zechstein Groups have conventionally been set to Lower and Upper Permian Epochs respectively. All the Rotliegend and the Zechstein sedimentary formations of the Northern Permian Basin have been deposited during the Late Permian and the Lower Permian only consists of volcanic rocks (Glennie et al. 2003).

Keeping the purpose of the thesis project into consideration, the focus is on Upper Rotliegend 2 Unit which extends from the Wordian age to the Early Wuchiapingian age (figure 2.6) of the Late Permian will be described below in section 2.3.2. The remaining Rotliegend Units will be described very briefly.

2.3.2 The Rotliegend Group

According to Deegan and Scull (1977), the sedimentary sequence of Rotliegend Group consists of continentally deposited clays, shales, sandstones and some minor conglomerates at places. Both Lower Rotliegend (LR) and the Upper Rotliegend 1 (UR1) Units are characterized by volcanics and are separated by the Saalian unconformity (Figure 2.6). While, the Upper Rotliegend 2 (UR2) and UR1 are separated by another unconformity called, "Altmark Unconformity" (Stemmerik et al. 2000).

The Upper Rotliegend 2 (UR2) sequence consists of four main facies: fluvial wadi facies, aeolian dune facies, lacustrine desert lake facies and evaporitic sabkha facies (Glennie et al. 1978; Glennie 1998).

The fluvial wadi deposits contain mainly micaceous and argillaceous sandstones and associated micaceous siltstones. Desiccation cracks and clay rip-rap clasts show subaerial exposure. The sandstones have some clay laminae, nodular anhydrite and early dolomite cement in southern part of Rotliegend Basin. This facies is dominant in Moray Firth and called Findhorn Formation (Ziegler 2006; Glennie 1998). Aeolian sandstones sequences are consist of well-defined planar bedding marked by sharp grain size differences. These facies in UK sector are referred to as Leman Sandstone, whereas, it is referred to as Auk Formation in Northern Permian Basin (Ziegler 2006). The lacustrine facies characterized by mainly red brown mudstone and minor siltstone (Glennie 1998). In southern UK areas it is referred to as Silverpit Formation, and called Fraserbugh Formation in the Northern Permian Basin (Ziegler 2006). The sabkha facies is characterized by poorly bedded clays, silts and sands at outer edge of desert-lake deposits (Glennie 1998). Mud cracks, sandstone dykes and nodular anhydrite are typical features of sabkha (Ziegler 2006).

Chapter 3
THEORETICAL BACKGROUND

3.1 Introduction

The properties of sandstone depend on its composition at shallow depth, temperature and stress history during burial. Provenance, transport and depositional environment control initial composition of sandstone. The most important factor in predicting reservoir quality at depth is the initial or primary clastic composition and the depositional environment (Figure 3.1) (Bjørlykke and Jahren 2010).

According to Bjørlykke and Jahren (2010), main diagenetic processes are:
(1) Near surface diagenesis.
(2) Mechanical compaction
(3) Chemical compaction
(4) Cementation

3.2 Near surface diagenesis

The primary sediment composition is altered by diagenetic reactions as soon as the sediments are deposited. Sediments are most susceptible to react with water or air or both by process of fluid flow and diffusion at burial depth of about <1 to 10 m. Diagenesis is caused by meteoric water near surface. Water starts to react and dissolve carbonates and other unstable minerals like feldspar and mica (Figure 3.2) (Bjørlykke and Jahren 2010), when it seeps down in the soil. Because it is fresh and under saturated with respect to minerals, carbonate cementation and K-feldspar leaching processes are of significant importance at this stage.

The carbonate cement is mainly derived from biogenic carbonates within the rock at shallow depth which becomes unstable below the redox boundary. Carbonates dissolve and re-precipitate as cement at shallow burial depth due to high reaction rates of carbonate minerals (Saigal and Bjørlykke 1987). Biological productivity controls carbonate minerals available in rocks and depends upon clastic sedimentation rate.

K-feldspar leaching, mica and precipitation of kaolinite significantly affect reservoir properties (Bjørlykke et al. 1992). Kaolinite is thermodynamically unstable in the presence of K-feldspar and it is transformed into illite during deep burial (120-140˚C). The transformation

of kaolinite into illite affects the permeability of rock while leaching of K-feldspar causes an increase in secondary porosity (Bjørlykke and Jahren 2010).

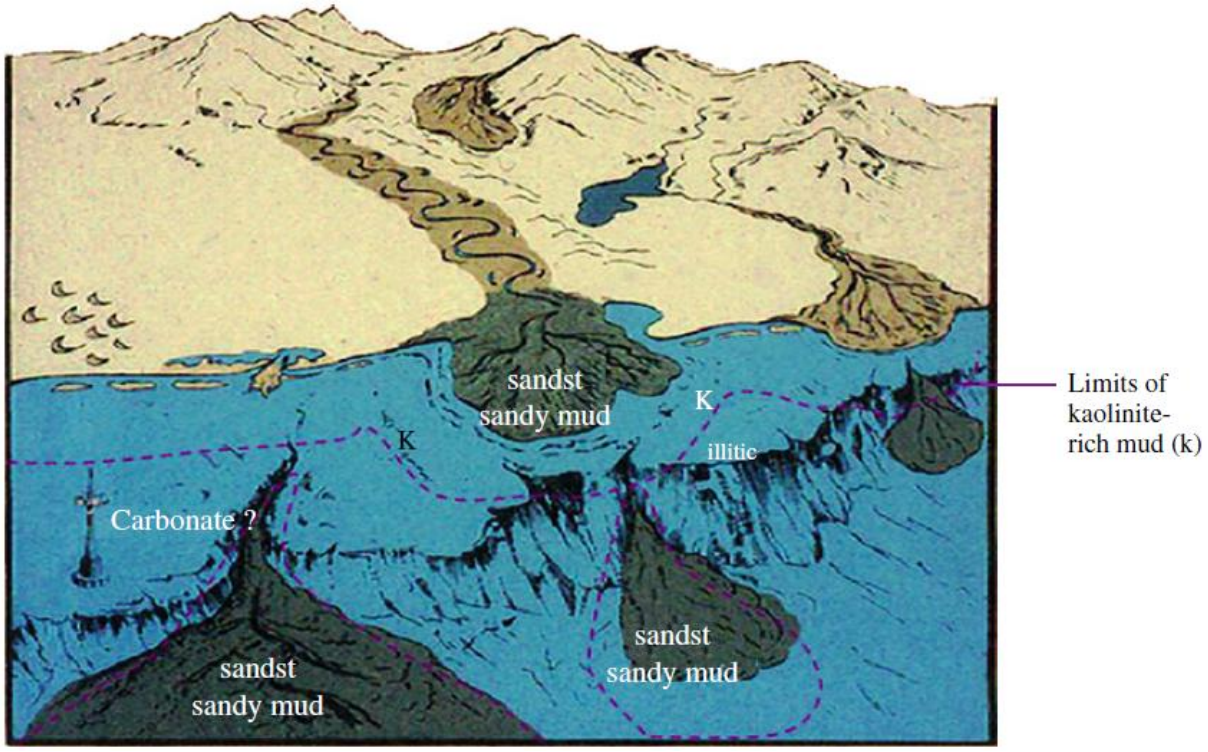

Figure 3.1 Showing a sedimentary basin on a continental margin (Bjørlykke and Jahren 2010).

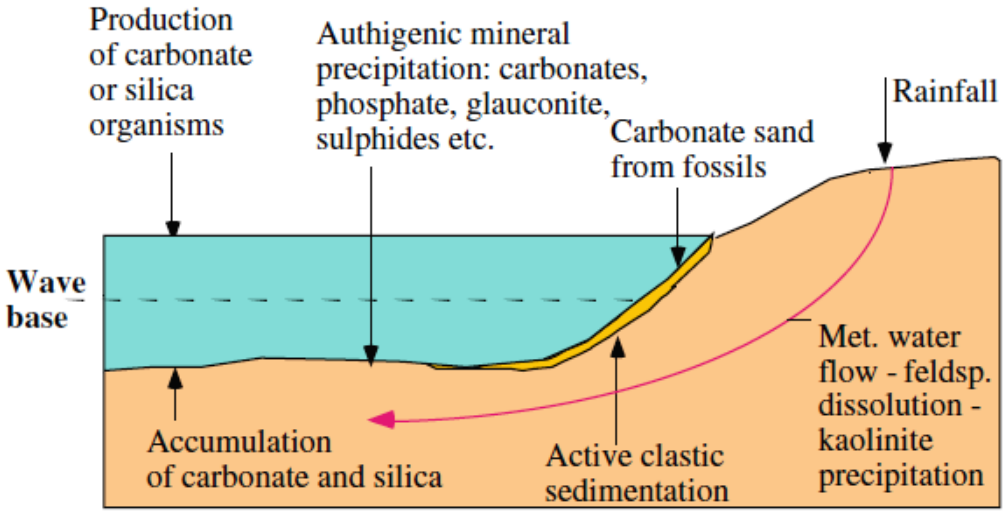

Figure 3.2 Schematic illustration of diagenetic processes in shallow marine environment (Bjørlykke and Jahren 2010).

These reactions of water with feldspar and micas can be written as follows (Bjørlykke and Jahren 2010):

$2K(Na)AlSi_3O_8 + 2H^+ + 9H_2O \longrightarrow Al_2Si_2O_5(OH)_4 + 4H_4SiO_4 + 2K^+ (2Na^+)$
Feldspar — Kaolinite — dissolved silica — dissolved cations

$2KAl_3Si_3O_{10}(OH)_2 + 2H^+ + 3H_2O \longrightarrow 3Al_2Si_2O_5(OH)_4 + 2K^+$
Muscovite — Kaolinite

3.3 Mechanical compaction

The initial space among the sand grains, measured as the intergranular volume (IGV) of the sediment is determined by grain size, sorting, shape and matrix content (Paxton et.al, 2002). IGV decreases as sediments are buried, which is function of mechanical compaction. Mechanical compaction causes grains to pack closely together (Figure 3.3) (Ajdukiewicz and Lander 2010). Experimental compaction shows that initial porosity (40-42%) of sandstone may reduce to 35-25% at 20-30 MPa (2-3 Km depth). This depends on grain strength and grain size (Chuhan et al. 2003).

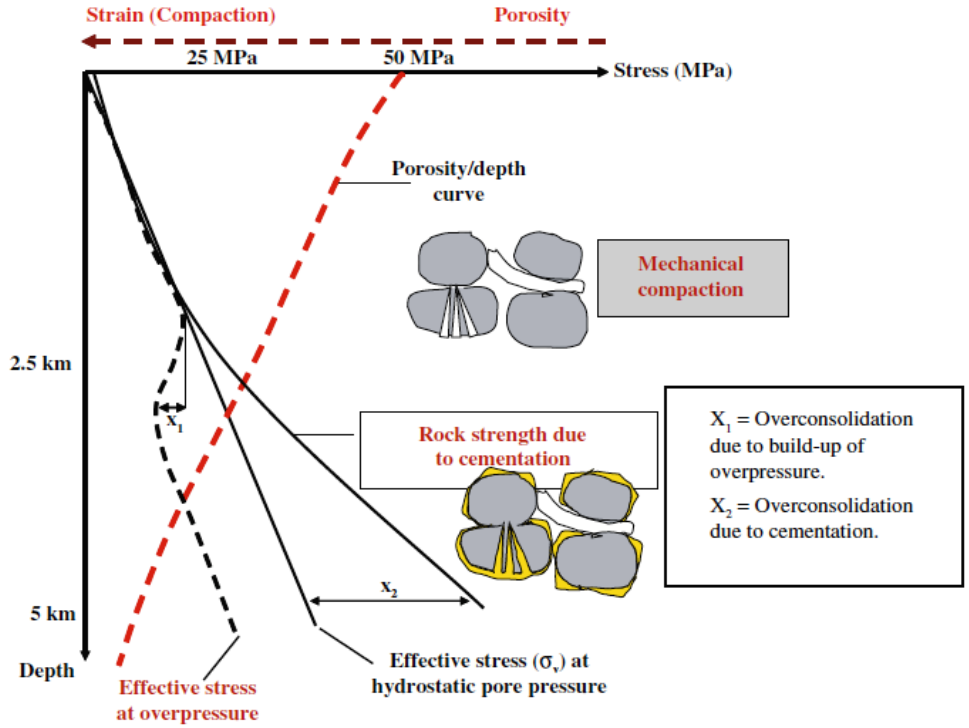

Figure 3.3 Sandstones mechanically compact as a function of effective stress (depth) by grain reorientation and grain breakage, before they become cemented at 80°C-100°C (Bjørlykke and Jahren 2010).

3.4 Sandstone reservoirs buried to intermediate depth (2.0–3.5 KM, 50–120°C)

Quartz cementation starts at intermediate depth which thus increases the strength of the rock and stops mechanical compaction. Chemical compaction is the main process acting on the reservoir from this depth onwards. About 2-4% quartz cement stops mechanical compaction and strengthen the rock. This means chemical compaction will be the main process acting on the reservoir. Albitization can also alter composition of reservoirs buried at this depth (Bjørlykke and Jahren 2010).

Quartz cementation starts to precipitate and modify porosity when temperature reaches 60°C to 80°C. Quartz cementation depends on time, temperature (as shown in Figure 3.4) and surface area available (Ajdukiewicz and Lander 2010; Walderhaug 1996). Porosity is decreased in both mechanical compaction and chemical compaction. Quartz cementation is limited by diagenetic clay coats over grains. Quartz cementation is main porosity destroying process in sandstones buried at intermediate depth (2.0-3.5 Km) (Bjørlykke et al. 1989). Quartz cementation will be discussed in detail later within this chapter.

K-feldspar may be albitized which may result in significant change in composition of sandstone reservoirs at intermediate burial depth. K-feldspar reacts with Na^+ which results in formation of Albite and releases K^+ (Bjørlykke and Jahren 2010). This reaction is shown below:

$$KAlSi_3O_8 + Na^+ \longrightarrow NaAlSi_3O_8 + K^+$$

K-feldspar Albite

Saigal et al. (1988)

Albitization starts at 2-3 Km burial depth (Saigal et al. 1988) and 30-50 % of original K-feldspar can be albitized at the same depth (Aagaard et al. 1990).

3.5 Deeply buried sandstones (>3.5–4 KM, >120°C)

The quartz cementation does not stop until all porosity is filled by quartz cement and temperature falls below 70 to 80°C due to uplift or other reasons (Walderhaug 1996). Quartz cementation continues until it destroys all porosity and when temperature reaches 200-300°C sandstone converts into hard quartzite during continuous burial (Bjørlykke and Jahren 2010).

Illitization only starts if kaolinite and K-feldspar are present together in reservoir and takes place at burial depths of about 3.7 to 4 Km (120-140°C) (Chuhan et al. 2000). Kaolinite and K-feldspar are thermodynamically unstable when they are present together in the reservoir as mentioned earlier. High activation energies are required for illitization which is available at deep burial. Illitization is probably the most important reasons for reduction of reservoir properties along with quartz cementation (Bjørlykke et al. 1992). The following equation represents the illitization reaction of kaolinite:

$$\underset{\text{K-feldspar}}{2K(Na)AlSi_3O_8} + \underset{\text{Kaolinite}}{Al_2Si_2O_5(OH)_4} \longrightarrow \underset{\text{Illite}}{KAl_3Si_3O_{10}(OH)_2} + \underset{\text{Quartz}}{SiO_2} + 2H_2O$$

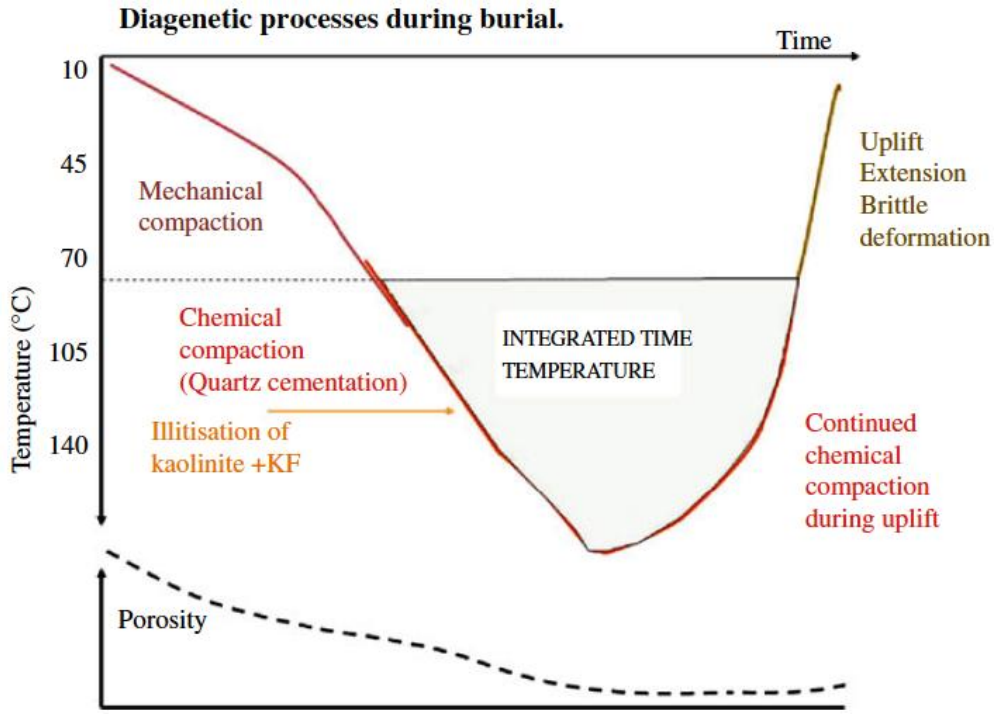

Figure 3.4 Diagenetic processes, mainly quartz cementation, as a function of temperature and time. Note that quartz cementation will continue also during uplift as long as the temperature exceeds 70–80◦C (Bjørlykke and Jahren 2010).

3.6 Quartz cementation

According to Worden and Morad (2009), three factors affect reservoir quality:
1) Porosity and Permeability
2) Degree of mechanical and chemical compaction
3) Amount and type of pore filling cement.

Sandstone reservoirs buried at 2-3 km depths lose their porosity from 35-45% (depositional porosity) to 15-20%. The main reason of porosity reduction at this depth is quartz cementation which kicks off at 70-80°C (Bjørlykke et al. 1989).

3.6.1 Origin of quartz cement in sandstones

There have been different suggestions and explanations about the source of silica until late 90's (e.g. McBride 1989). External sources and dissolution process were two main explanations regarding silica source. A large flux of water in sandstone is mainly considered an external source, but later it was ascertained that external sources have no role in quartz cementation. Bjørlykke (1994) calculated that 108 cm^3 water passing through each cm^2 of sandstone will result in quartz cementation, which is naturally impossible. Most of the authors believe source of silica is mainly from the illite-mica induced dissolution (I-MID) which was introduced by Oelkers et al. (2000).

"Dissolution at grain contacts requires stress, and the process is often called Pressure Solution, but the degree of stress needed is relatively moderate" (Bjørlykke and Jahren 2010). Rutter and Elliott (1976) introduced that silica solubility is controlled by pressure. However, Bjørkum (1996) accentuated on the critical role of the temperature and trifling role of pressure for silica dissolution in diagenetic rocks. According to Fisher et al. (2000), illite clay or mica and quartz grain contacts are the preferred sites of dissolution. These contacts are called stylolites. The quartz overgrowth is formed due to the transportation of dissolved silica at stylolites to the grain surfaces by diffusion (Figure 3.5). Precipitation will take place away from the stylolites where the silica will be oversaturated with respect to quartz (Bjørlykke and Jahren 2010).

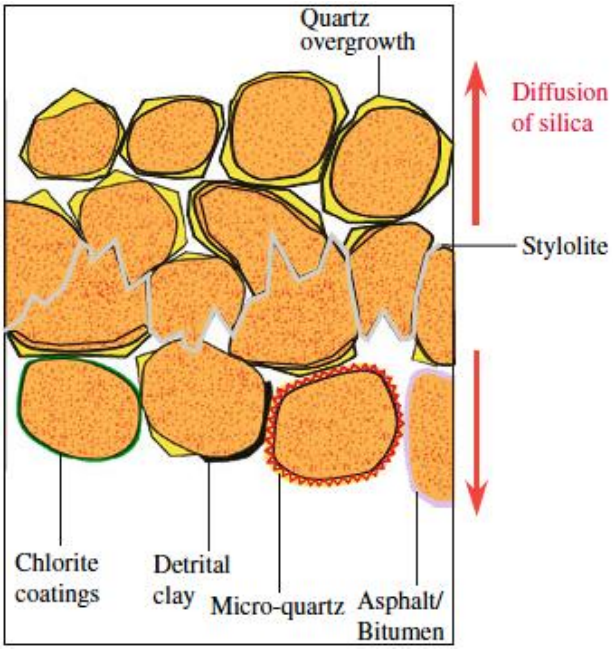

Figure 3.5 Schematic illustration of a stylolite. The dissolved silica is transported away from clay rich stylolite by diffusion (Bjørlykke and Jahren 2010).

3.6.2 Factors influencing quartz cementation

Temperature effects quartz cementation in two ways, by affecting the diagenetic processes which result in release of silica or by affecting quartz dissolution, diffusion and precipitation. Thus "Temperature affects both the thermo-dynamics and the kinetics of geochemical process that cause quartz cementation". Rate of quartz cementation is increased exponentially by a factor of 1.7 for every 10°C as a function of temperature (Walderhaug 1996). Reservoir must attain temperature of about 60°C to start quartz cementation. Quartz cementation does not start before this temperature (Bjørlykke and Jahren 2010). Quartz overgrowth and quartz cementation increases significantly during deep burial diagenesis (>2.5 km) with temperatures 90^{o}C-130°C (Giles et al. 1992; Gulyas et al. 1993). Porosity is reduced by precipitation of quartz cement which is also a function of surface available for quartz cementation. Slowly subsiding basins may witness quartz cementation for tens of millions of years at low temperatures (<100°C). Inversely at high temperatures cementation may take place for shorter time span (Morad et al. 1994).

3.7 Porosity preserving mechanisms

During progressive burial in sandstones, quartz cementation destroys all porosity unless it is hindered by some porosity preserving mechanism (Bjørlykke and Jahren 2010).
There are several porosity preserving mechanisms, and some will be discussed below. Grain coats are the most important porosity preserving mechanisms in preserving good porosity at depth about 5 Km.

3.7.1 Hydrocarbon emplacement

According to Johnson (1920) hydrocarbons in sandstone reservoirs can also influence the porosity. But recently it was thought that hydrocarbon bearing reservoirs have good porosity (Emery et al. 1993). However, now most of the authors are of the view that hydrocarbon presence does not have great effect on porosity (Aase and Walderhaug 2005; Barclay and Worden 2000b; Ramm and Bjørlykke 1994; Walderhaug 1994).

It has been found in the North Sea that hydrocarbon bearing reservoirs have slightly improved porosity while there hardly any change on reservoir quality across the water contacts (Giles et al. 1992; Ramm and Bjørlykke 1994).

Walderhaug (1994) proved that hydrocarbon emplacement in sandstones does not really hinder the quartz cementation and cementation continues even in the presence of hydrocarbon (Walderhaug 1990).

3.7.2 Fluid overpressure

The increase in effective stress mainly drives reduction in compaction related porosity. The vertical effective stress at grain contacts is reduced by fluid overpressure. A potential for porosity preservation is provided by early overpressure until significant quartz cementation occurs (~90°C) (Walderhaug 1994). Overpressures may also limit quartz cementation by delaying the onset of intergranular pressure solution, eliminating a primary source of silica. Overpressure developed at a later stage has a minor effect on porosity (Jahren and Ramm

2000). Porosity normally lost due to compaction, is held open by overpressure, resulting in preserved porosity at deeper burial depths.

3.7.2 Clay coats

Clay coatings are considered one of the most important preserving porosity mechanisms in sandstones (Anjos et al. 2009; Taylor et al. 2004; Bloch et al. 2002; Ehrenberg 1993; Pittman et al. 1992; Thomson 1979; Heald and Larese 1974). It has been observed that sandstones with a lot of clay coatings have highly preserved porosity and less quartz cementation than the sandstones with poor clay coatings. Clay coatings include chlorite, smectite and illite.
The most important clay coating which effectively preserves the porosity by controlling the quartz cementation is authigenic chlorite, because it forms continuous layers around detrital quartz grains (Taylor et al. 2010). According to Bloch et al. (2002) chlorite coating is most effective in porosity preserving than the other clays which do not stop quartz cementation completely.

Illite has been reported less as a grain coating than chlorite coatings (Taylor et al. 2010). Pore filling illite is found in sandstone reservoirs present at a burial depth of 3, 5-4km in Haltenbanken and the North Sea basin. This indicates that illite precipitation occurs above 120^{o}C-140°C as suggested by Ehrenberg (1990). According to Storvoll et al. (2002), it has been shown that illite may form grain coatings, but uncertainty lies about the timing of grain coating development, relative to the quartz cement precipitation which starts at 2,5-3km (90^{o}C-100°C) . A precursor mineral is necessary for the development of authigenic illite (Aagaard et al. 2000).

Numerical models of quartz cementation given by Bloch et al. (2002) and Lander et al (2008) show that reservoirs which are deeply buried and are at higher temperatures require full grain coats to preserve porosity.

3.7.3 Microquartz coats

Microquartz coating is also a very effective porosity preserving mechanism in deeply burried sandstones. Scanning Electron Microscope (SEM) is used to detect the presence of micro-quartz coating because it is too small to be observed in standard optical microscope. According to (Taylor et al. 2010), micro-quartz is rapidly crystallized from silica supersaturated solution and siliceous sponge spicules dissolve to maintain the silica saturation even at very low temperatures. This has been observed in several of the Upper Jurassic reservoir rocks from the North Sea, where the micro-quartz is believed to originate from Rhaxella sponges (Bjorlykke and Jahren 2010). Micro-quartz coating prevents the quartz cementation and considered as primary reason behind the good qualities of many deeply buried, up to 5 km, reservoirs in the North Sea (Bjorlykke and Jahren 2010). The reservoir intervals containing microcrystalline quartz coats have lower amounts of quartz overgrowth and higher intergranular porosity than sandstones lacking micro-quartz (Bjørlykke and Jahren 2010).

Chapter 4
METHODS AND DATA

4.1 Well information and data set

The project is based on the study of two wells 1/3-5 and 2/10-2, located on Hidra high and Grensen Spur respectively in Central Graben. The well information is downloaded from Norwegian Petroleum Directorate website and compiled into a well data summary sheet.

Table 4.1 Well summary sheet for petrophysical evaluation (NPD 2012).

	Well 1/3-5	**Well 2/10-2**
Structural element	Hidra high	Grensen spur
UTM zone	31	31
Wellbore contents	Dry	Oil
RKB elevation (m)	35	26
Water depth (m)	71	71
Total depth (MD) [m RKB]	4850	4164
Bottomhole temp. (^{o}C)	172	148
Porosity	Good	-
Permeability	Low	-
Deepest penetrated age	Early Permian	Early Permian
Oldest penetrated fm.	Rotliegend GP.	Rotliegend GP.

4.2 Well correlation

The main objective of the well correlation was to correlate the reservoir sandstone part of Permian Rotliegend Group in both the wells. The correlation has been done by using several wire line logs.

The wire line logs can provide information related to porosity, lithology, presence of hydrocarbons or other related parameters. The logs can also be used to further derive petrophysical properties, e.g. using cross-plots as in the petrophysical analysis.

The following logs have been used for the correlation; Gamma ray, sonic, neutron porosity, bulk density. Gamma ray and sonic logs are used in combination to mark the lithology while porosity is calculated by using neutron porosity and bulk density logs in combination.

The correlation has been done by using Petrel software. The software is introduced by Schlumberger and used for reservoir modeling, well correlation and seismic interpretation. Only correlation is performed in this project using this software.

4.3 Petrophysical evaluation

After the well correlation is finished and all the well tops set, the logs are exported from Petrel and imported into Interactive Petrophysics (IP) software. This software enables the logs to be cross-plotted against each other, and allows a more thorough analysis of the log values. Any wire line-log values could potentially be plotted, but for this thesis the focus is on porosity, so a number of cross plots are used to show the good porosity preservation in two wells. e.g Porosity vs Depth, Density and Gamma ray color coded with Neutron Porosity etc.

4.4 Petrographic analysis

Petrographic analysis has been done using Optical Microscopy and Scanning Electron Microscopy (SEM) on the samples from wells 1/3-5 and 2/10-2.

4.4.1 Optical microscopy

4.4.1.1 Thin section observations

All ten thin sections have been examined under a Nikon Optiphot-Pol petrographic microscope. The polished thin sections are examined with respect to composition, grain size, grain shape and sorting (Figure 4.1). Other general observations regarding compaction of the sand stones such as grain contacts, quartz overgrowth, grain coating have also been noted down and pictures are taken to document them.

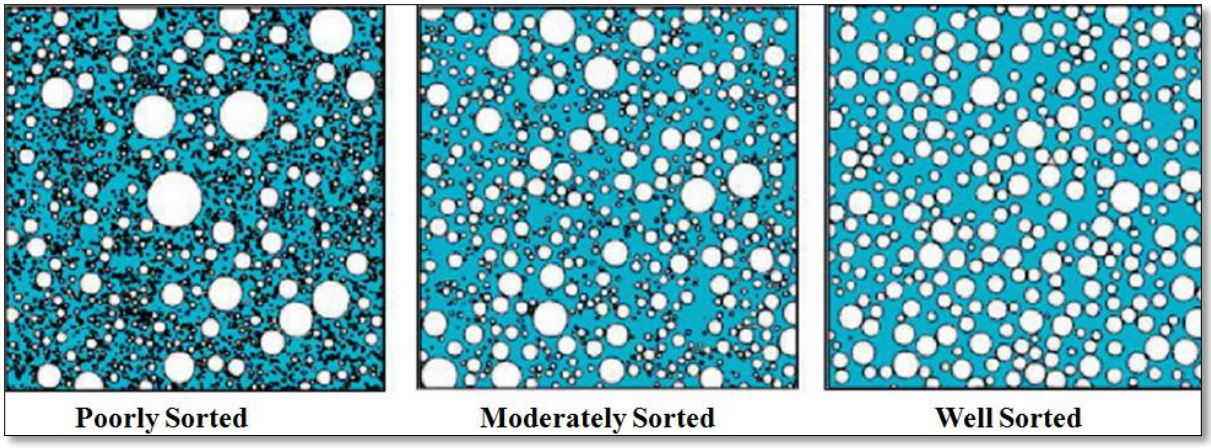

Figure 4.1 Degree of sorting presented by Chuhan et al. (2003).

4.4.1.2 Point counting

Point counting has been done for all ten thin sections to estimate the porosity and composition. An automatic counter and a mechanical stage, in addition to standard polarization microscope are used to perform point counting. 300 points are counted on each thin section on the basis of set parameters;
1) Quartz 2) Feldspar 3) Rock Fragments 4) Matrix 5) Quartz cement 6) Carbonate cement 7) Authigenic clay 8) Total Porosity

4.4.1.3 Intergranular volume (IGV)

Intergranular volume (IGV) as defined by Paxton et al. (2002) is the sum of intergranular porosity, intergranular cement and depositional matrix.

Intergranular Volume (IGV) = cement + depositional matrix + intergranular porosity

Point counting results have been used to calculate IGV (Intergranular volume). IGV is used to measure the compaction in sandstones. In sandstone samples from these two wells IGV varies from 29.1 % to 52.1 %.

Table 4.2 Thin sections of study area with their depths.

Well Name	Sample depth (m)
2/10-2	4152.60
	4157.60
	4159.70
	4159.20
	4160.20
	4163.20
1/3-5	4807.50
	4809.50
	4812.60
	4813.60

4.4.2 Scanning electron microscopy (SEM)

SEM analysis has been done on samples using JEO2 JSM-6460LV Scanning Electron Microscope (SEM) with a LINK INCA Energy 300 Energy Dispersive X-Ray (EDX) system. Two types of samples have been studied under SEM. These include thin sections coated with carbon and freshly fractured samples from core material which are mounted over stubs and coated with gold. All 10 samples mounted over stubs are studied. And 8 samples are chosen for carbon coating in a way that it covered the high and low porosity zones (Table 4.3).

Table 4.3 Selected samples prepared for SEM examination.

Well name	Structural element	Thin section	Carbon coated	Stubs
1/3-5	Hidra high	4	4	4
2/10-2	Grensen spur	6	4	6
Number of samples		10	8	10

4.5 Quartz cementation and porosity algorithm

Walderhaug (1996) presented a mathematically simple kinetic model where quartz cementation and porosity loss are presented as functions of time and quartz cement is sourced from stylolites and thicker zones of clay- and mica-catalyzed quartz dissolution. He also discussed how his model can handle the effect of factors such as grain size, percentage of detrital quartz, clay coatings, and different temperature histories.

The model imitates the situations where quartz is sourced from stylolites and grain interpenetration is negligible. The modeled sandstone volume is located in between stylolites

and does not include the stylolites. Moreover, only the precipitation of quartz is modeled, and compaction is inhibited in the sandstone volume by the onset of quartz cementation and stabilizing the sandstone framework. Thus the porosity loss is equal to the volume of quartz precipitation. Quartz cementation is modeled as a continuous process rather than as episodic cementation events.

According to Walderhaug (1996), at constant temperature, the volume of quartz cement, Vq (in cm^3), precipitation in a 1-cm^3 volume of sandstone with quartz surface area A (in cm^2) during time t (in s) can be calculated as

$$Vq = MrAt/\rho \quad (1)$$

Where M is the molar mass of quartz (60.09 g/mole), r is the rate of quartz precipitation in mole/cm^2s, and ρ is the density of quartz (2.65 g/cm^3). Both experimental data (Rimstidt and Barnes 1980) and studies of quartz-cemented sandstones (Walderhaug 1994a) indicate that quartz precipitation rate can be expressed as a logarithmic function of temperature:

$$r = a10^{bT} \quad (2)$$

where T is temperature (°C) and a, b are constants with units of moles/cm^2 s and 1/°C, respectively. When the temperature history of sandstone is given as time-temperature points linked by linear functions, as is typically the case for existing basin modeling systems, T can be replaced by linear functions of time, and equation 2 can be rewritten as

$$r = a\ 10^{b(c_n t + d_n)} \quad (3)$$

where c_n is heating rate (°C/s), d_n is the initial temperature (°C), and the index n refers to the relevant segment of the temperature history curve. Based on equations 1 and 3, the amount of quartz cement Vq precipitated in a volume of sandstone from time t_0 to t_m can be calculated as the sum of a series of integrals where each integral gives the volume of quartz precipitated during each time step:

$$V_q = \frac{M}{\rho} A_o a \int_{t_0}^{t_1} 10^{b(c_1+d_1)} dt$$

$$+ \frac{M}{\rho} A_1 a \int_{t_1}^{t_2} 10^{b(c_2 t+d_2)} dt + \cdots \frac{M}{\rho} A_{m-1} a \int_{t_{m-1}}^{t_m} 10^{b(c_m t+d_m)} dt \quad (4)$$

The volume of quartz cement (*Vq)* precipitated from time t_0 to t_m is calculated as a sum of integrals for two reasons: (1) each segment of a sandstone's temperature vs. time curve normally will have a different slope, resulting in changes in values for the *c* and *d* coefficients throughout the burial history of a sandstone and (2) the quartz surface area where quartz precipitation takes place will vary as cementation proceeds. Thus, one must recalculate the quartz surface area after an increment of quartz cement has precipitated so that the adjusted surface area can be used in the following time step. Solving the integrals in equation 4 gives

$$V_q = \frac{MA_o a}{\rho b c_m \ln 10} [10^{b(c_1 t+d_1)}]_{t_0}^{t_1} + \frac{MA_1 a}{\rho b c_2 \ln 10} [10^{b(c_1 t+d_1)}]_{t_1}^{t_2}$$

$$+ \cdots \frac{MA_{m-1} a}{\rho b c_m \ln 10} [10^{b(c_m t+d_m)}]_{t_{m-1}}^{t_m} \quad (5)$$

In the special case of temperature remaining constant, the volume of quartz cement precipitated is calculated using equation 1 because constant temperature gives $c = 0$, resulting in an undefined value for equation 5.

Following Lasaga (1984), initial quartz surface area, A_0, is estimated as the cumulative surface area of spheres with a diameter, *D*, equal to the grain size and with total volume equal to the fraction of detrital quartz, *f*, in a unit volume, *V*, of the sandstone. This gives the equation

$$A_0 = 6fV/D \quad (6)$$

If the detrital quartz has variable grain size, the cumulative surface area of the quartz in each grain size class is calculated with equation 6, and the total quartz surface area is found by

taking the sum of the quartz surface areas for each grain size. As discussed in following sections, this simple method does not take into account factors such as variations in grain shape, surface roughness, and the lateral extent of grain contacts. However, increased surface area due to the first two factors would be counteracted by decreased surface area due to the grain contacts. In the following calculations the change in quartz surface area caused by precipitation of quartz cement is considered to be proportional to the porosity loss caused by quartz precipitation. Quartz surface area, *A*, when an amount of quartz cement *Vq* has precipitated, can therefore be expressed as

$$A = A_0 (\phi_0 - Vq)/\phi_0 \quad (7)$$

Where ϕ_0 is the porosity when quartz cement precipitation starts.

Equations 5 and 7 provide a sufficient mathematical basis for calculating the evolution of quartz cementation and porosity loss in sandstone as a function of temperature history. The following calculations use Walderhaug's (1994) estimates for the values of a and *b* coefficients: *a* = 1.98' 10–22 moles/cm^2 s and *b* = 0.022°C–1.

Finally, when surface area is expressed by equation 7 and temperature changes at a constant rate, equation 5 may also be solved analytically:

$$Vq_2 = \phi_0 - \left(\phi_0 - V_{q_1}\right) \exp \frac{-MaA_0}{\rho\phi_0 bc\ ln10} \left(10^{bT_2} - 10^{bT_1}\right) \quad (8)$$

Where Vq_2 is the amount of quartz cement (cm^3) precipitated from time T_1 to T_2, and Vq_1 is the amount of quartz cement present at time T_1. However, equations 5 and 8 give the same results when sufficiently small time steps, typically 1 m.y., are used in equation 5.

The following work flow delineates the whole thesis work.

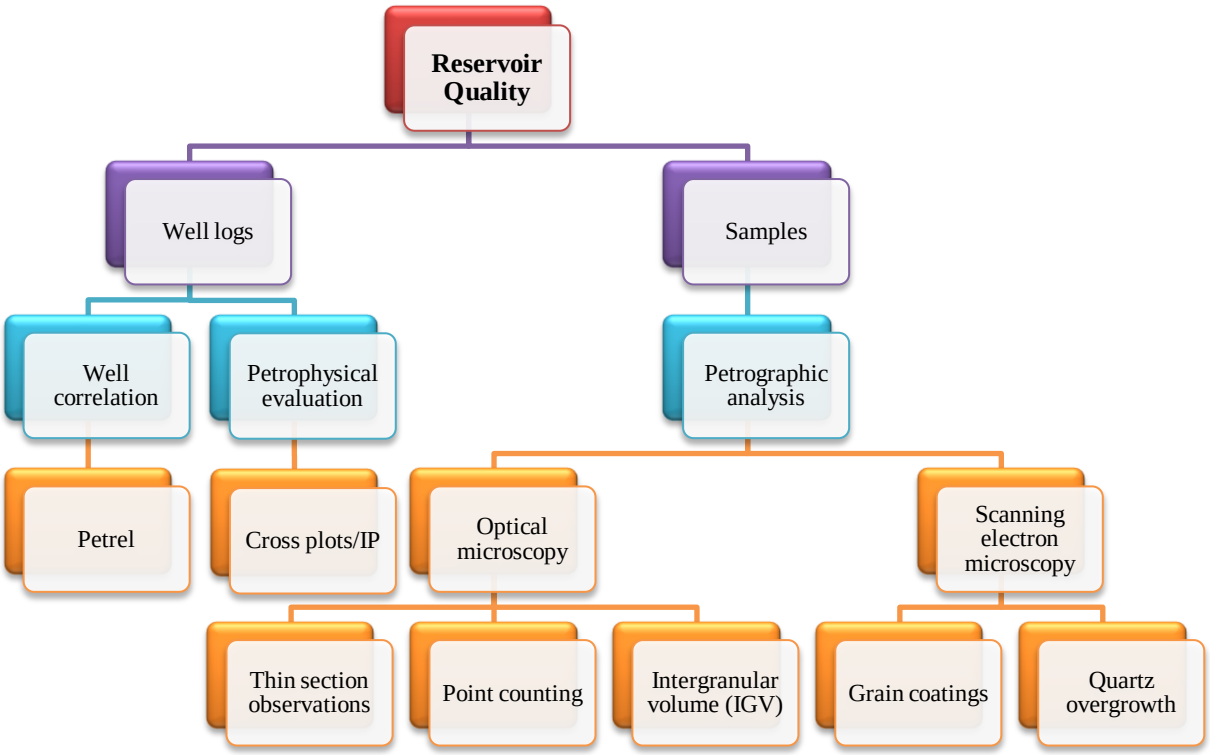

Chapter 5
WELL CORRELATION AND PETROPHYSICAL ANALYSIS

5.1 Introduction

The aim of this chapter is to correlate Rotliegend sandstone units in wells 1/3-5 and 2/10-2 and investigate the petrophysical properties of cored intervals in study area. The correlation enables to identify the lithology and its variation in both the wells. The purpose of petrophysical analysis is to determine the porosity values from the well logs and to identify the porous and non-porous zones in the cored intervals.

Table 5.1 Well summary sheet for petrophysical evaluation. The data is issued by Norwegian Petroleum Directorate (NPD).

	Well 1/3-5	**Well 2/10-2**
Structural element	Hidra high	Grensen spur
UTM zone	31	31
Wellbore contents	Dry	Oil
RKB elevation (m)	35	26
Water depth (m)	71	71
Total depth (MD) [m RKB]	4850	4164
Bottomhole temp. (^{o}C)	172	148
Porosity	Good	-
Permeability	Low	-
Deepest penetrated age	Early Permian	Early Permian
Oldest penetrated fm.	Rotliegend GP.	Rotliegend GP.

5.2 Results

5.2.1 Well correlation

The Upper Rotliegend 2 Unit in the study area mainly consists of sandstones and claystones. The fluvial conglomeratic sandstones are probably derived from Old Red Sandstones. Aeolian sandstones are formed by the reworking of unconsolidated fluvial deposits (Glennie et al. 2003). The sandstone interval in well 1/3-5 is considered clean as it is characterized by low gamma ray, low density response and showing boxcar or cylindrical gamma ray trend (Emery and Mayers 1996). While claystones in sandstone interval from well 2/10-2 are characterized by high gamma ray response (>100 API units) and apparently gamma ray is showing fining/dirtying upward trend (Emery and Mayers 1996).

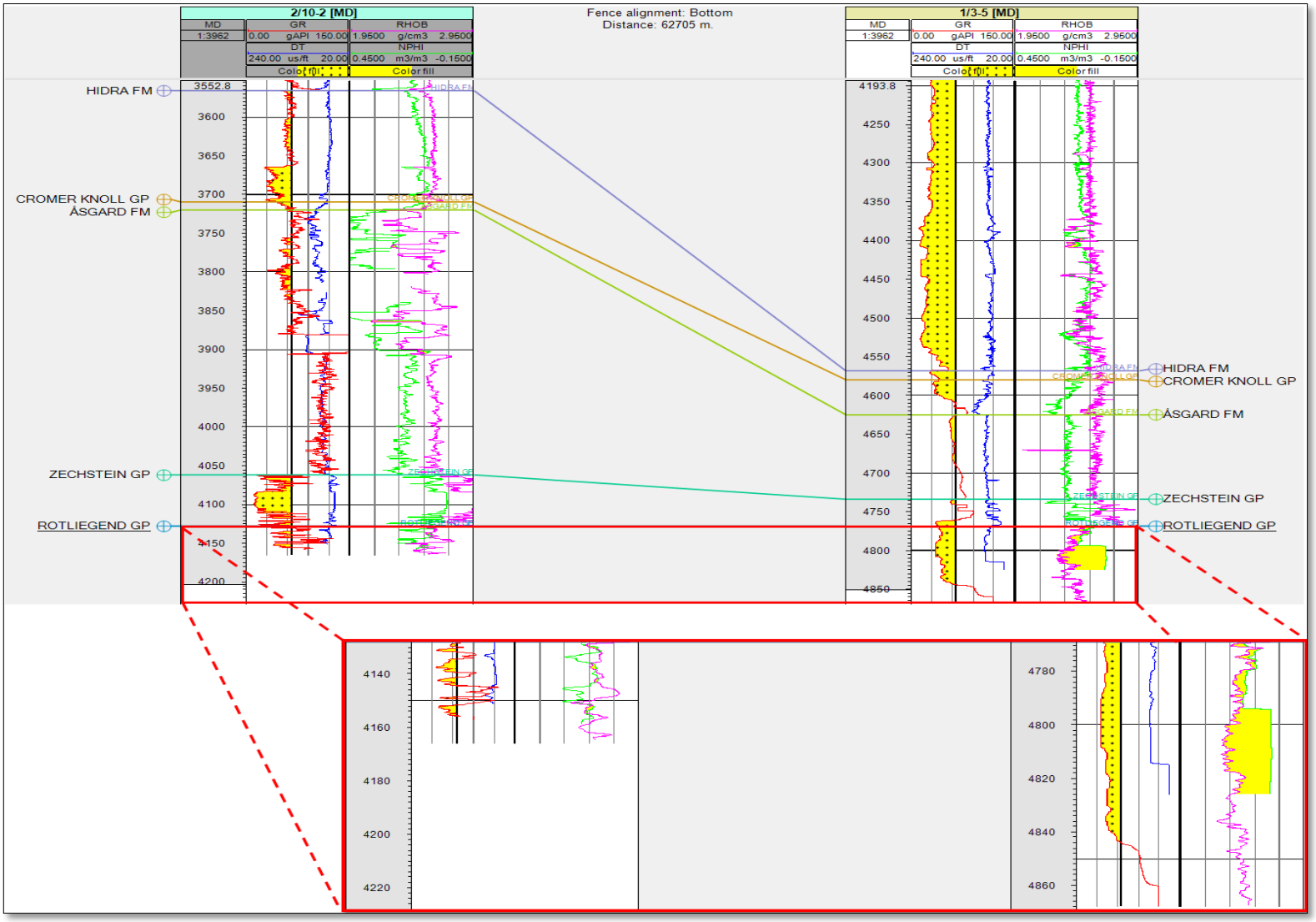

Figure 5.1 Correlation of well 1/3-5 and Well 2/10-2. The zoomed in part shows only Upper Rotliegend 2 Unit.

5.2.2 Petrophysical analysis

To gain more information from petrophysical properties of wire line logs petrophysical analysis has been carried out. Several parameters are plotted against each other to get better understanding of lithology and porosity distribution in the wells.

Cross plots

Several cross plots have been made to investigate the porosity variation in Rotliegend sandstone in wells 1/3-5 and 2/10-2.

Neutron porosity log for specific Rotliegend sandstone interval is plotted with the depth (Figure 5.3) to find out the porosity variation with increasing depth for both the wells. The well 2/10-2 has higher gamma ray log values indicating some claystone intervals. A histogram for interval 4128m-4164m is generated. From the histogram (Figure 5.2) it is evident that claystone and sandstone make up two different populations of gamma ray values, separated at about 60 API. This information is used to filter out porosity contributions from the claystone in all the porosity plots.

The porosity values for well 2/10-2 vary between 5% and 22%, and show average porosity about 8 % (Figure 5.4) at interval 4128m-4164m. Likewise, the average porosity value for well 1/3-5 is about 14% at interval 4769m-4850m. The porosities of cored intervals from both wells are shown in appendix A.

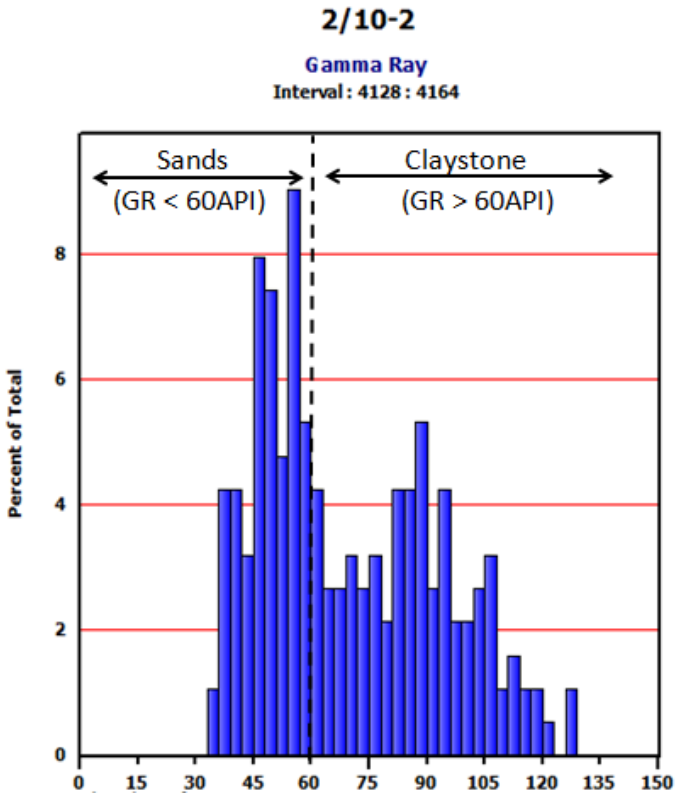

Figure 5.2 Gamma ray (API) distributions for the Rotliegend sandstone of well 2/10-2. Also showing sands (GR < 60API) and claystone (GR > 60API) intervals.

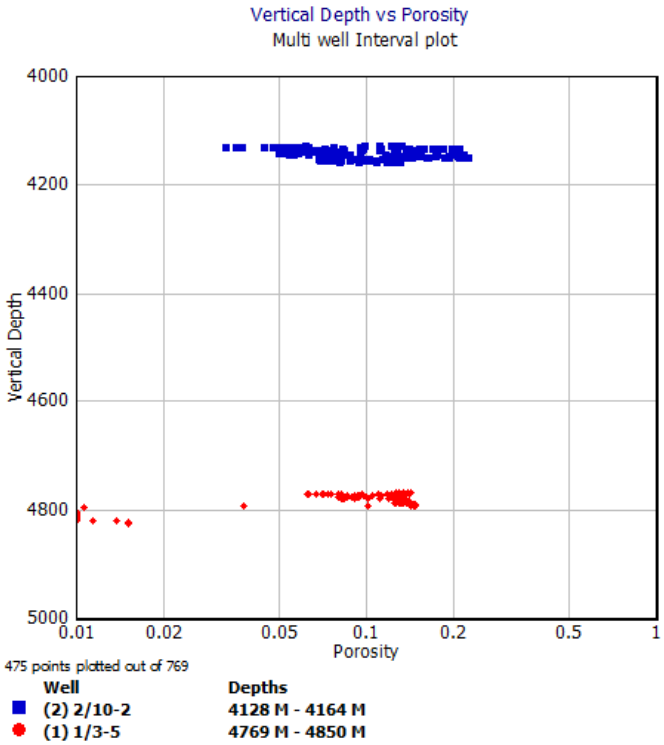

Figure 5.3 Porosity (%) values for the Rotliegend sandstone plotted against depth (m). The color key refers to the well name.

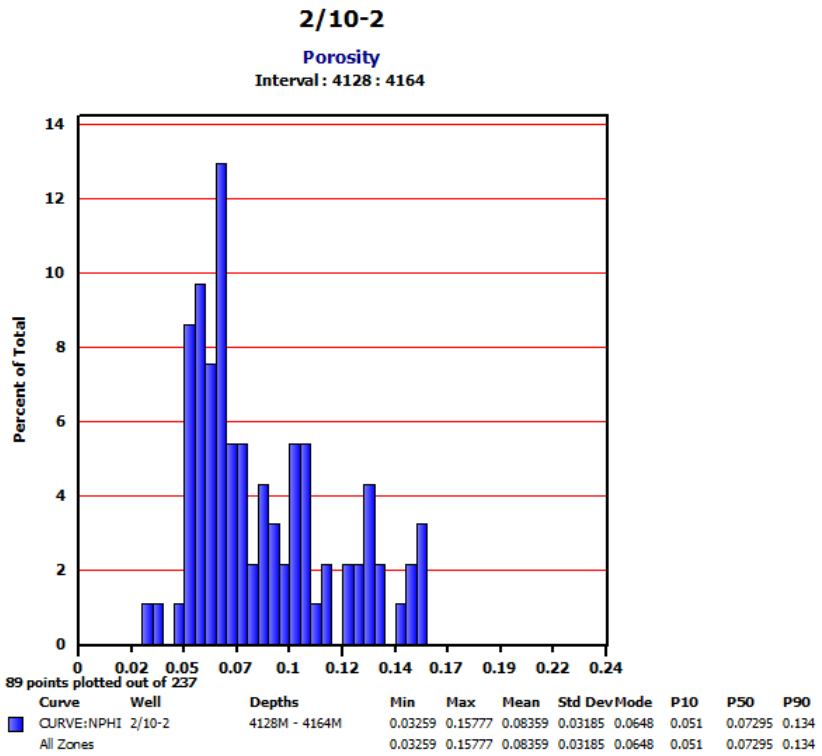

Figure 5.4 Porosity (%) distribution histogram of sandstone (GR < 60API) for well 2/10-2. Also showing mean porosity as 8.3%.

Figures (5.5 and 5.6) show two other cross plots from well 2/10-2 between density and gamma ray color coded with neutron porosity for the interval 4128m-4164m. Note that gamma ray cutoff value 60 API is applied to separate the claystone part from sandstone. The sandstone interval has average density about 2.58 g/cc (Figure 5.7), low porosity and low gamma ray values. Another cross plot between P-wave and density color coded with depth (Figure 5.8) clearly shows that the interval 4128m-4164m has relatively high P-wave velocity about 4500 m/s as compared to the interval 4769m-4850m in well 1/3-5 that has P-wave velocity about 3500 m/s, this indicates that the interval is low porosity and high density sandstone.

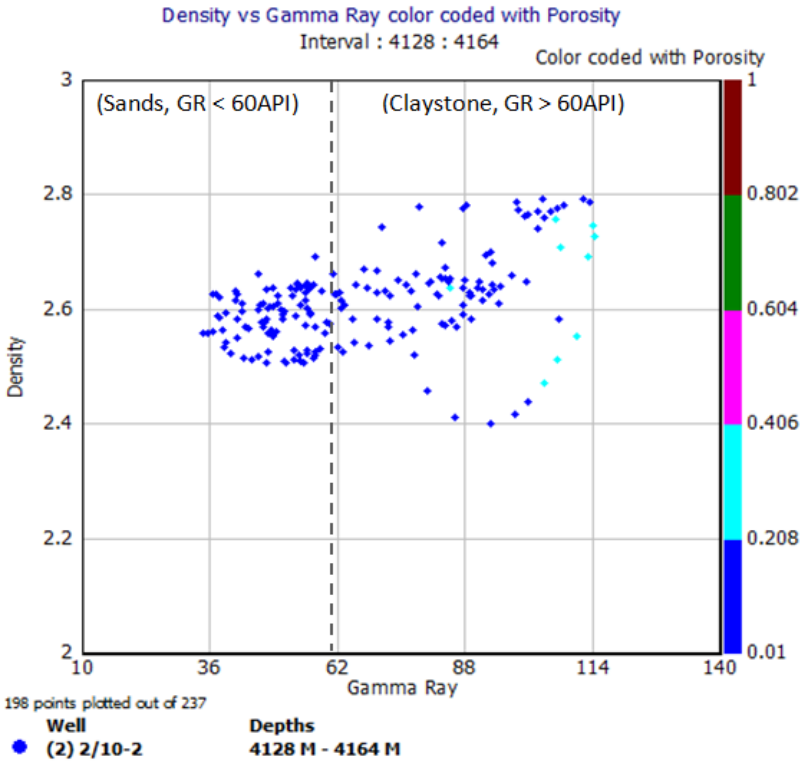

Figure 5.5 Cross plot between Density (g/cc) and Gamma Ray (API) color coded with Porosity (%) of well 2/10-2.

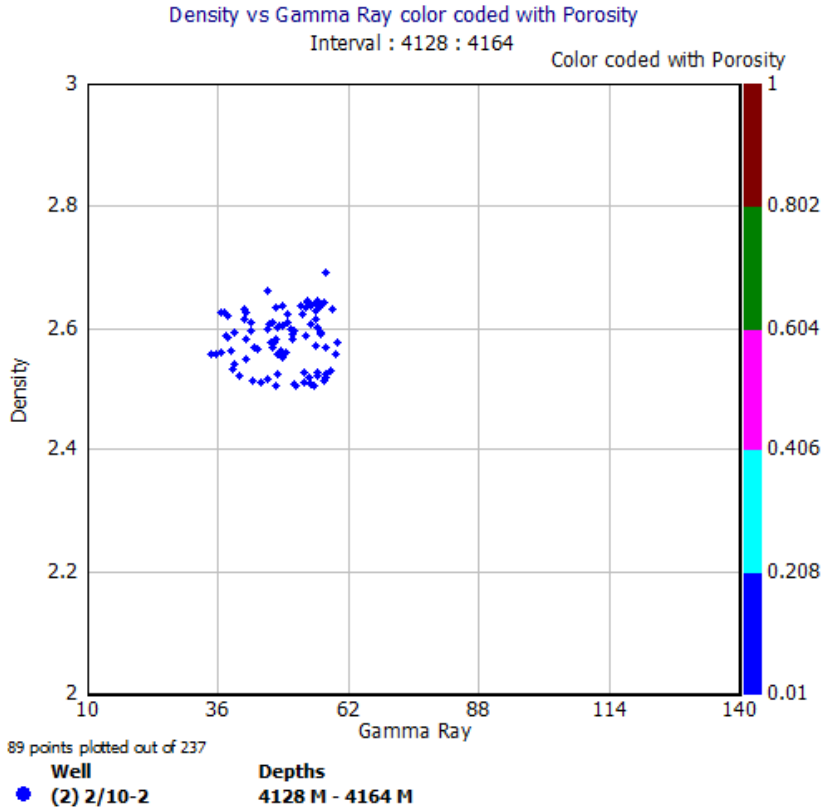

Figure 5.6 Cross plot between Density (g/cc) and Gamma Ray (API) color coded with Porosity (%) showing only sandstone (GR < 60API) in well 2/10-2.

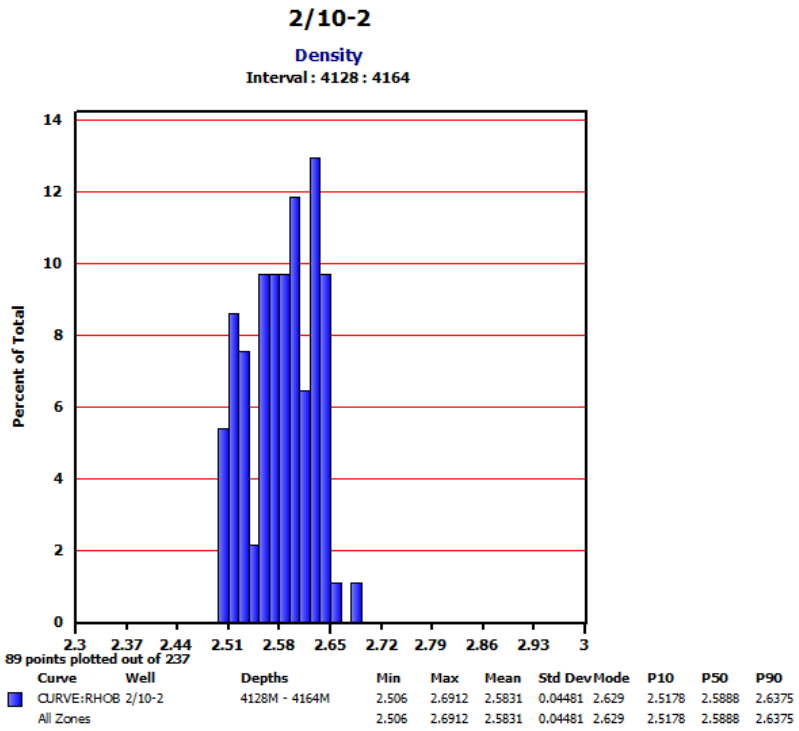

Figure 5.7 Histogram showing density (g/cc) distribution in sandstone (GR < 60API) of well 2/10-2. Also showing mean density 2.58 g/cc.

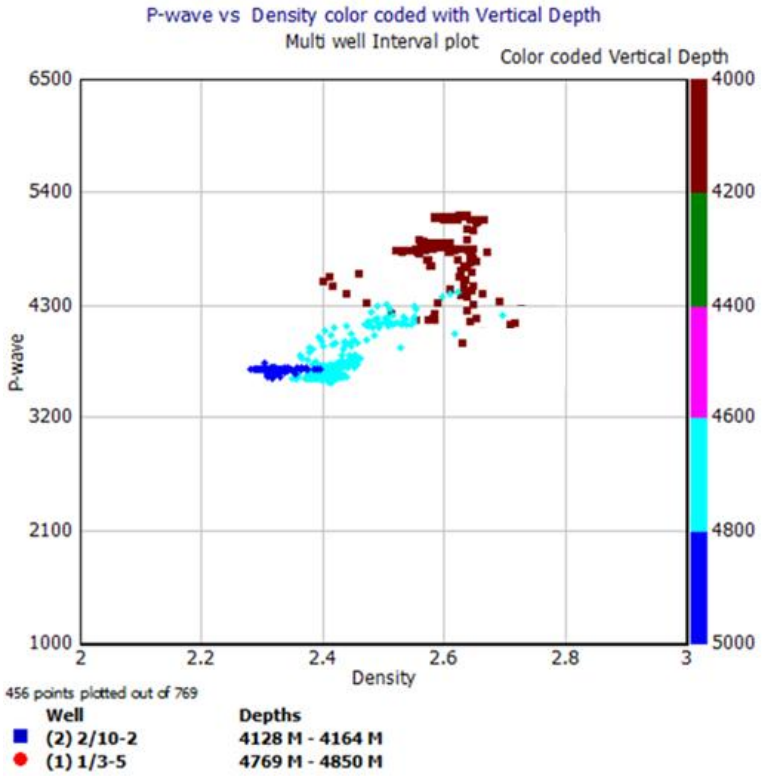

Figure 5.8 Cross plot between P-wave (m/s) and Density (g/cc) color coded with Depth (m), showing only sandstones (GR < 60API) from wells 2/10-2 and 1/3-5.

The cross plot (Figure 5.9) for well 1/3-5 shows that the sandstone interval 4769m-4850m has low gamma ray value from 35 API to 50 API. The sandstone interval has average density about 2.39 g/cc (Figure 5.10) and has more porosity. Note that a cross plot between P-wave and density color coded with depth (Figure 5.8) shows that the interval 4769m-4850m has low P-wave velocity about 3500 m/s as compared to the interval 4128m-4164m in well 2/10-2 that has P-wave velocity about 4500 m/s, this indicates that the interval is porous and low density sandstone.

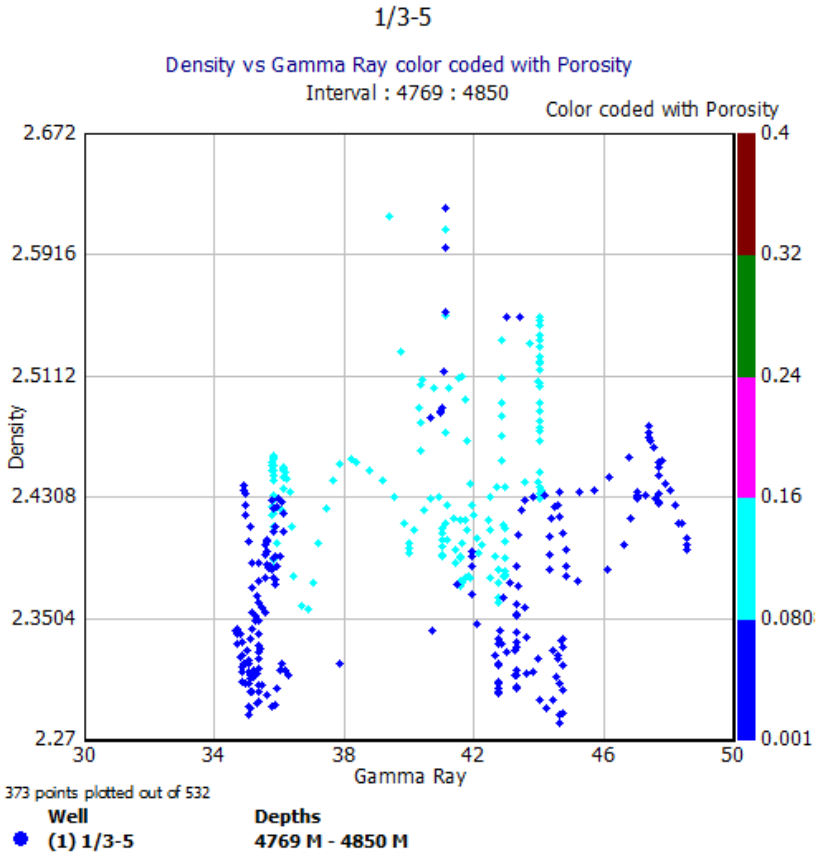

Figure 5.9 Cross plot between Density (g/cc) and Gamma Ray (API) color coded with Porosity (%), showing sandstone (GR < 60API) in well 1/3-5.

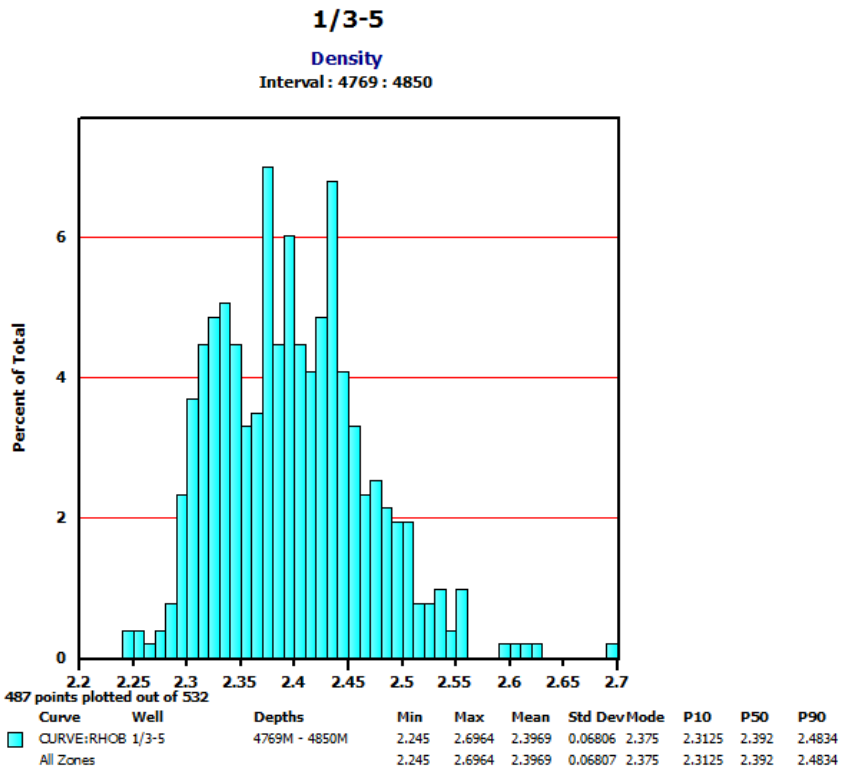

Figure 5.10 Histogram showing density (g/cc) distribution in sandstone (GR < 60API) of well 1/3-5. Also showing mean density 2.39 g/cc.

Chapter 6
PETROGRAPHIC ANALYSIS

6.1 Optical microscopy

A petrographic and mineralogical analysis has been performed on the sandstone samples to find out any kind of relationship between mineralogy and the preserved porosity of sandstone. The purpose of this analysis is to investigate the reason behind the well preserved porosity in the sandstone samples at this depth. The main focus has been on the presence of grain coating, which is later on analyzed under the scanning electron microscope (SEM). The effect of grain composition, grain size and sorting on porosity is also determined by thin section analysis.

All 10 thin sections of Rotliegend Sandstone from wells 2/10-2 and 1/3-5 have been point counted under a polarizing microscope to get information about the composition and the porosity of the sandstone. Thin section analysis includes point counting results, estimation of sorting, calculation of IGV, petrographic classification and provenance studies.

6.1.1 Results

6.1.1.1 Point counts

The point counting is performed on all 10 samples to get a quantitative analysis of sandstone quality and composition. Figure 6.1 shows the results from the point counting.

Table 6.1 Results from point counting analysis, divided into corresponding wells.

Formation	Well	Depth (mRKB)	Rock composition			Matrix	Authigenic Clays	Iron Oxide	Cement		Total Porosity	IGV
			Qtz.	Flds.	Lith. Frag.				Quartz	Carbonate		
Rotliegend Sandstone	2/10-2	4152.60	47	4.3	5	7.6	17.6	0	0.3	14.6	3.6	43.7
		4157.60	51	1.4	3	1	13	0	0	22	8.6	44.6
		4159.20	49.3	1.4	2	2	14.3	0	0	21	11	48.3
		4159.70	48.6	2.3	3	1	24	0	0.6	18.3	2.2	46.1
		4160.20	50.3	1.6	5	6.6	26	0	0	9.6	0.9	43.1
		4163.20	36.6	7	4.3	3	19.3	0	0	8.3	21.5	52.1
	1/3-5	4807.50	58	7.3	2.6	0	7	2.5	2	4	16.6	32.1
		4809.50	60.6	5	5.3	1	10	3.3	1.3	2.5	11	29.1
		4812.60	59.6	5.9	4.3	0	9	3.6	3	3.3	12.2	30.2
		4813.60	53.6	8.7	6.5	0	7	5.6	1	0.6	18	31.2

6.1.1.1.1 Point count results

In figures (6.2a, b) point count results of all 10 samples are presented based on parameters; detrital quartz, matrix, authigenic clays, iron oxide, quartz cement, carbonate cement and porosity. Some amounts of carbonate cement and authigenic clays are found in the samples from well 2/10-2, while samples from well 1/3-5 have high amounts of detrital grains and correspondingly low carbonate cement and authigenic clay contents.

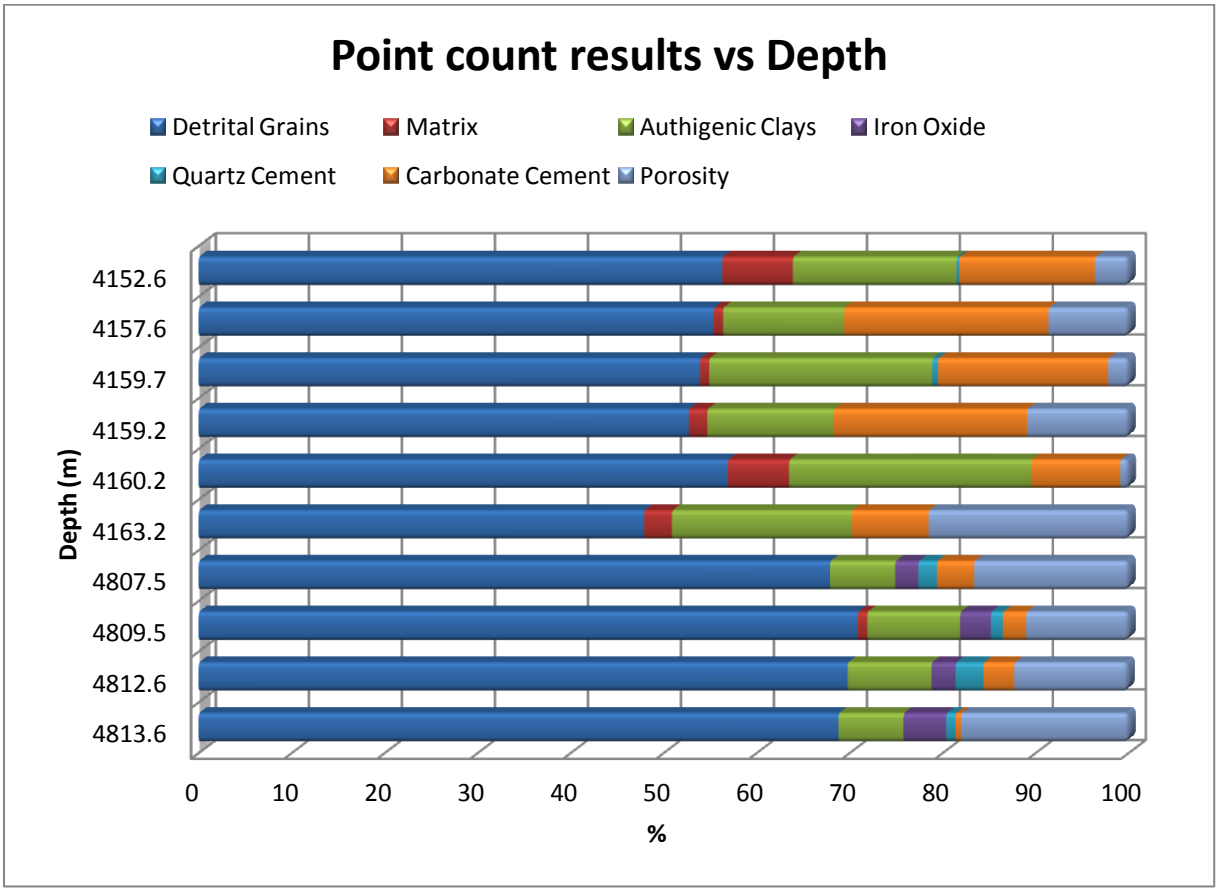

Figure 6.2a Point counting results displayed corresponding to parameters against depth.

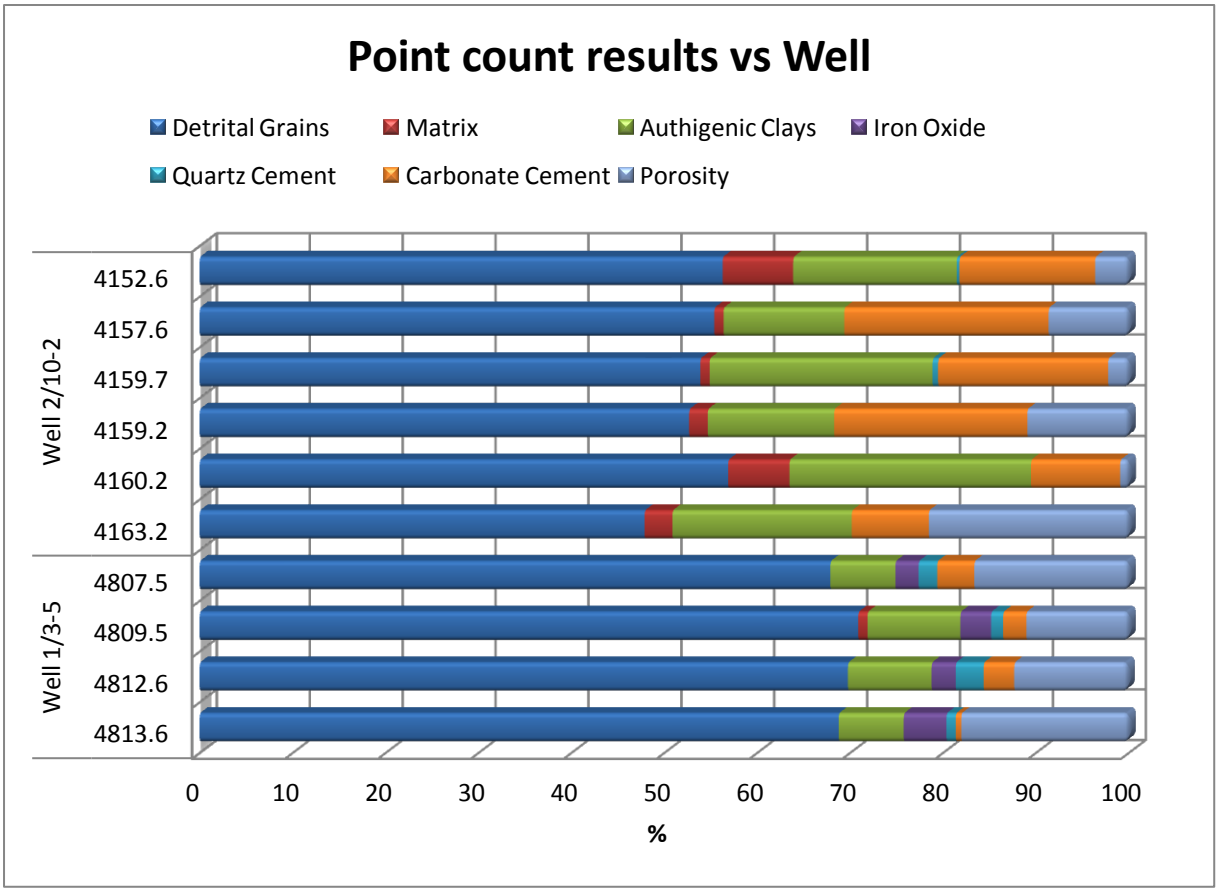

Figure 6.2b Point counting results displayed corresponding to parameters against well.

6.1.1.1.2 Petrographic classification

The point count results have further been used to find out sandstone composition by dividing it into three components; quartz, feldspar and rock fragments, and plotting them on a petrographic classification diagram (Figure 6.3). All the samples from Rotliegend sandstone contain an ample amount of detrital quartz and less than 10% of fine grained matrix and thus fall within the definition of arenites. The entire samples plot within Pettijohn (1975) defined arenites area (Figure 6.3). According to Adams et al. (1986), sandstones containing more than 95% quartz are considered mineralogically mature. This is confirmed by the thin section analysis (6.2.2), which shows that most of the samples fall between texturally sub-mature to mature as defined by Folk (1951).

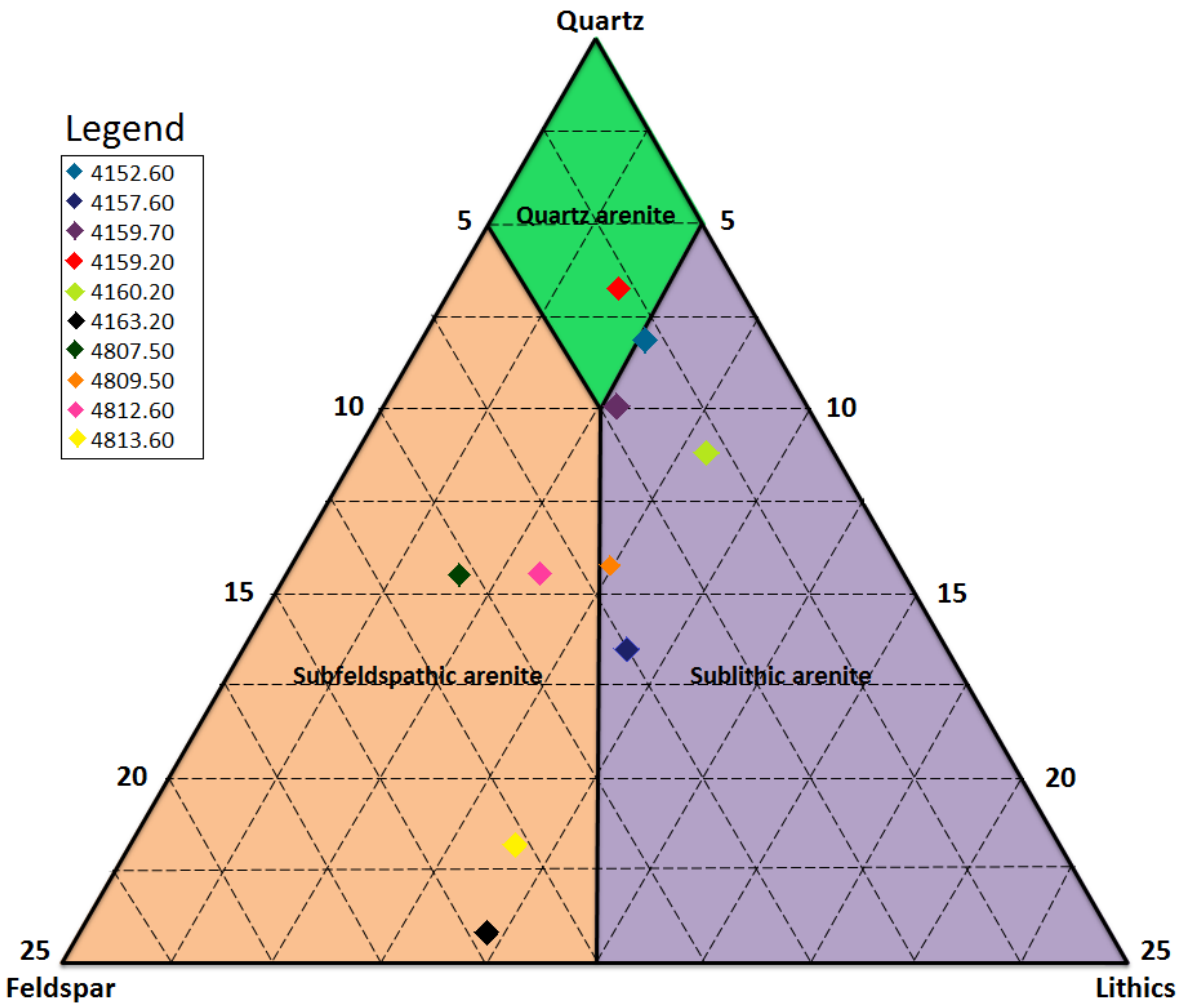

Figure 6.3 Petrographic classification of arenites (Pettijohn 1975). All the samples have been plotted and color-coded according to their depth.

6.1.1.1.3 Provenance studies

The detrital composition of the clastic rocks is significantly related to the tectonic settings of their source area (Miall 2000). Two ternary diagrams (QFL and QmFLt) are used to demonstrate the detritus provenance (Dickinson 1985). The plot of the composition of all 10 samples from Rotliegend sandstone shows provenance from a cratonic interior (Figures 6.4 and 6.5). The mineralogy is typical of continental settings (Glennie 1972; Heeremans et al. 2004).

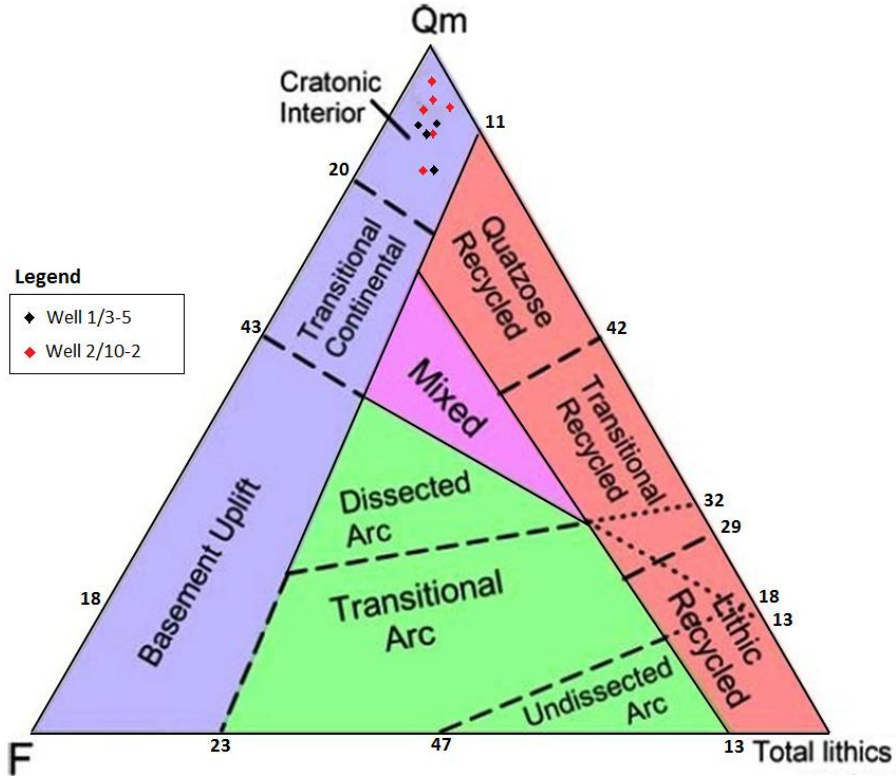

Figure 6.4 Interpretation of sandstone composition and provenance from the petrography of sandstone shows a cratonic interior provenance (Dickinson 1985).

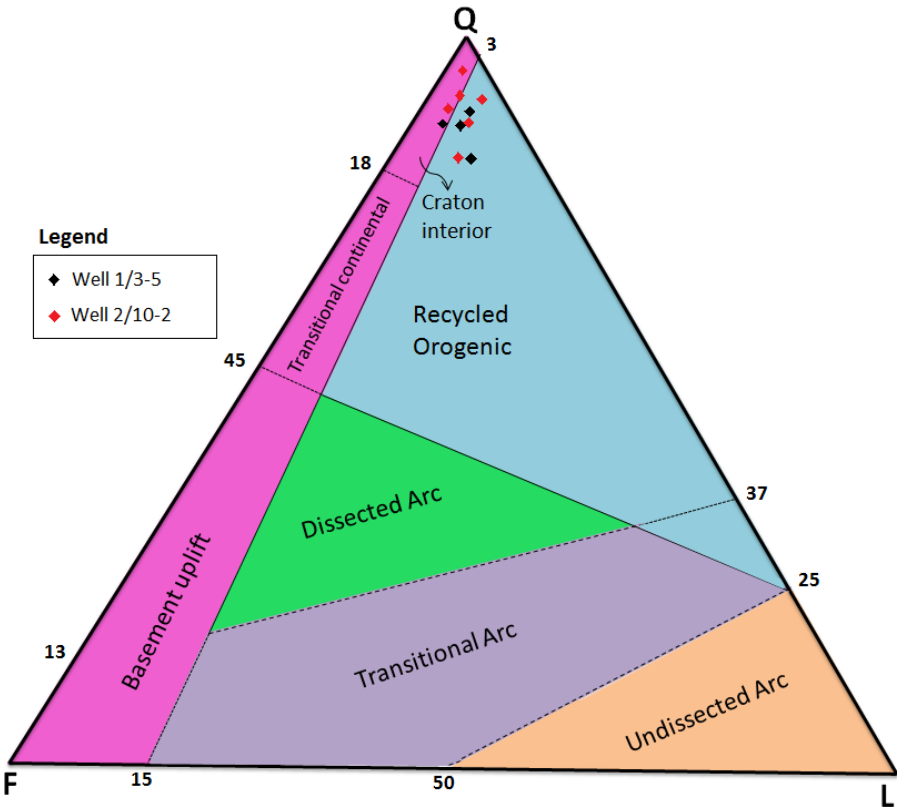

Figure 6.5 The detrital mineral composition plot shows cratonic interior or recycled orogenic source of Rotliegend sandstone (Dickinson 1985).

6.1.1.1.4 Total porosity

The total porosity is one of the parameters in point counting and represents the porosity in the samples. Since the secondary porosity is observed to be negligible in point counting, so total porosity is used for both primary and secondary porosities. The histogram gives the overview of highly varying porosity values (Figure 6.6a, b). The porosity counts vary from 0.9% to 21.5%. By calculating the mean porosity of Rotliegend sandstone in both the wells (Table 6.2), it is evident that over all porosity in well 1/3-5 is higher than that of in well 2/10-2; mean porosities are 14.45% and 7.69% respectively. The samples from 4163.2 m and 4813.6 m are highly porous. The sample from depth 4160.2 m contains low porosity.

Table 6.2 Calculated mean counted percentage of total porosity for each well.

Mean Porosities (%)									
Rotliegend Sandstone									
Well 2/10-2						**Well 1/3-5**			
7.69						14.45			
4152.6	4157.6	4159.2	4159.7	4160.2	4163.2	4807.5	4809.5	4812.6	4813.6
3.6	8.6	2.2	11	0.9	21.5	16.6	11	12.2	18

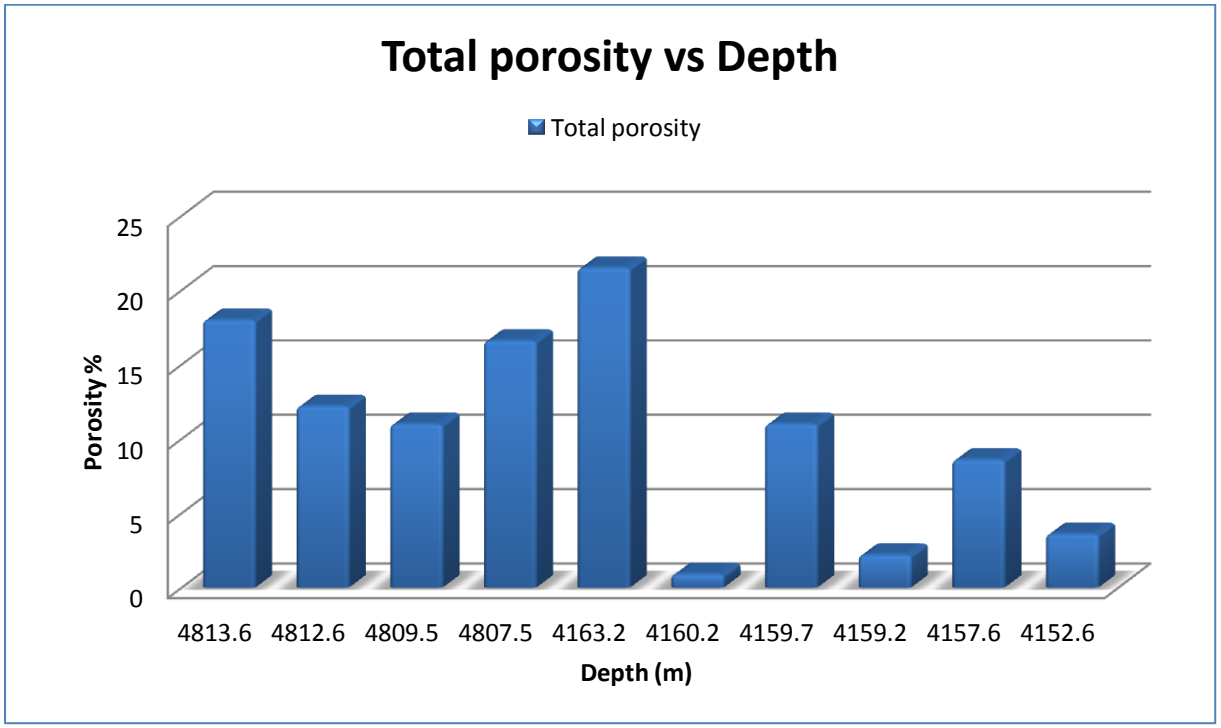

Figure 6.6a Histogram of the counted percentage for total porosity against depth.

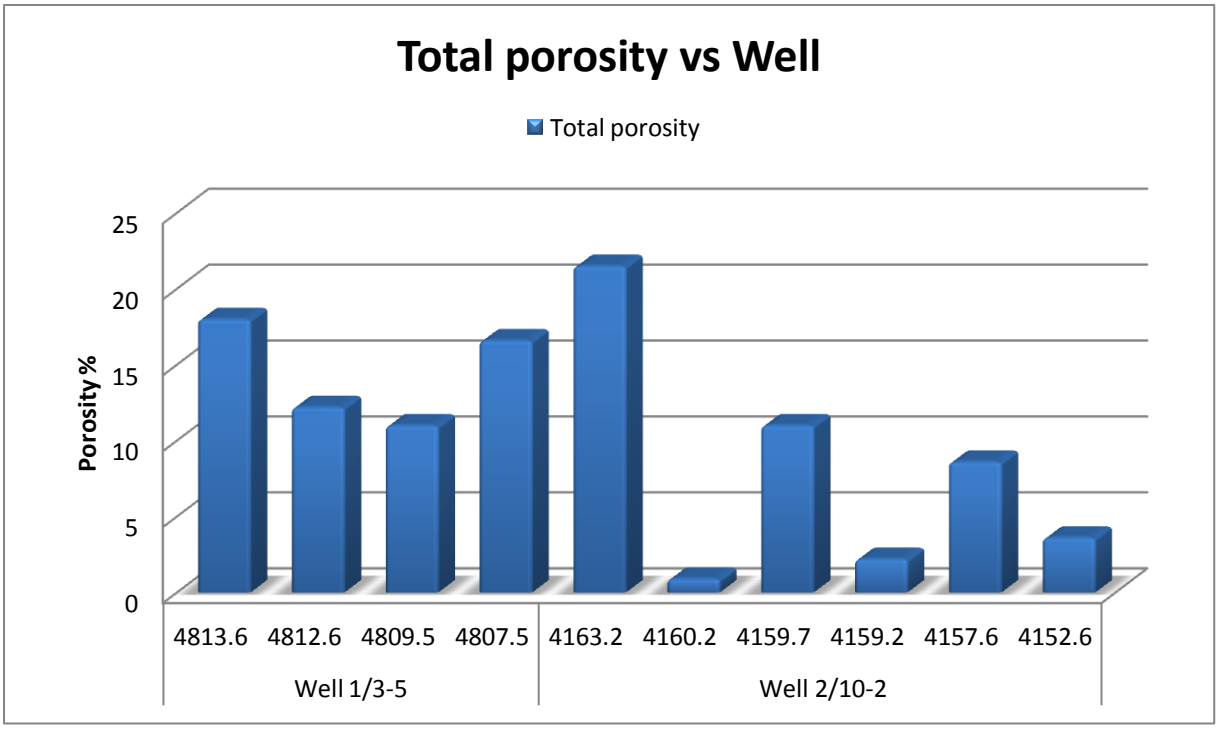

Figure 6.6b Histogram of the counted percentage for total porosity against wells.

Low porosity is often related to advanced diagenesis of sandstone. At great depths the quartz cementation mainly causes porosity reduction. The counted percentages of porosity and quartz cement are displayed together in Figure 6.7a to see if any relationship existed within these samples. Quartz cementation is very less, and histogram shows that highest porosity value is present in shallow sample while highest quartz cementation percentages are found in deep samples (Figure 6.7a). And there is also a coupled relationship between these two parameters; in some samples with high porosity the quartz cementation is very low and vice versa.

The samples from 4163.2 m and 4813.6 m are highly porous and have very low quartz cementation. The sample from depth 4160.2 m is very low in both quartz cementation and porosity.

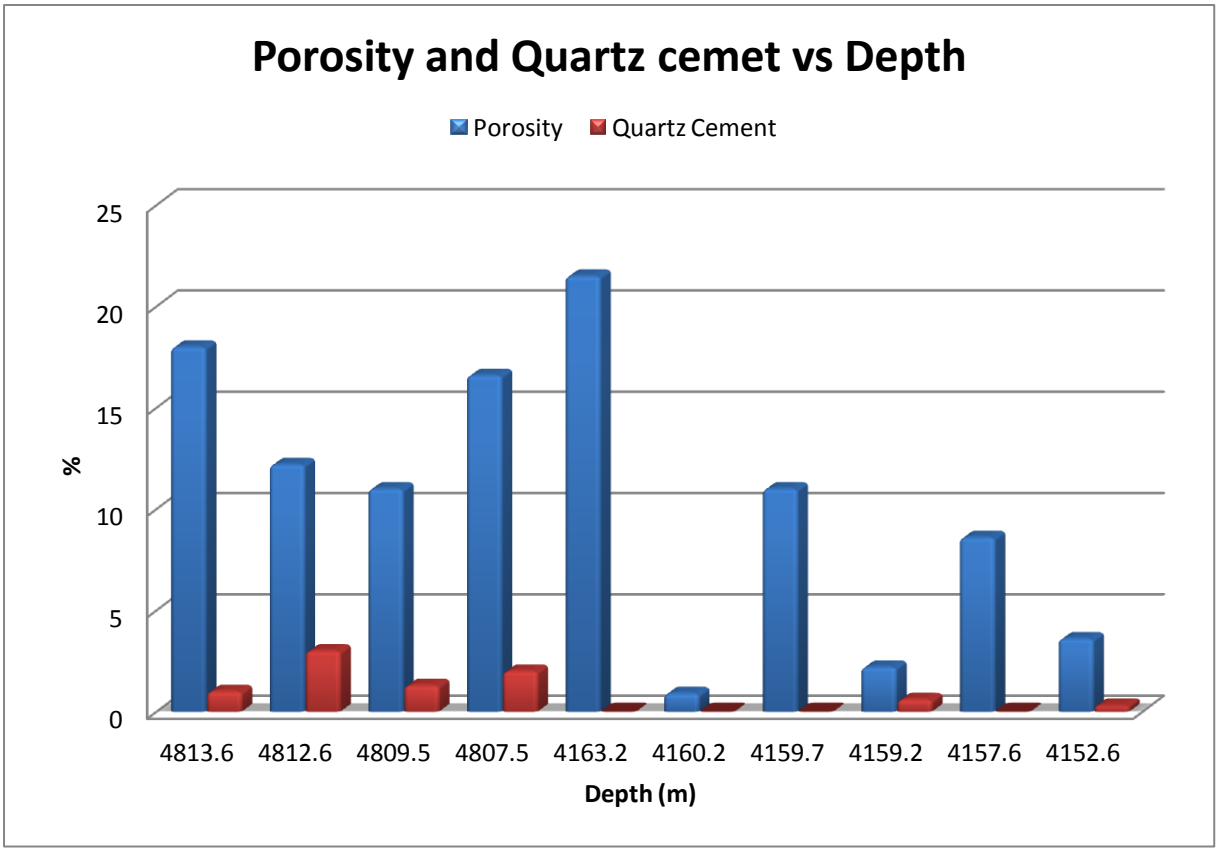

Figure 6.7a Histogram with the comparison of porosity and quartz cement, arranged by increasing depth.

As the same parameters are arranged according to wells, it is evident that although quartz cementation is not much but still it has an effect on porosity and samples that contain the least quartz cementation have high porosity. The samples from well 1/3-5 have more quartz cementation than that of well 2/10-2 (Figure 6.7b). The sample at depth 4163.2 m from well 2/10-2 contains no quartz cement and has highest porosity.

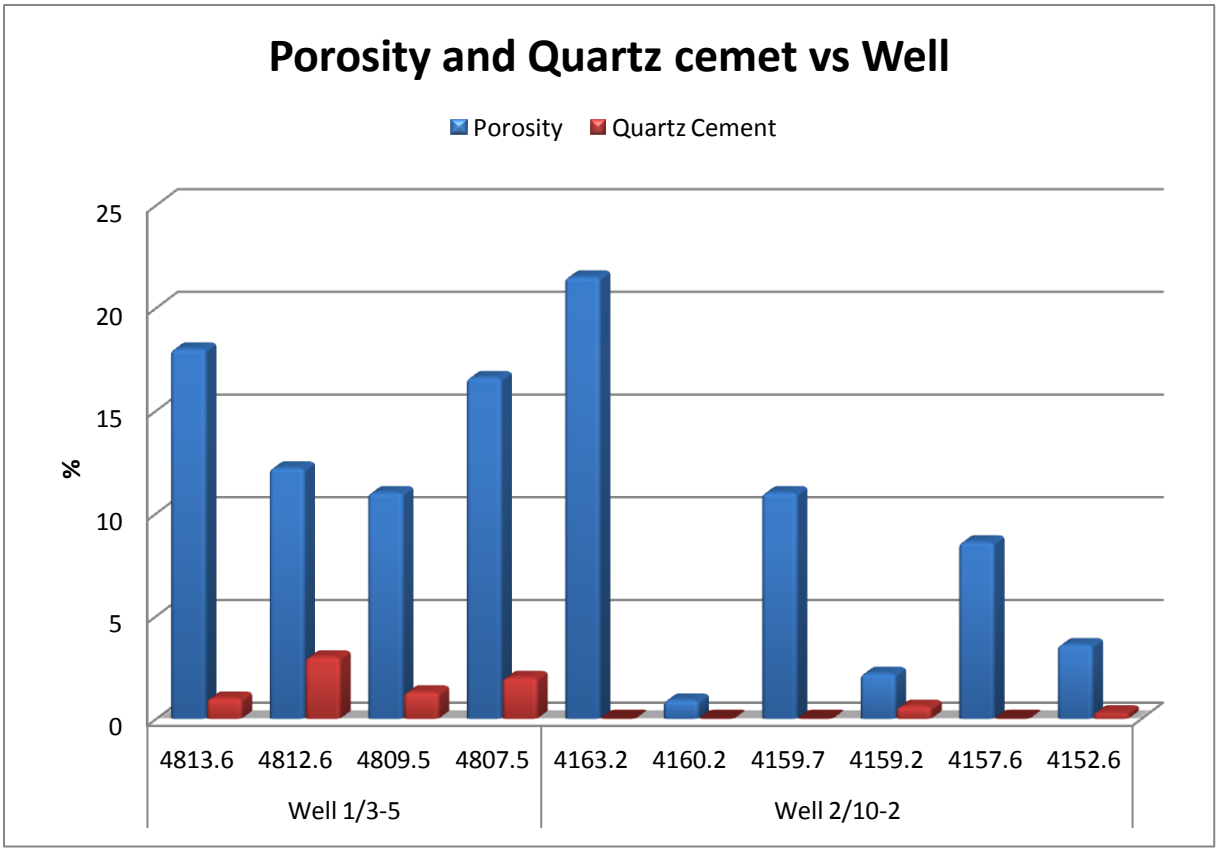

Figure 6.7b Histogram with the comparison of porosity and quartz cement, arranged by wells.

6.1.1.1.5 Authigenic clays

According to Bjørlykke (1998), authigenic clays can also give a clue about the diagenesis that sandstone has gone through. During the point counting analysis authigenic clays and feldspar content have been point counted. Feldspar is point counted as a whole irrespective of its types. Later on, SEM analysis has confirmed most of the feldspar as K-feldspar.

Authigenic clays in all the samples are mostly present as grain coating but some of the clays are also present in pore spaces causing porosity reduction. The counted percentages of authigenic clays (Table 6.3) and porosity are displayed together in histogram (Figure 6.8a, b) to see if there is any coupled relationship within these samples.

The counted percentages of porosity and authigenic clays are displayed together in Figure 6.8a to see if there is any relationship within these samples. Amounts of authigenic have been observed more in samples from well 2/10-2 than in samples from well 1/3-5. Later on from SEM analysis it was revealed that samples from well 2/10-2 contained authigenic clays as

both pore-filling kaolinite and illite coating while well 1/3-5 only contained illite coating. And there is also a coupled relationship between these two parameters; in some samples with high porosity the authigenic clay content is low and vice versa. The sample from depth 4160.2 m is very low in porosity and very high in authigenic clay content.

Table 6.3 Calculated mean counted percentage of authigenic clays for each well.

Authigenic clays (%)									
Rotliegend Sandstone									
Well 2/10-2						**Well 1/3-5**			
18.86						8.25			
4152.6	4157.6	4159.2	4159.7	4160.2	4163.2	4807.5	4809.5	4812.6	4813.6
17.6	13	13.3	24	26	19.3	7	10	9	7

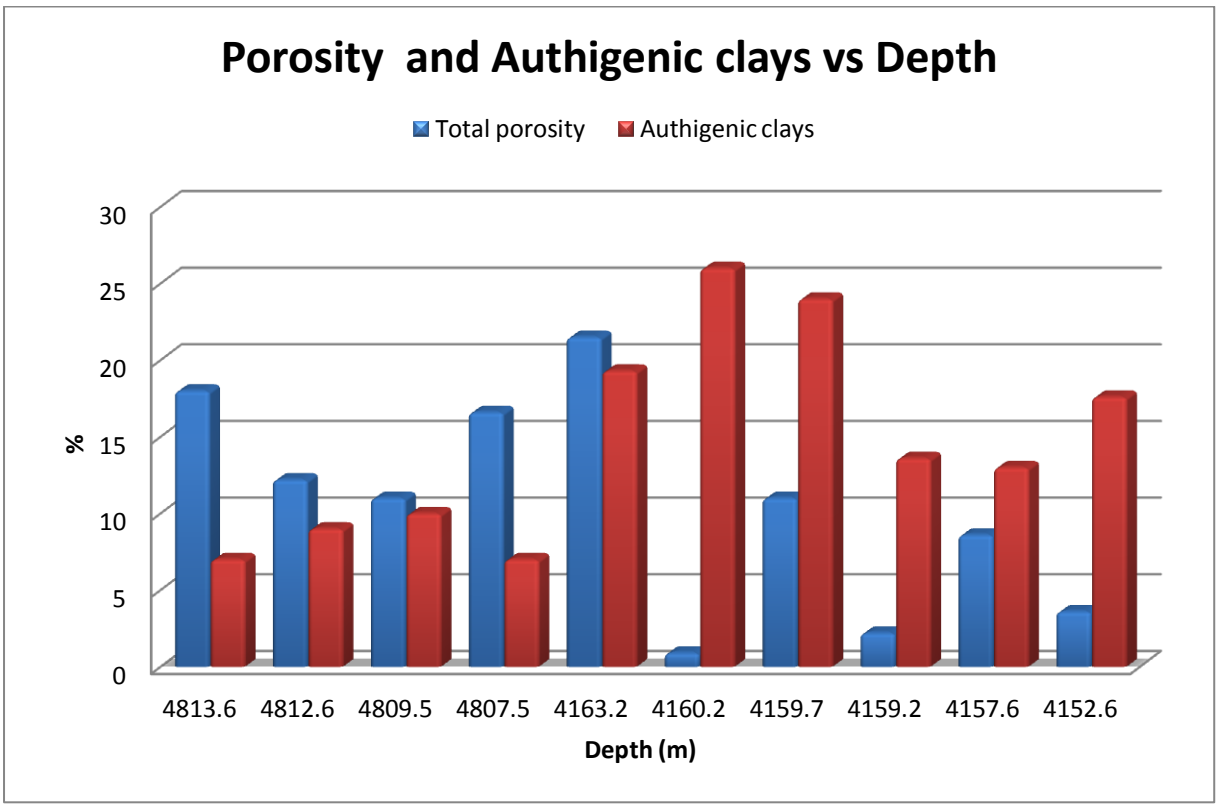

Figure 6.8a Histogram with the comparison of porosity and authigenic clays, arranged by increasing depth.

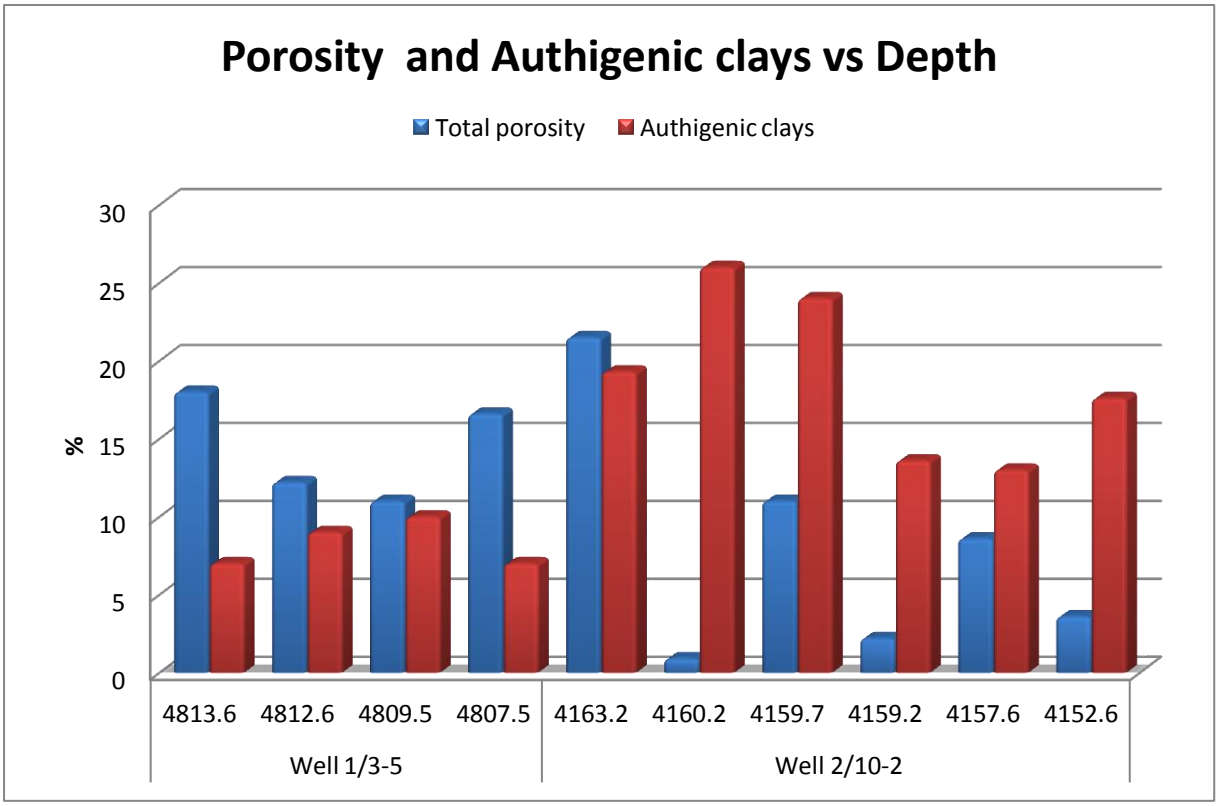

Figure 6.8b Histogram with the comparison of porosity and authigenic clays, arranged by wells.

6.1.1.1.6 Carbonate cement

Carbonate cementation at early diagenesis stages in sandstone can also cause reduction in the primary porosity. Carbonate cement is also one of the parameters in point counting analysis. Irrespective of types, carbonate cement is point counted. But SEM confirmed that most of this carbonate cement is ankerite, dolomite and calcite at places.

The counted percentages of carbonate cement are displayed together with porosity in histogram (Figure 6.9a, b) to see if there is any relationship with in the samples.

Table 6.4 Calculated mean counted percentage of carbonate cement for each well.

Carbonate cement (%)									
Rotliegend Sandstone									
Well 2/10-2						**Well 1/3-5**			
15.63						2.6			
4152.6	4157.6	4159.2	4159.7	4160.2	4163.2	4807.5	4809.5	4812.6	4813.6
14.6	22	20.8	18.3	9.6	8.3	4	2.5	3.3	0.6

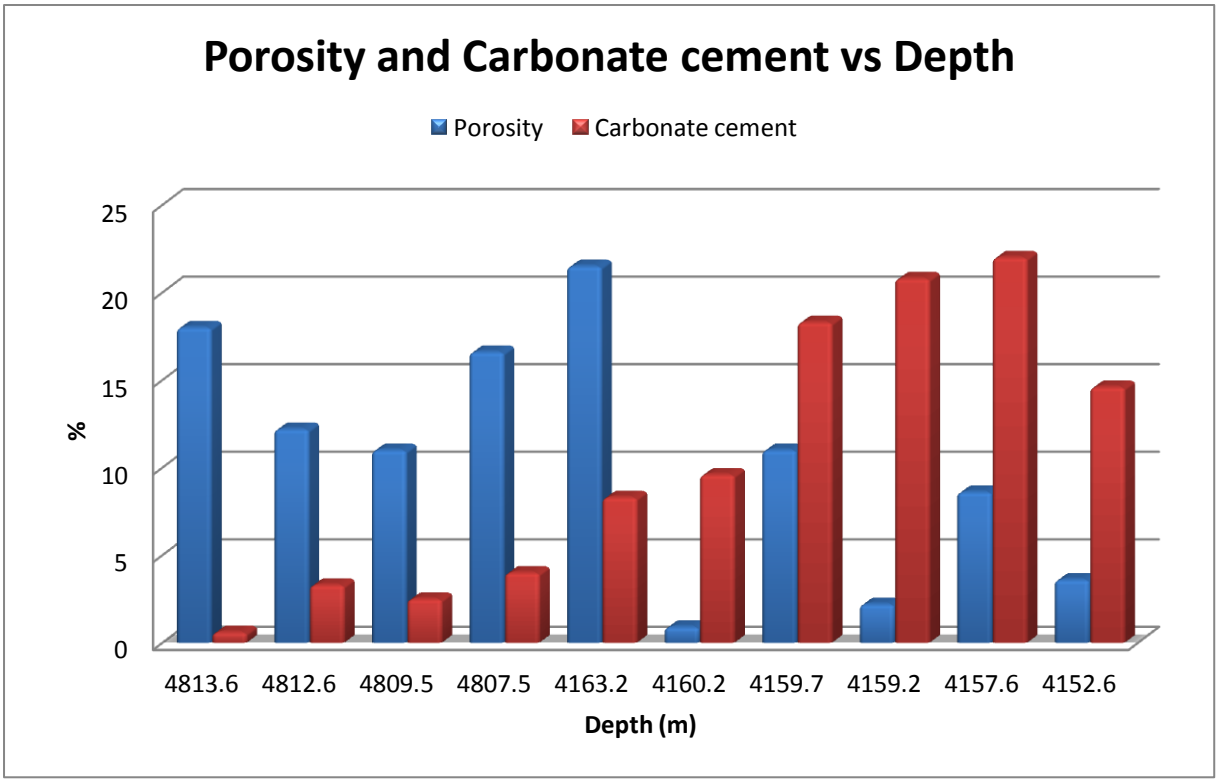

Figure 6.9a Histogram with the comparison of porosity and carbonate cement, arranged by increasing depth.

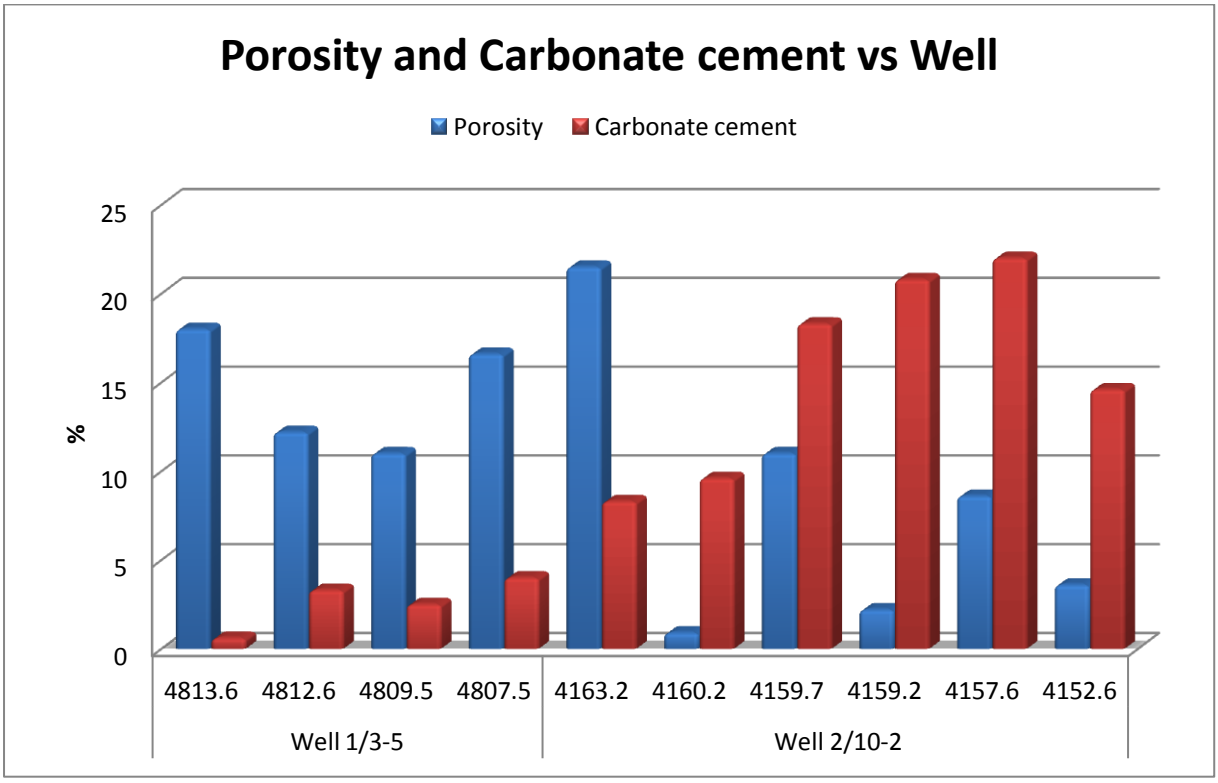

Figure 6.9b Histogram with the comparison of porosity and carbonate cement, arranged by wells.

6.1.1.2 Intergranular volume (IGV)

To get the amount of contribution from compaction and cementation to the porosity loss, the intergranular volume was calculated from the point counting analysis results (*Intergranular Volume (IGV) = cement + depositional matrix + intergranular porosity*).

The intergranular volume values from all samples are arranged separately both according to the depth and wells, and presented in Figures (6.10a, b). The average IGV value for well 2/10-2 is 46.31% and ranges from 43.1% to 52.1%. The reason for high IGV is high amount of early carbonate cement and authigenic clays. Likewise, the average IGV value for well 1/3-5 is 30.65% and varies between 29.1% and 32.1%. The reason for low IGV is that the samples from this well are more mechanically compacted.

Table 6.5 Calculated average IGV for each well.

Average IGV (%)									
Rotliegend Sandstone									
Well 2/10-2						**Well 1/3-5**			
46.1						30.65			
4152.6	4157.6	4159.2	4159.7	4160.2	4163.2	4807.5	4809.5	4812.6	4813.6
43.7	44.6	48.3	46.1	43.1	52.1	32.1	29.1	30.2	31.2

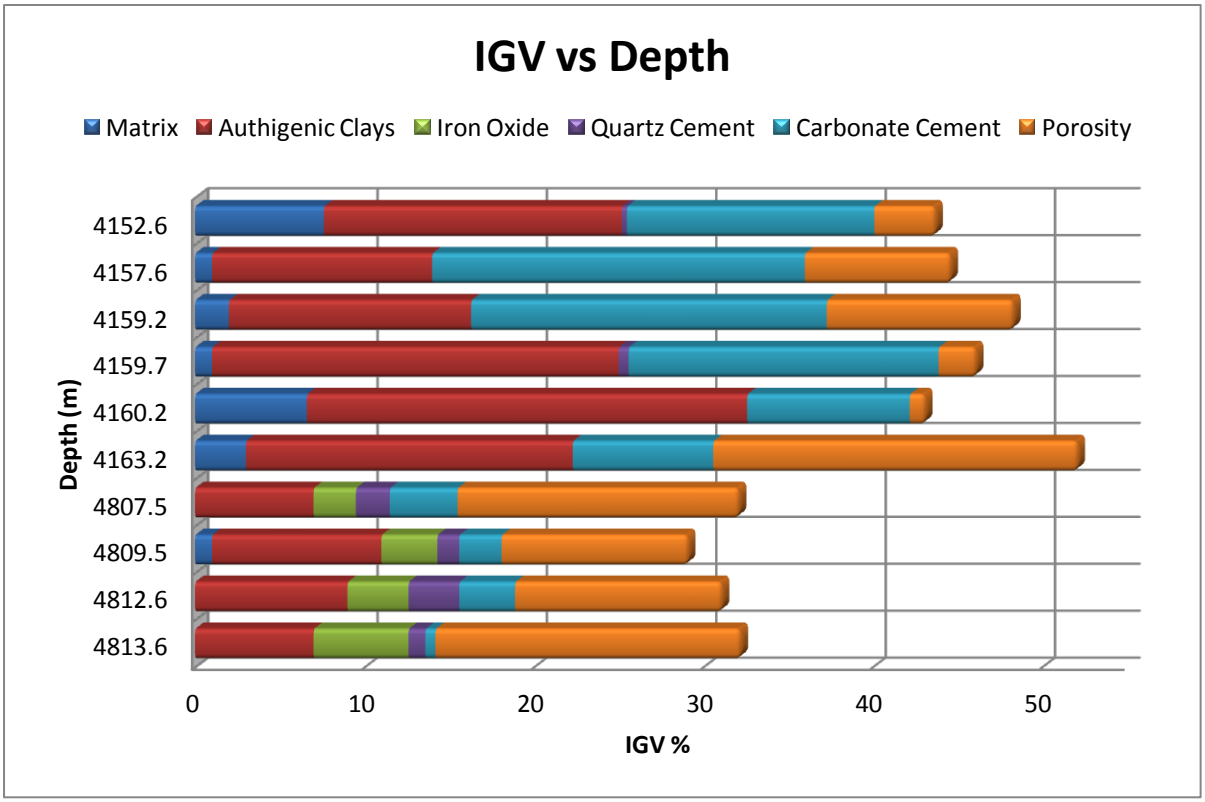

Figure 6.10a Overview of calculated IGV, arranged by increasing depth.

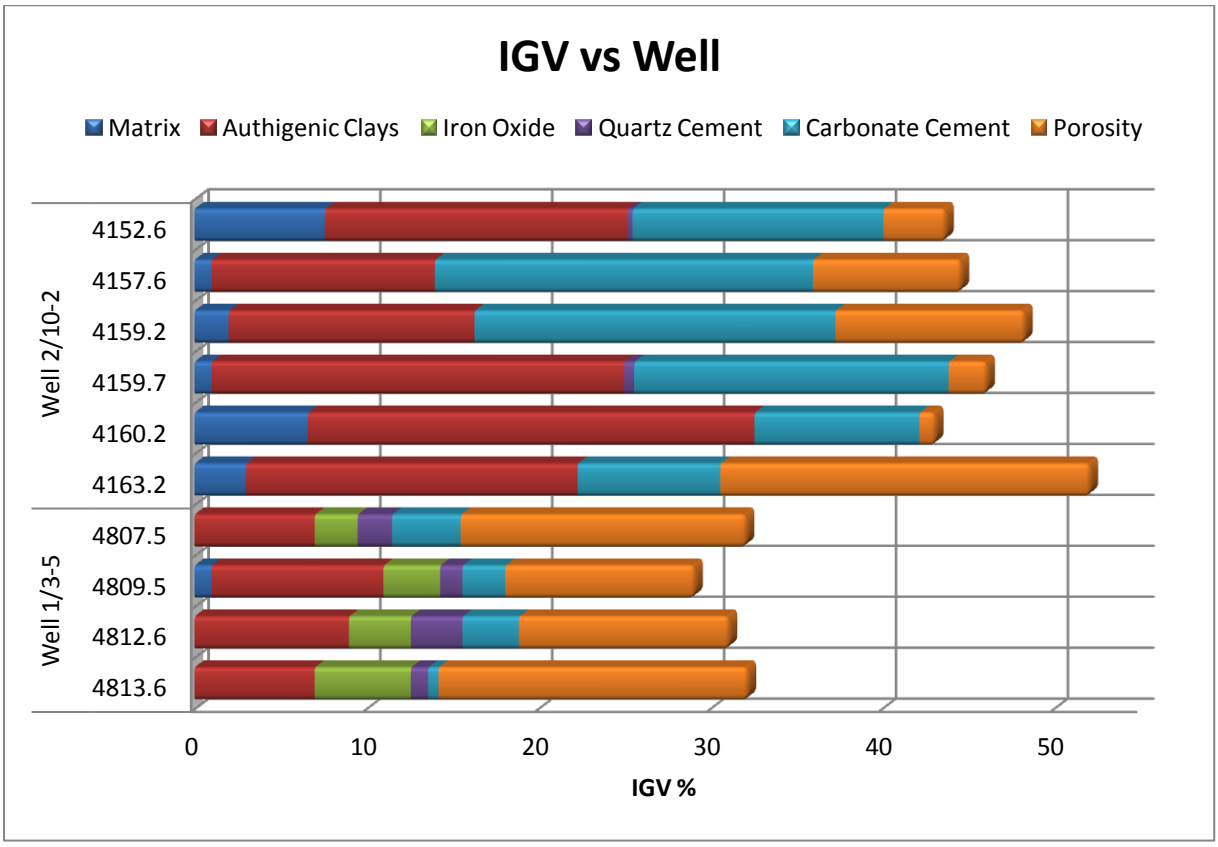

Figure 6.10b Overview of calculated IGV, arranged by wells.

Textural characteristics

A visual appraisement of grain size, shape and sorting was performed on all ten thin sections to see how the mentioned parameters vary within these samples. The result table is presented in appendix B. The analysis has also been done to find out if these parameters had any noticeable effect on calculated intergranular volume (IGV). The same results have been used to determine the maturity of sandstone.

Grain size, shape and sorting are plotted against the calculated IGV in three separate diagrams (Figure 6.11a, b, and c).

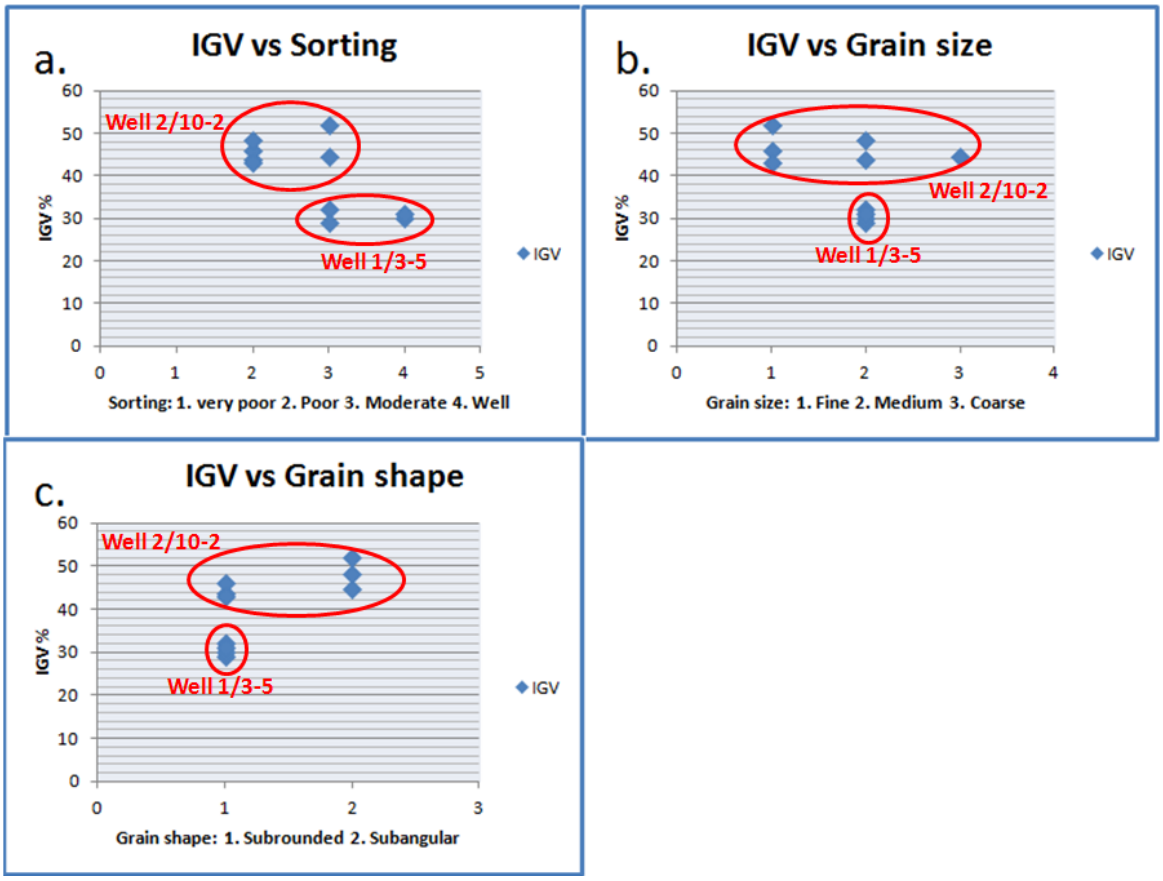

Figure 6.11 a) Diagram shows relationship between degree of sorting and calculated IGV. b) IGV plotted against grain size. c) IGV plotted against grain shape.

Textural maturity

The results of visual estimation of grain size, grain shape and sorting are used to infer the maturity of sandstone.

Table 6.6 Four stages of textural maturity. Revised from Folk (1951).

I. Immature stage	II. Submature stage	III. Mature stage	IV. Supermature stage
Sediments contain considerable clay and fine mica. The grains are poorly sorted and angular.	Sediments contain very little or no clay. The grains are poorly sorted and angular.	Sediments contain no clay and well sorted, but the grains are still subangular.	Sediments contain no clay, is well sorted, and the grains are rounded.

As none of the samples contain that significant amount of detrital clay content so the immature stage can be excluded following the definition of textural maturity by Folk (1951). According to the definition of maturation by Folk (1951) most of the samples from both the wells have subangular to subrounded grains and mostly moderate to well sorted, showing that they are texturally mature.

Detrital matrix

Detrital matrix is one of the parameters counted in point counting analysis. The amount of counted detrital matrix is compared to calculated IGV (Figure 6.12) to find out whether or not a difference in the amount of detrital matrix has any effect on mechanical compaction.

The average amount of detrital matrix from point counted analysis shows that well 2/10-2 has more amount of detrital matrix (Table 6.7) and hence high IGV values, while well 1/3-5 has very low amount of detrital matrix and low IGV values.

Table 6.7 Calculated average amount of detrital matrix for each well.

Amount of detrital matrix (%)									
Rotliegend Sandstone									
Well 2/10-2						**Well 1/3-5**			
3.53						0.25			
4152.6	4157.6	4159.2	4159.7	4160.2	4163.2	4807.5	4809.5	4812.6	4813.6
7.6	1	1	2	6.6	3	0	1	0	0

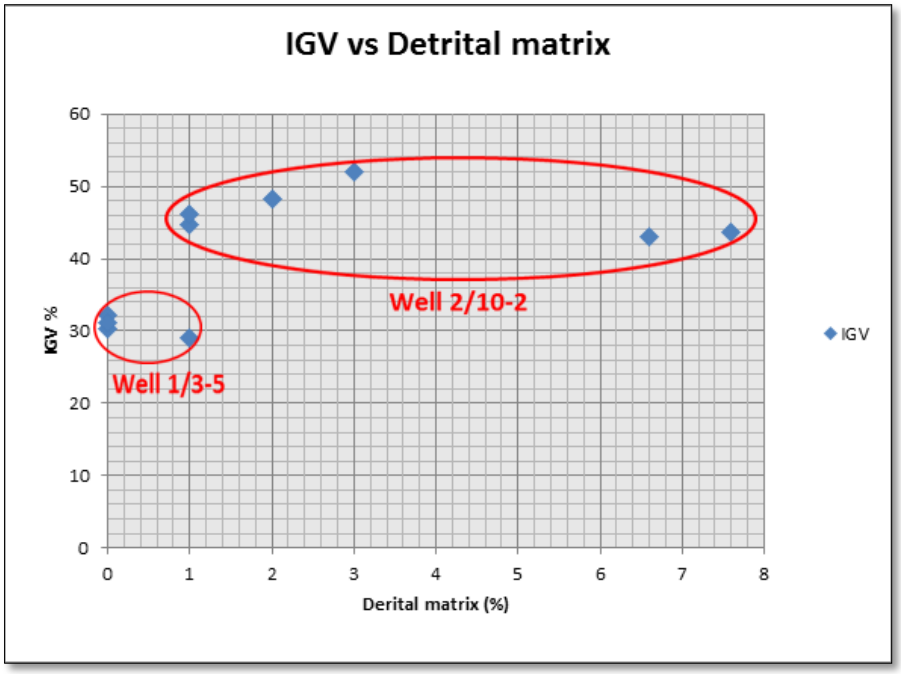

Figure 6.12 IGV plotted against the counted amount of detrital matrix.

Carbonate cement

Amount of carbonate cement from point counting analysis is plotted against the corresponding calculated IGV values (Figure 6.13) to see the effect of carbonate cement on IGV.

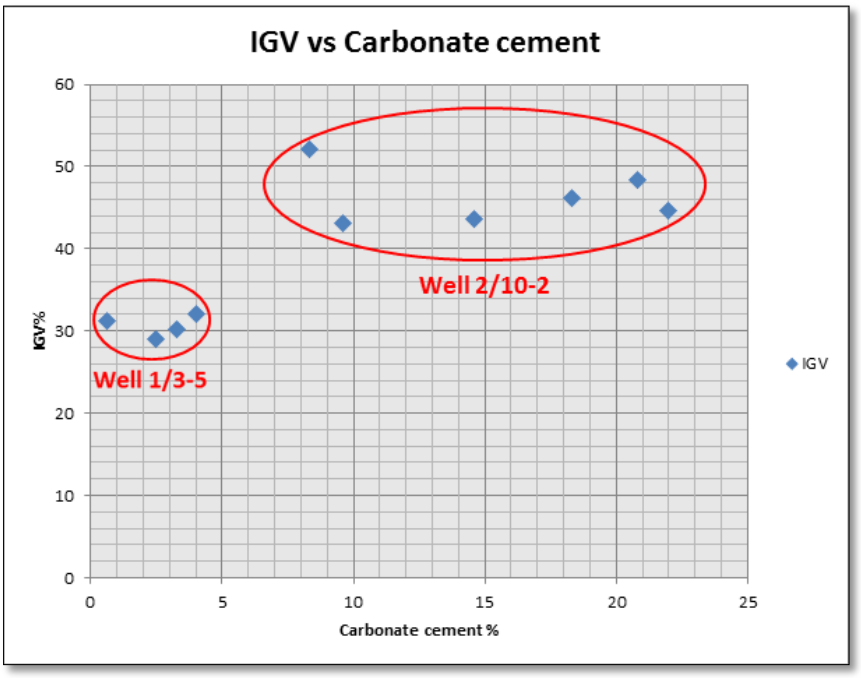

Figure 6.13 IGV plotted against the counted amount of carbonate cement.

Authigenic clays

Amount of authigenic clays from point counting analysis is plotted against the corresponding calculated IGV values (Figure 6.14) to see the effect of authigenic clays on IGV.

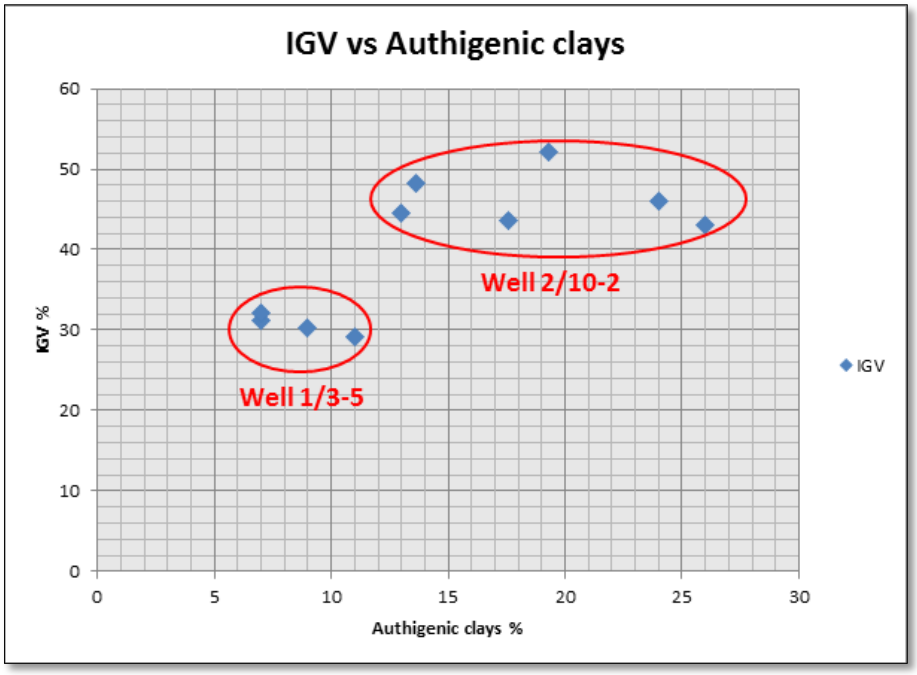

Figure 6.14 IGV plotted against the counted amount of authigenic clays.

Depth

IGV is plotted against the increasing depth to see how it varies with depth.

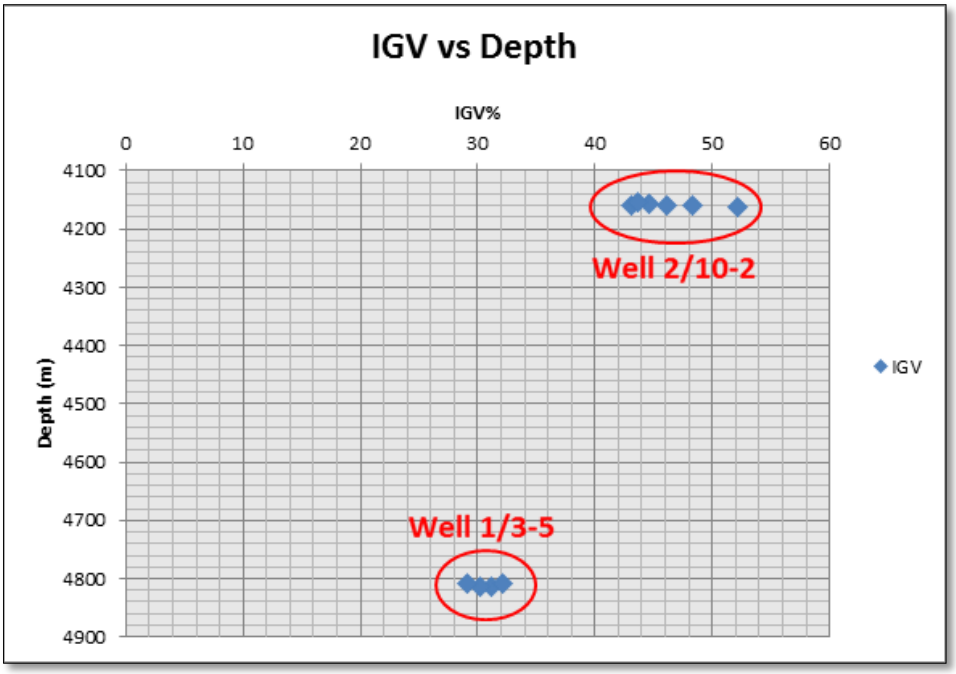

Figure 6.15 IGV plotted against increasing depth.

6.1.1.3 Thin section observations

An optical microscope with an attached camera has been used to take the images of selected thin sections. These images are further used to demonstrate some of the observations made in point count analysis.

Figure 6.16a and b shows the ankerite cement observed in some of the samples from well 2/10-2, here represented by a sample from 4152.60 m. Some samples from well 2/10-2 have shown abundance of pore-filling kaolinite, figure 6.16a and b shows the presence of pore-filling kaolinite from 4163.20 m. The muscovite has been point counted as matrix in most of the samples (Figure 6.17a and b).

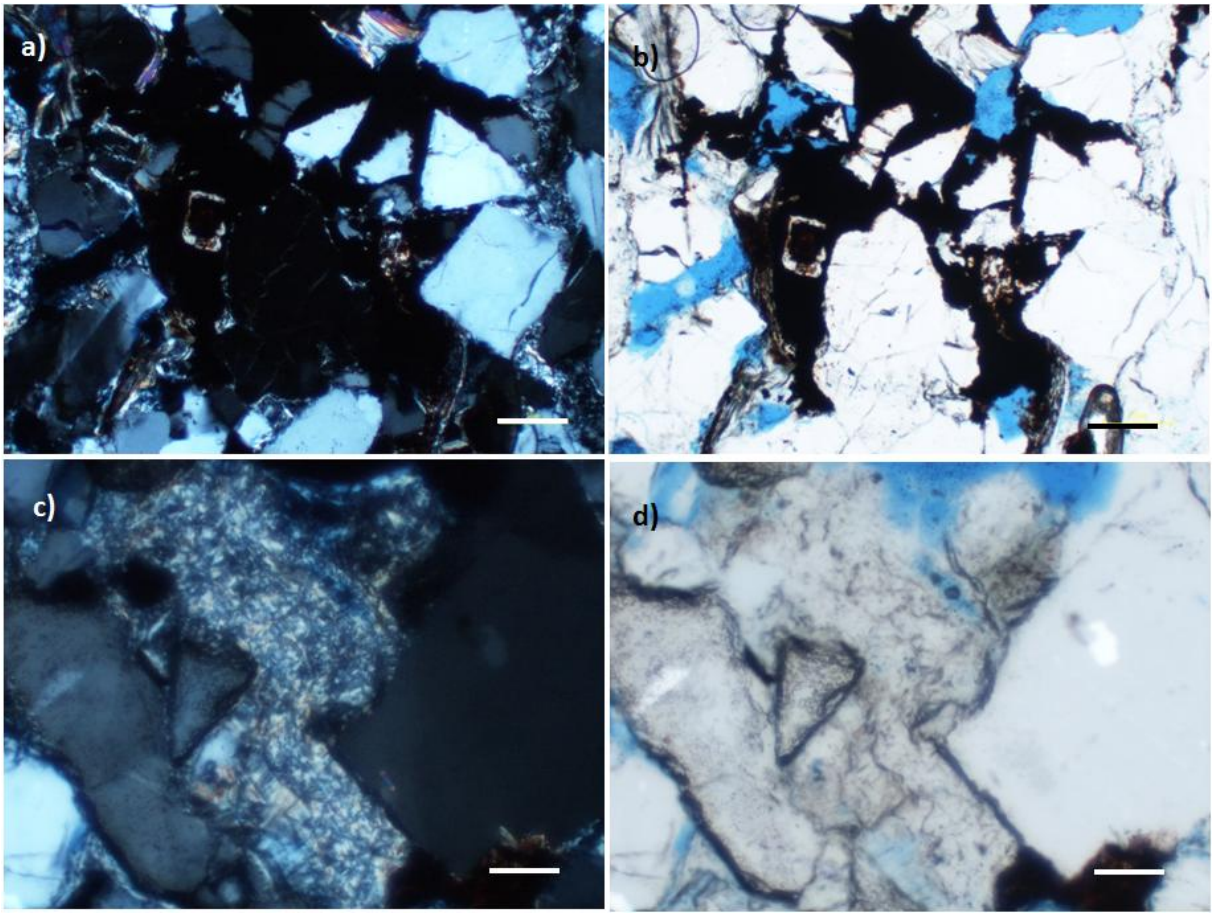

Figure 6.16 Images of thin sections taken in an optical microscope. White scale bar equals 50 µm. a) Amounts of ankerite cement (dark brown) is seen in crossed polars from 4152.60 m (well 2/10-2). b) Same image as in a), taken in plane light. c) Abundance of pore-filling kaolinite is observed in crossed polars from 4163.20 m (well 2/10-2). d) Same image as in c), taken in plane light.

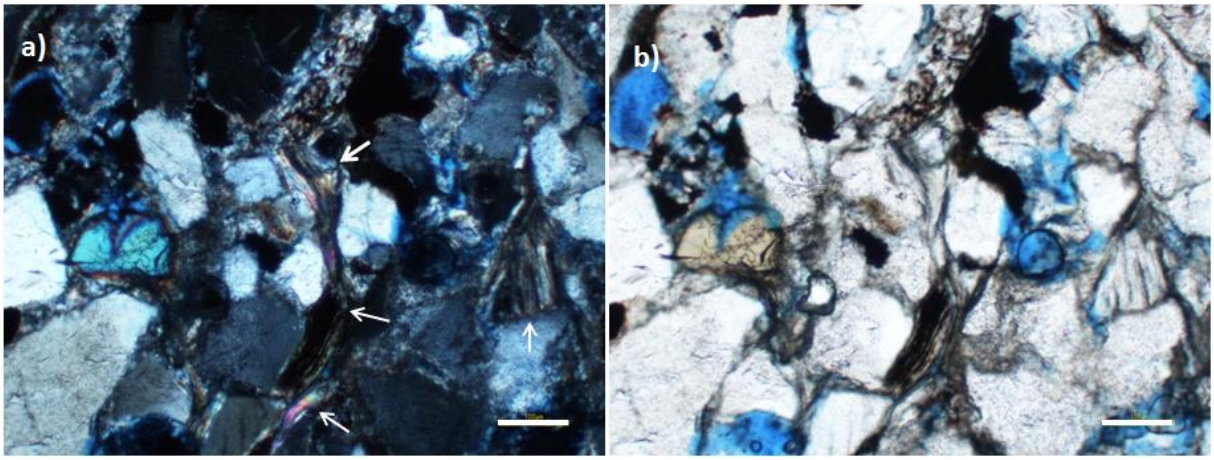

Figure 6.17 Image of a thin section taken in an optical microscope. White scale bar equals 100 µm. a) white arrows showing ductile deformation of muscovite grain as a result of mechanical compaction, from 4152.60 m (well 2/10-2). b) Same image as in a) taken in plane light.

6.2 Scanning electron microscopy (SEM)

All the samples have been further investigated under scanning electron microscope with special emphasis on cementation, authigenic clays, k-feldspar and porosity. The grain coatings are also inspected in detail in sample examination.

6.2.1 Results

6.2.1.1 Grain coatings

Most of the samples have been examined to find out the type of coating and to see how much this coating is covering the grains. Stub mounted samples from well 1/3-5 are investigated with regards to quartz overgrowths and authigenic clay coatings. Whereas, stub mounted samples from well 2/10-2 have been examined with regards to authigenic clay coatings because there is hardly any quartz overgrowth seen both under optical microscope and scanning electron microscope.

In all the 10 samples, most of them showed considerable amounts of coating covering whole grains. Illite with flaky to honey comb appearance is observed as coatings in almost all the samples (Figure 6.18). The rim forming clays surrounding quartz grains have also been identified in SEM analysis which acted as nucleation for authigenic illite (Figure 6.20). Very small amounts of quartz overgrowth are found on detrital quartz grains in the samples from well 1/3-5 and it is observed that these are the specific samples where some of the grains are not fully covered by illite coatings. Most of the stubs are heavily illite coated hence none of them have shown considerable quartz overgrowth (Figure 6.21).

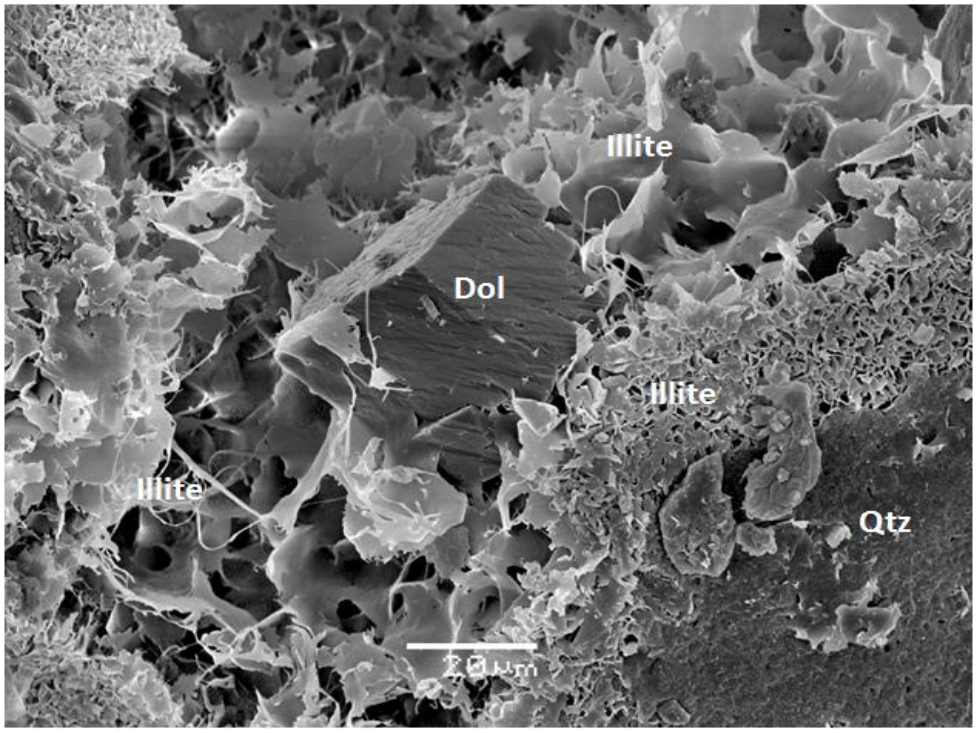

Figure 6.18 A SEM image from 4807.50 m in well 1/3-5 showing a quartz grain is coated with flaky to honey comb illite. A dolomite crystal (Dol) is also peering out of the grain surface.

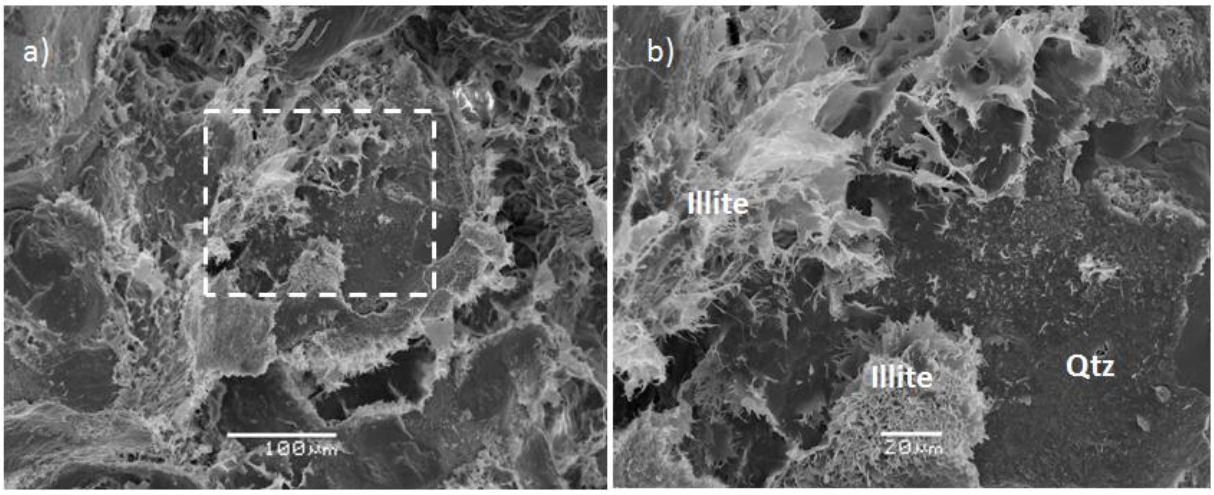

Figure 6.19 a) A SEM image showing quartz grains fully covered with illite coating. b) The close-up showing the part of a illite coated surface of quartz grain leaving no place for quartz cemenation. (The image has been taken from 4812.60 m in well 1/3-5)

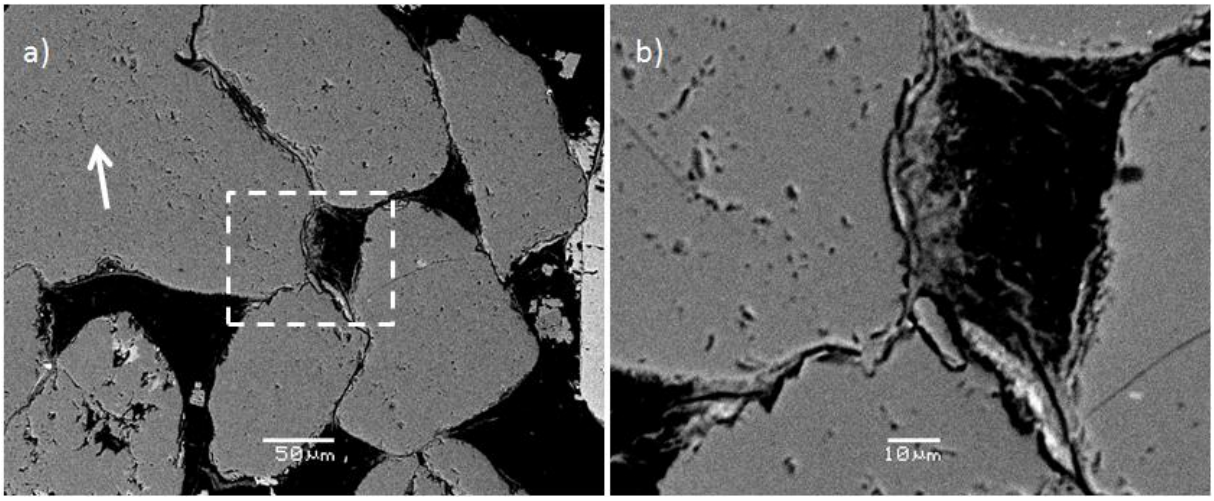

Figure 6.20 a) A backscattered image showing illite coating covering the grain, but part of the grain with no illite coating is quartz cemented (white arrow). b) Enlarged part of the image showing authigenic illite nucleating from clay rim surrounding the grains. (The image has been taken from 4807.50 m in well 1/3-5)

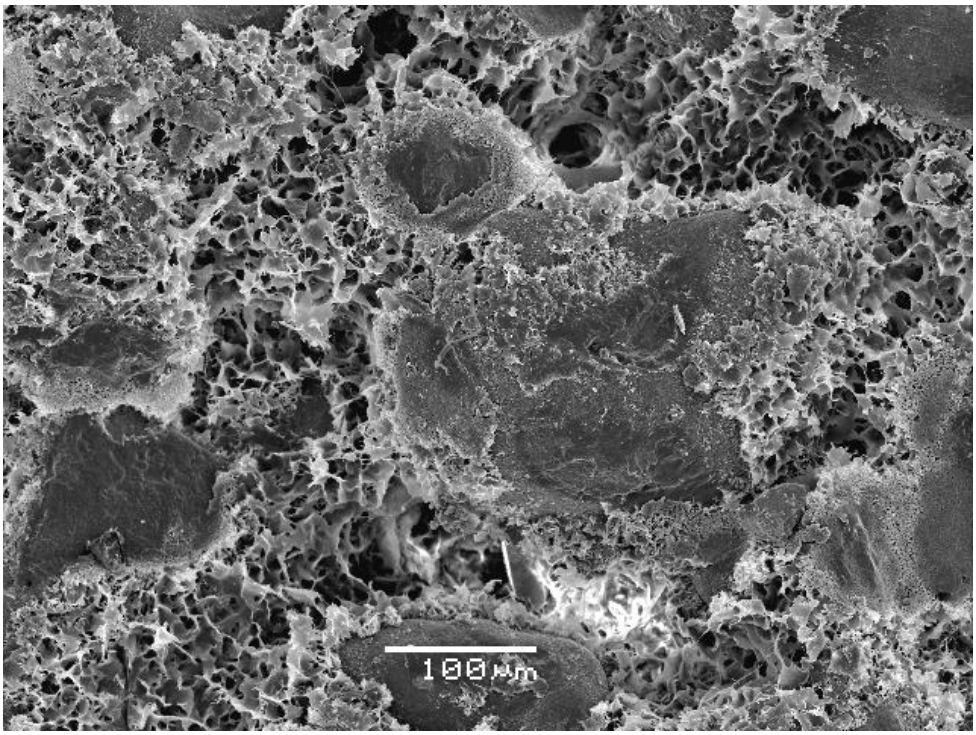

Figure 6.21 An example of one of the heavily illite coated samples. Illite is almost everywhere in the sample, although it has effectively inhibited quartz cementation but severely damaged the permeability of the sample. (The image has been taken from 4807.50 m in well 1/3-5)

6.2.1.2 Quartz overgrowth and porosity

To confirm the results of quartz cementation and porosity from point count analysis and for further investigation detail pictures are taken in scanning electron microscope. The observations from all the sampled studied under optical microscope and scanning electron microscope closely matched, showing that there is hardly any quartz overgrowth found in the samples from well 2/10-2, whereas if not considerable but some quartz cementation is found in the samples from well 1/3-5 (Figure 6.22).

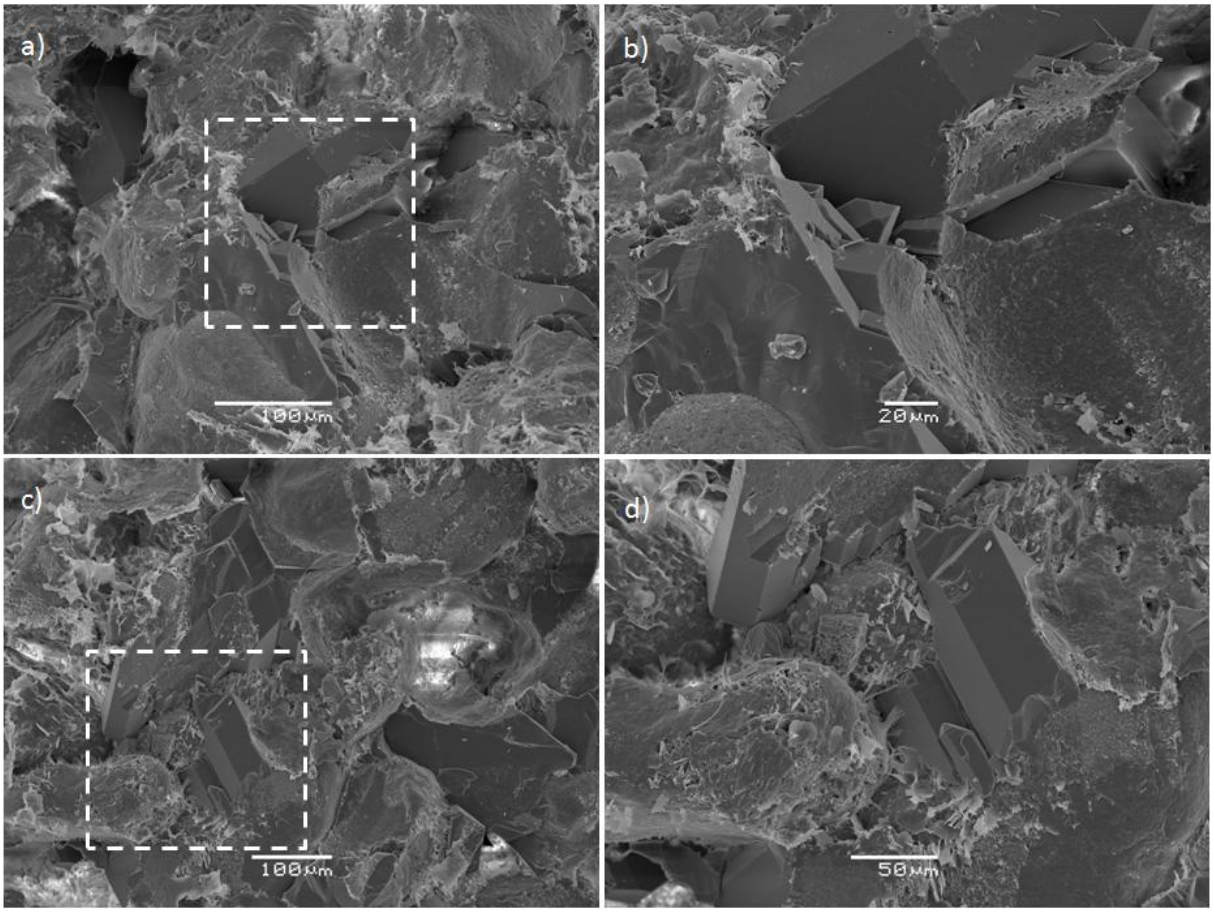

Figure 6.22 Relatively more quartz cementation/overgrowth found in samples from well 1/3-5. a) SEM image from well 1/3-5 (4812.60m) showing some amount of quartz overgrowth. b) The close-up showing detailed image of a tiny overgrowing quartz crystal among the bigger ones. c) SEM image from 4807.50 m in well 1/3-5 showing another example of quartz over growth. d) Enlarged part of the image shows that quartz grains without illite coating have allowed quartz cementation to take place.

The samples that appear to have some quartz cementation are from well 1/3-5. Although quartz cementation is not considerable but still it has influenced the porosity. The carbon coated thin sections from this well have also been examined using cathode luminescence (Figure 6.23). By exposing these thin sections to cathode luminescence (CL), the quartz overgrowth can be visually separated from the detrital grain. The original quartz grain illuminate stronger than the cement in most cases, causing a luminescence contrast enabling a differentiation of detrital grain and over growth.

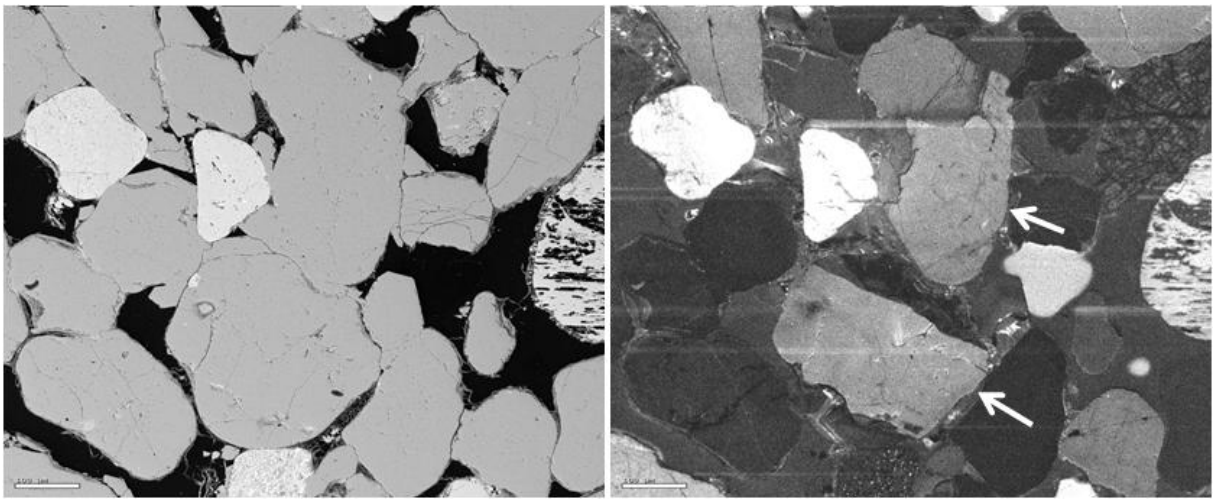

Figure 6.23 A SEM image from 4812.60 m in well 1/3-5 to the left and the same area when exposed to luminescence to the right. Note the difference in the shape between the cemented grains and the illuminated original detrital quartz grains (with white arrows) to the right.

Figure 6.24 shows that some of these samples have been so much mechanically compacted that signs of grain crushing have been observed which later on filled with quartz cement. When samples are exposed to cathode luminescence it appears that they also have some quartz overgrowth (Figure 6.25). This may indicate that sands have been more compacted together rather than only cemented by quartz.

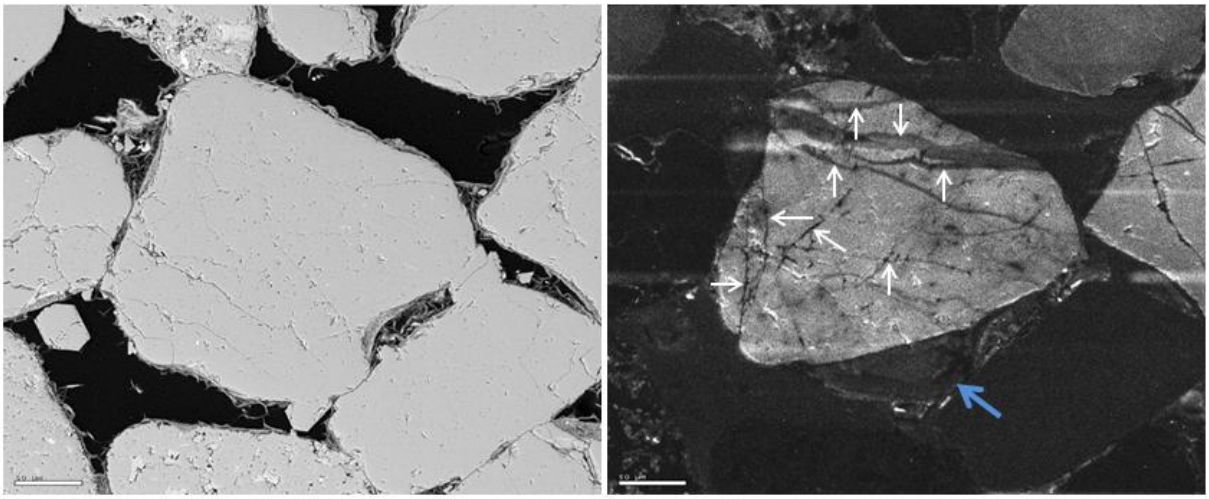

Figure 6.24 A SEM image from 4809.50 m in well 1/3-5 to the left and the same area when exposed to luminescence to the right. Note that the grain has been crushed due to mechanical compaction and the fractures (white arrows) have been filled with quartz cement, the blue arrow shows the quartz overgrowth on the illuminated original detrital grain to the right.

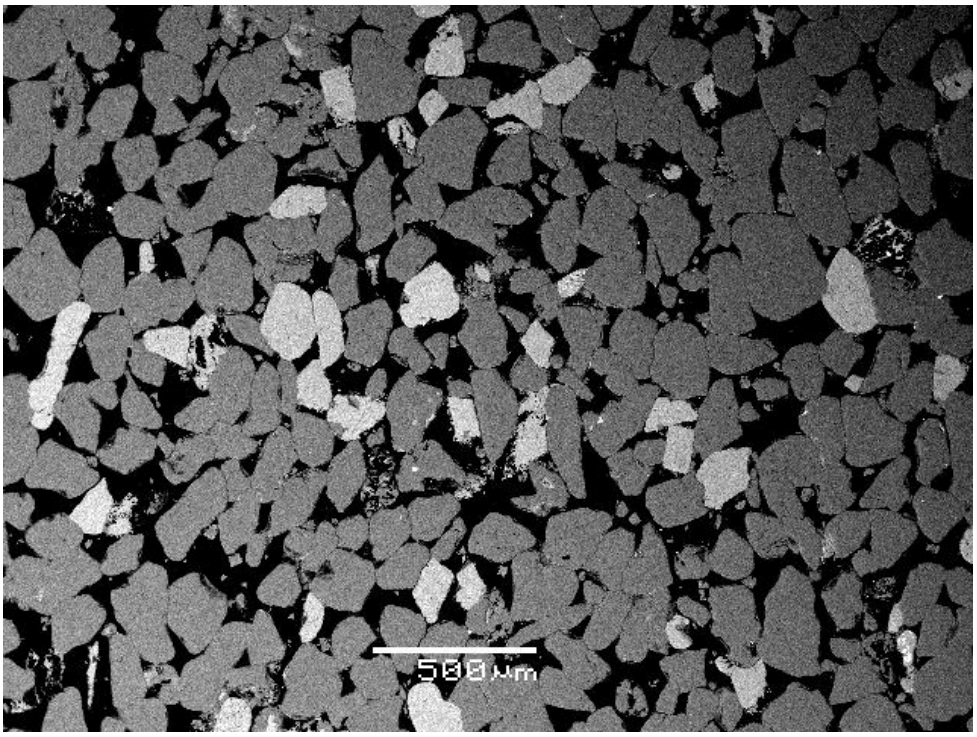

Figure 6.25 A backscattered electron image showing an overview of the porosity and grains in a sample from well 1/3-5 (4807.50 m).

6.2.1.3 Authigenic clays and porosity

Out of all authigenic clays causing porosity reduction, kaolinite and illite have been found as pore filling clays. Although most of Illite has been identified as coating but some of the illite has also been present in pores. The amounts of authigenic clays estimated in the point count analysis, and under scanning electron microscope closely match. Most of the samples from well 2/10-2 contain both pore filling kaolinite and illite. They clay minerals appear to be authigenic as they possess their characteristic morphology. The kaolinite is easily recognized by its stacked booklet shape in the form of vermicular aggregate built up (Figure 6.26 and Figure 6.27). The stacked booklet morphology of kaolinite is preserved in the sample at 4 km depth. The samples from well 2/10-2 have shown illitization of kaolinite to some extent.

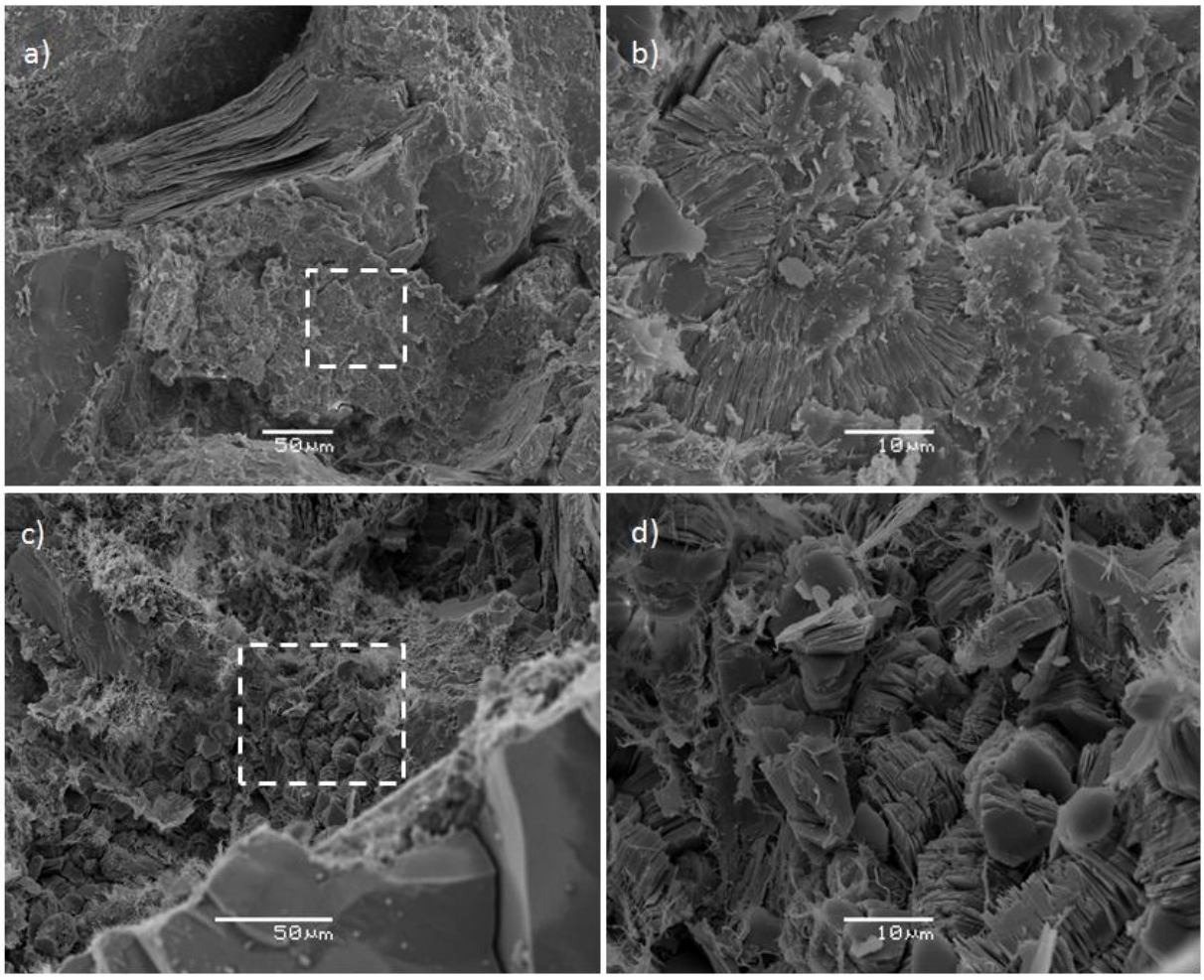

Figure 6.26 Kaolinite is abundant in well 2/10-2. a) SEM image from 4159.20 m (well 2/10-2) showing amounts of authigenic pore filling kaolinite. b) Enlarged part of the image shows that kaolinite booklets have been stacked together to form vermicular aggregate. c) SEM image shows another pore filling reducing porosity. d) Enlarged part showing illitization of some of the kaolinite.

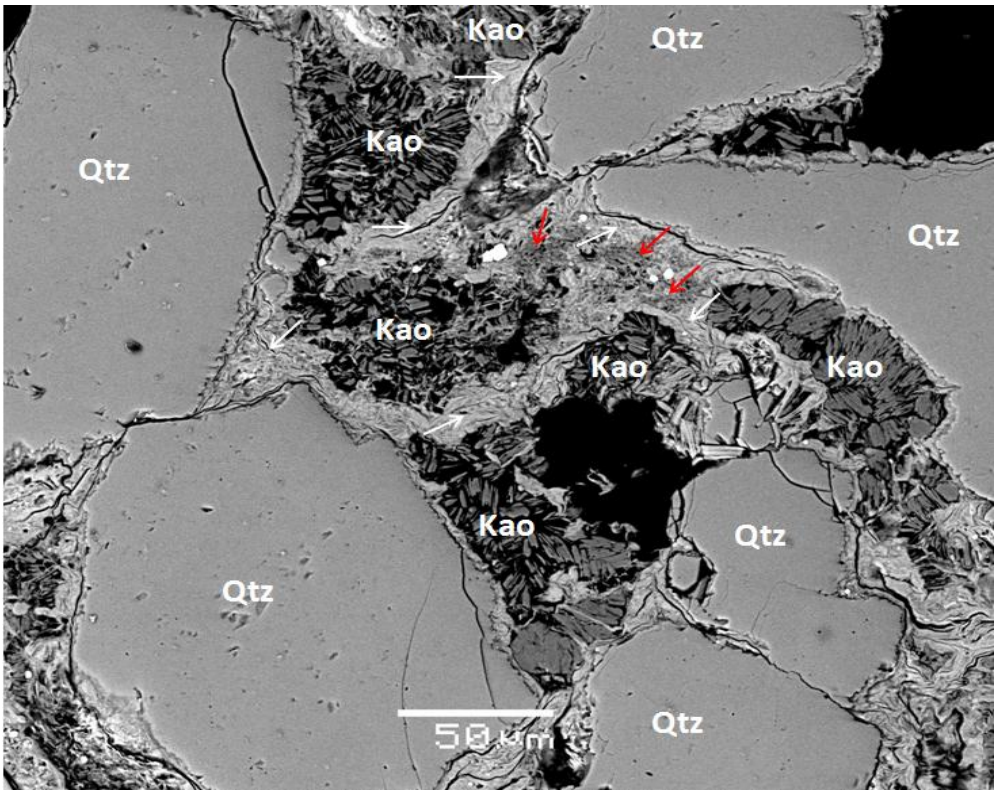

Figure 6.27 A backscattered electron image from 4163.20 m in well 2/10-2 showing authigenic pore filling kaolinite (Kao), illite (white arrows) and carbonate cement (red arrows) reducing the porosity.

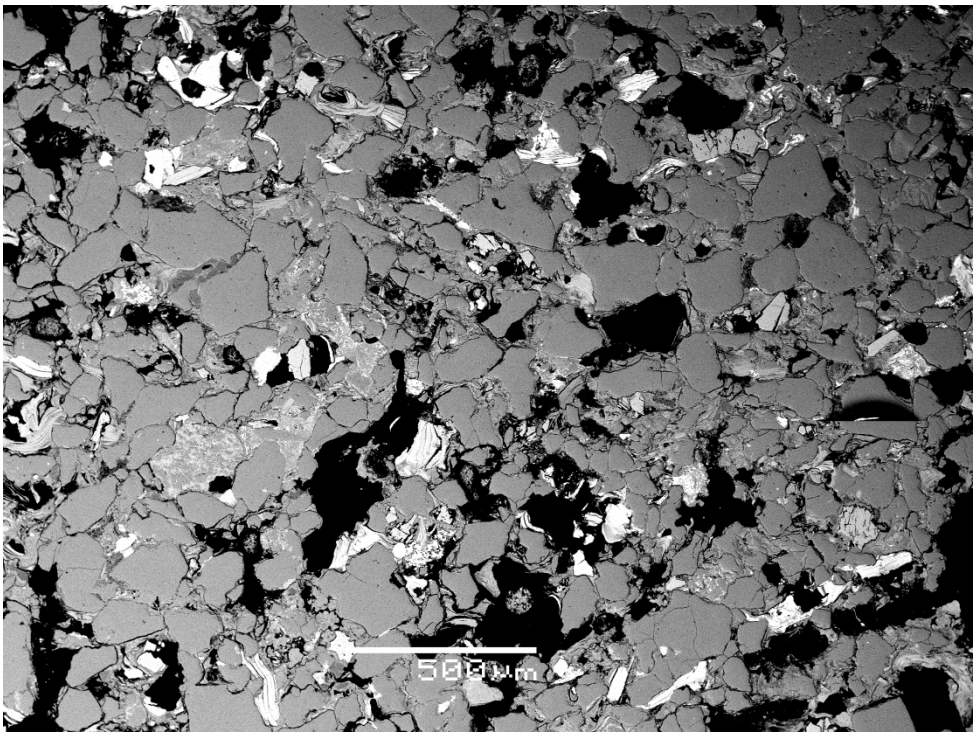

Figure 6.28 A backscattered electron image showing an overview of the porosity and grains in a sample from well 2/10-2 (4163.20 m).

6.2.1.4 Carbonate cement and porosity

The results of carbonate cementation from point counted analysis have been further investigated in detail under SEM analysis. The results from both the analysis closely matched, confirming that samples from well 2/10-2 contain more carbonate minerals as a result of early carbonate cementation. Most frequently found carbonate minerals as cement are dolomite and ankerite, whereas calcite and siderite are found at places (Figure 6.29). The carbonate cement is present in the pore spaces, hence destroying the porosity in most of the samples in well 2/10-2. On the other hand samples in well 1/3-5 have rare quantity of carbonate cement.

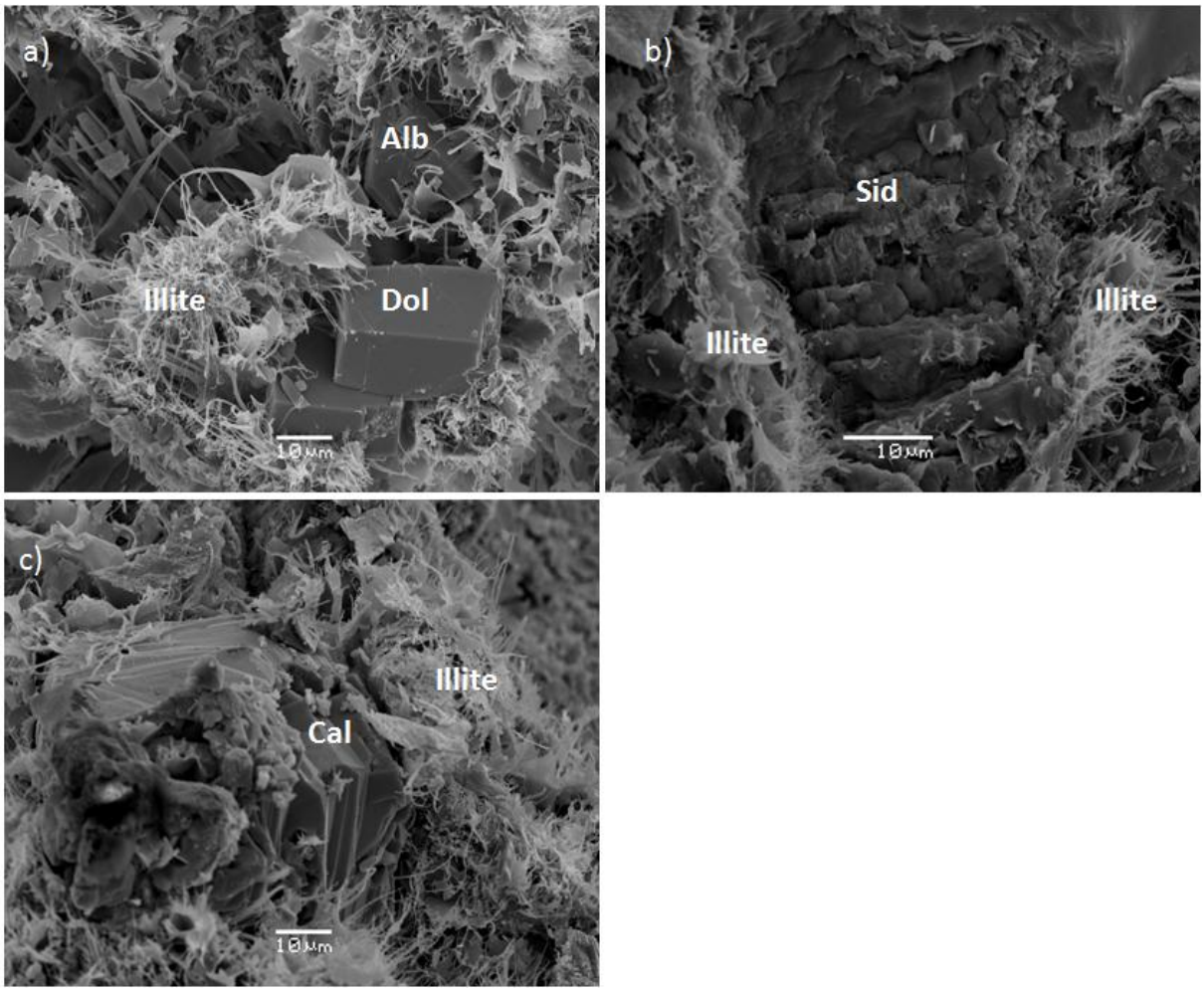

Figure 6.29 Carbonate cement is abundant in well 2/10-2. a) SEM image from 4157.60 m (well 2/10-2) showing dolomite (Dol) crystal as carbonate cement. b) SEM image from 4152.60 m (well 2/10-2) shows siderite (Sid) crystal as carbonate cement. c) SEM image from 4157.60 m (well 2/10-2) shows that the sample has calcite (Cal) crystals at places.

6.2.1.5 Feldspar

The amounts of feldspar, especially k-feldspar have been compared to clay minerals under scanning electron microscope.

The samples from well 2/10-2 have abundant large dissolved k-feldspar grains. The grains are observed with the replacement of k-feldspar by albite. The process is visually identified by darker albitized patches on light grey k-feldspar. K-feldspar grains in this well appear to have more dissolution porosity. However, less dissolution of k-feldspar grains is observed in the samples from well 1/3-5.

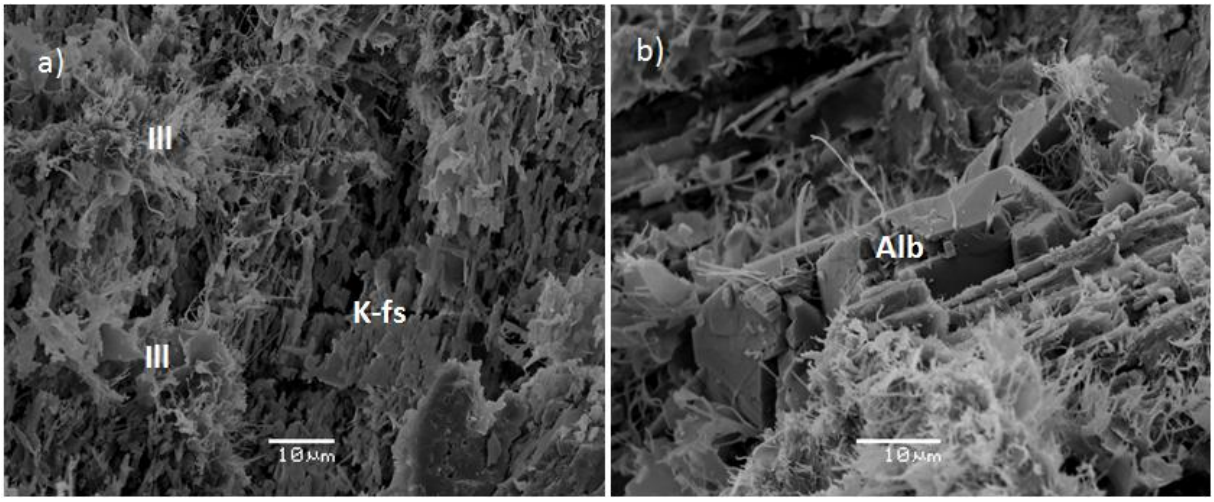

Figure 6.30 a) Illitization (Ill) of k-feldspar (k-fs) grain from 4152.60 m in well 2/10-2. b) SEM image from 4157.60 m in well 2/10-2 has an albite (Alb) grain.

6.2.1.6 Other minerals

Many minerals other than quartz, feldspar and authigenic clays have also been observed in stub mounted samples and carbon coated thin sections under scanning electron microscope.

The samples contain several grains of barite (Figure 6.31a), apatite (Figure 6.31b) and a grain of zircon (Figure 6.32).

Some albite is also witnessed in the samples but the abundance is very difficult to quantify because it has almost the exactly same weight as the quartz grains, and nearly same shade in backscattered electron images.

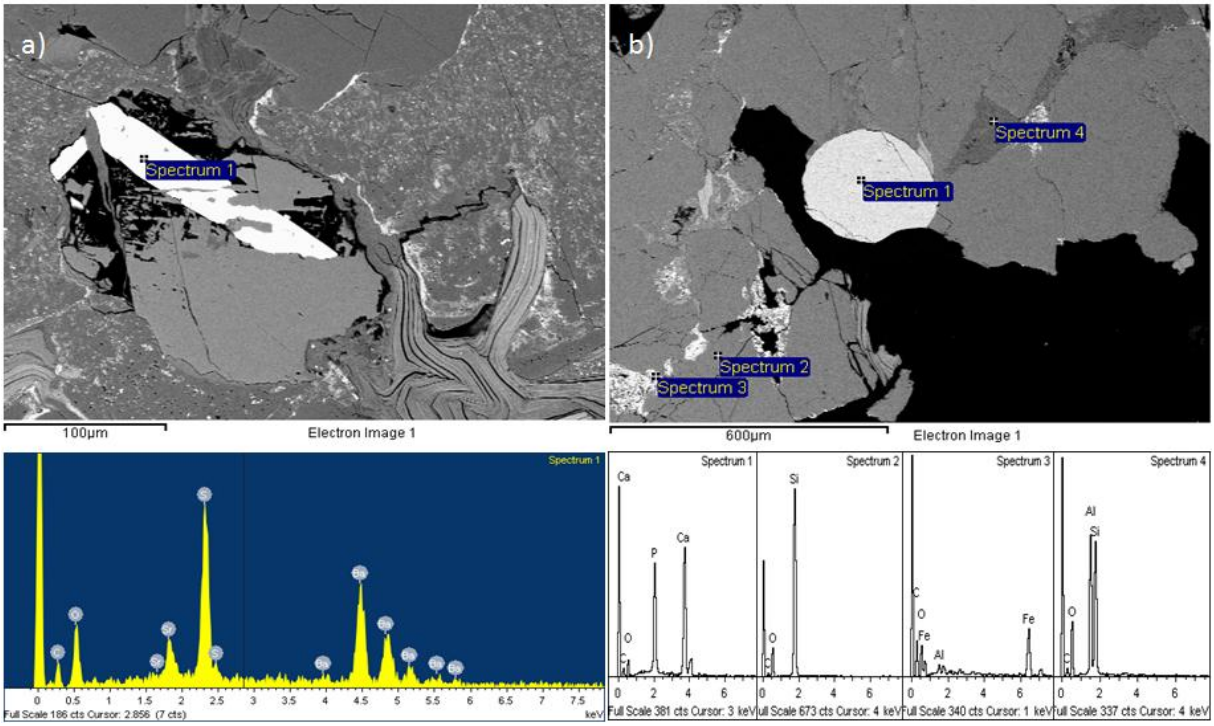

Figure 6.31 a) A backscattered electron image from 4159.20 m in well 2/10-2 shows the presence of barite crystal (spectrum 1) in dissolved feldspar. b) Another backscattered electron image from the same sample showing apatite (spectrum 1), quartz (spectrum 2), Fe-Al oxide (spectrum 3) and kaolinite (spectrum 4).

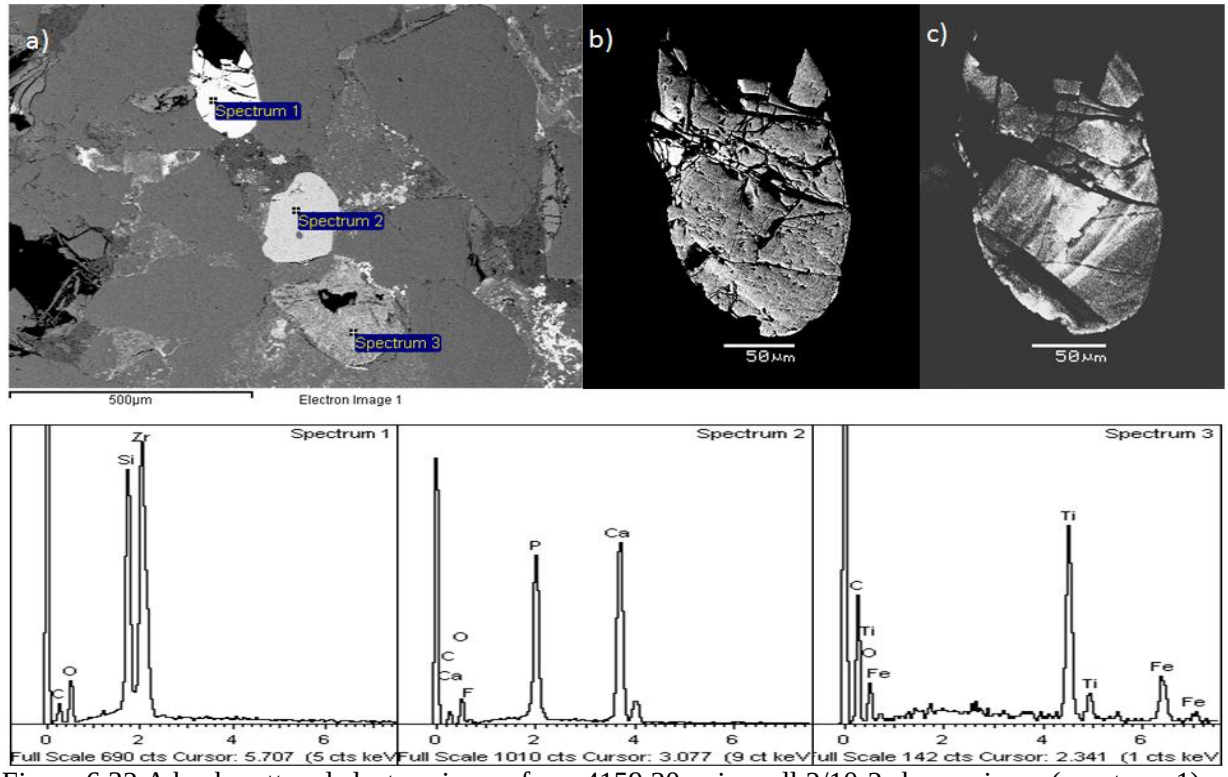

Figure 6.32 A backscattered electron image from 4159.20 m in well 2/10-2 shows zircon (spectrum 1), apatite (spectrum 2) and Fe-TiO (spectrum 3). b) Enlarged part showing only zircon. c) When the same enlarged part exposed to cathode luminescence.

Chapter 7
QUARTZ CEMENTATION AND POROSITY ALGORITHM

For many years it has been suggested that during intermediate and deep burial of quartz rich sandstones, the porosity loss is a function of quartz cementation and shallow burial is dominated by mechanical compaction. The modeling algorithm described in chapter 4 is supposed to be employed to simulate mechanical compaction and quartz cementation, and predict the porosities at greater depths. Since the amount of quartz cementation in the samples from both the wells was too low to be modeled, it was preferred to discuss the reason that has almost completely inhibited the quartz cementation, leaving tiny effect on the porosity loss even at depths greater than 4 km.

According to Walderhaug (1996), temperature and time are two factors which mainly effect quartz cementation. Following formula is used to calculate the average geothermal gradient for wells 1/3-5 and 2/10-2.

$$Geothermal\ gradient = dt/dz = \frac{\mathrm{B.H.T} - \mathrm{M.A.S.T}}{\mathrm{T.D}}$$

Where dt/dz is geothermal gradient (^{o}C/km), B.H.T is borehole temperature (^{o}C), M.A.S.T is mean annual surface temperature (^{o}C) and T.D is total depth in kilometers.
The borehole temperatures for wells 1/3-5 and 2/10-2 are 172^{o}C and 148^{o}C respectively, while depths are 4.8km and 4.1km respectively (Table 5.1). Mean annual surface temperature is taken 7^{o}C for Stavanger area. The calculated average geothermal gradient from both the wells is 33^{o}C per kilometer.

The geothermal gradient (Figure 7.1) and burial history curve (Figure 7.2) are generated and corresponding burial temperature and time are calculated at different depths for two wells.

Table 7.1 Corresponding temperature and time against different depths along two wells.

Depth (km)	Temperature (^{o}C)	Time (million years)
0	7	290
1	40	255
2	73	220
3	106	185
4	139	160
5	173	120

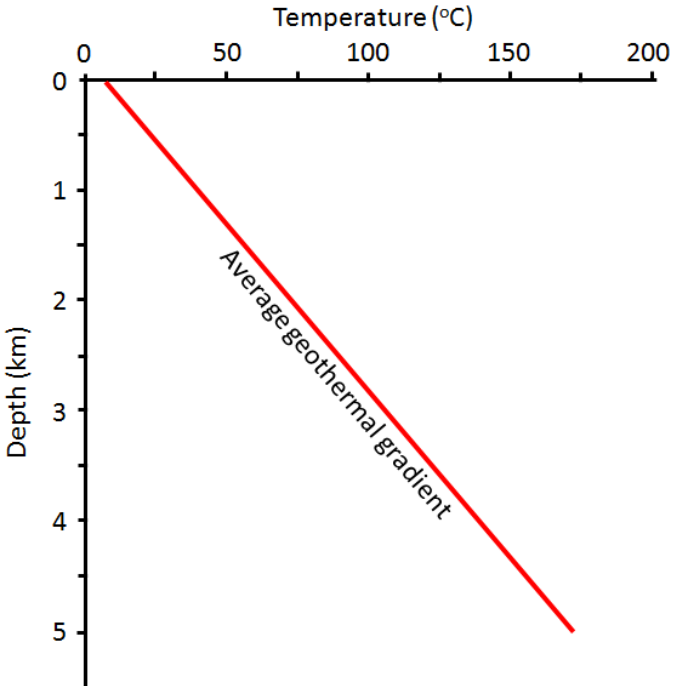

Figure 7.1 Average geothermal gradient generated for wells 1/3-5 and 2/10-2.

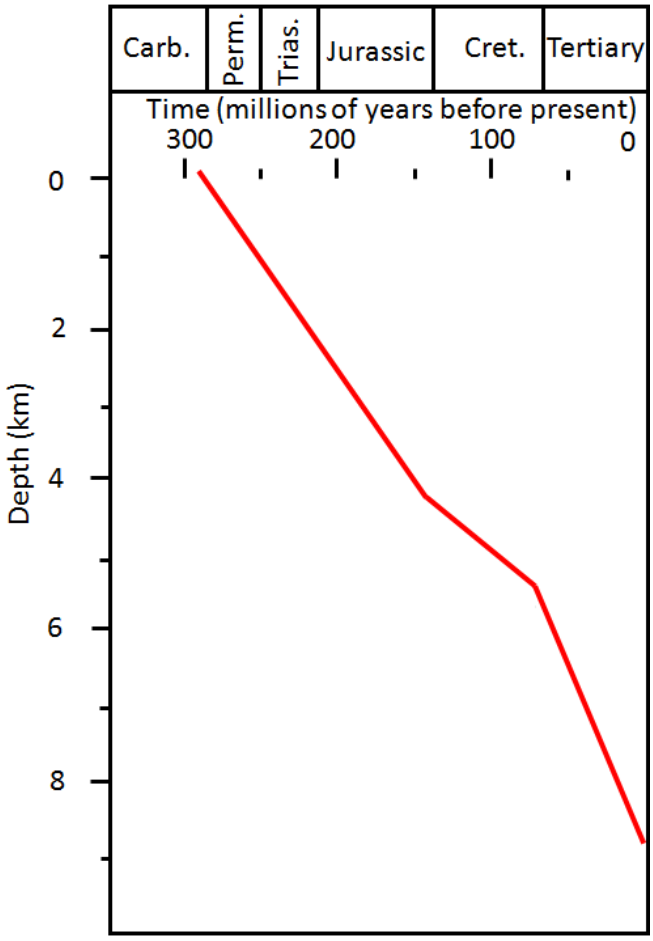

Figure 7.2 Burial-history curve for the Rotliegend sandstone in Central Graben (modified from Ziegler 2006).

Effect of grain size

Fine grained sandstones are observed to be more heavily quartz cemented than coarse grand sandstones (Walderhaug 1996). The reason is that small grains have more surface area available for quartz cementation. The experiments from Heald and Renton (1966) have shown that fine quartz grains become quartz cemented more rapidly than coarse quartz grains.

Effect of mineralogy

The surface area available for quartz cementation is also affected by nonquartz grains, hence keeping the other factors equal, quartzarenites will be more heavily quartz cemented than arkoses of same grain size (Walderhaug 1996). More rapid quartz cementation in pure quartzarenites compared to arkoses has been observed in experimental studies of Heald and Renton (1966).

Effect of temperature history

According to some authors (e.g., Schmoker and Gautier 1988; Schmoker and Higley 1991) sandstone porosity is considered to be a function of thermal maturity but it has been very hard to model the effect of temperature history on quartz cementation and porosity. However, the effect can be easily measured with this model. Walderhaug (1996) proved from different experiments that quartz cementation increases with increasing temperature and also explained that porosity loss per unit time at constant temperature decreases as a function of time due to the decrease in quartz surrounding area as cementation proceeds.

Effect of clay coatings

The inhibiting effect of clay coatings on quartz cementation has been documented in numerous papers (e.g., Heald and Larese 1974; Thomson 1979; Ehrenberg 1993; Byrnes and Wilson 1994), thus quartz cementation models should also consider this factor.
All the samples from wells 1/3-5 and 2/10-2 have very good clay coatings around the quartz grains. Samples from well 1/3-5 are medium grained but two samples at depths 4812.60 m and 4807.50 m, and approximately at temperature 167^{o}C have more quartz cementation with

3% and 2% respectively (Table 6.1), which is negligible considering this burial depth. The effect clay coating actually has overshadowed all the other factors.
The petrographic studies have revealed that quartz cementation took place on few grain surfaces which were not fully coated with clays.

Walderhaug (1996) modeled the effect of clay coatings by introducing the clay coating factor, C, which represents the quartz grains coated by clay into equation 7 (Chapter 4).

$$A = (1-C)\, A_0\, (\phi_0 - Vq)/\, \phi_0 \qquad (9)$$

Almost no quartz cementation means that there was no surface area available for quartz precipitation or all the quartz grains are fully coated with clays.
When all the quartz grains are coated with clay, C has the value 1, quartz surface area A is 0 and no quartz cement precipitates. Coatings of quartz grains by other minerals, such as carbonate cements, also reduce the available surface area for quartz cementation in the same way but less porosity is preserved due to filling of most or all the pore spaces by the cementing material (Walderhaug 1996).

According to Bjørlykke and Jahren (2010), a strong reduction in porosity and permeability due to quartz cementation has been observed in sandstone reservoirs between 3.5 and 4.5 km (120^{o}C-160^{o}C). The rate of quartz cementation increases as an exponential function of temperature which may increase by a factor of 1.7 for every 10^{o}C temperature increase (Walderhaug 1996). The precipitation of quartz cement is also a function of surface area available for quartz cementation (Figure 7.3).

A linear trend is drawn on the basis of quartz cementation and compaction curve at constant temperature of 120^{o}C, showing that the volume is fully quartz cemented in 50 million years (Figure 7.3). This trend line is an exponention for quartz growth rates in the reservoirs with more than 10% porosity remaining and less than 15% quartz cement formed assuming an initial porosity of 25% (Walderhaug et al. 2001). This is the case for all the reservoir rocks investigated in this study. Using the linear trend, amount of quartz cement has been calculated as 3.5% at 73^{o}C. As discussed earlier that quartz cement increases exponentially by the factor of 1.7 with every 10^{o}C temperature increase. It means that the sandstone reservoirs should have had at least 15% cement at the present temperature of about 140^{o}C (4km) in the study

area, which actually is not the case here. The long residence time at temperature above 140°C (Table 7.1) would indicate that these reservoirs should have been fully cemented.

Only 3% of quartz cement has been observed in the samples, indicating how efficiently grain coating has preserved porosity and hindered quartz cementation.

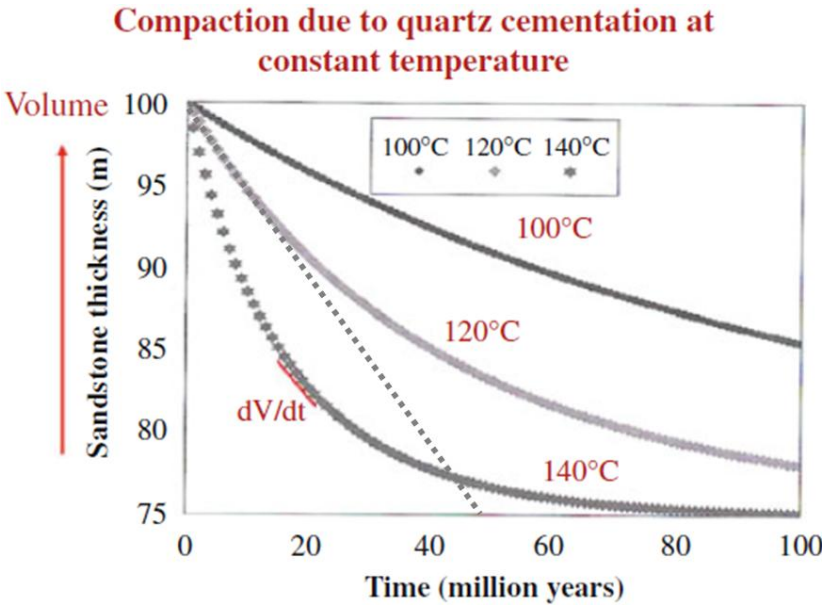

Figure 7.3 Modeling of quartz cementation and chemical compaction due to quartz dissolution and cementation as a function of time and temperature (from Walderhaug et al. 2001). We see that the rate of porosity loss (compaction, *dv*/*dt*) is highest at high temperatures and also when the porosity is still relatively high. A linear trend is drawn using the 120°C curve.

Chapter 8
DISCUSSION

8.1 Mechanical compaction

The intergranular volume (IGV) is defined as the sum of intergranular porosity, cement and depositional matrix and also describes the intergranular porosity before the onset of chemical compaction (Paxton et al. 2002). Quartz cementation starts at about 2km burial depth (70^{o}C) which stabilizes the grain framework and prevents the further mechanical compaction (Bjørlykke and Jahren 2010). According to Paxton et al. (2002), the mechanical compaction reduces the IGV (depositional porosity) from 40% to 26% at the burial depth of 2.5 km.

From the point count analysis of all the sandstone samples, the calculated IGV ranges mainly from 29% to 48% (Table 6.1), where low IGV values showing that some of samples have experienced maximum mechanical compaction, while high IGV values representing early depositional porosity preservation. Preservation of intergranular volume may be caused by early carbonate cementation or overpressure that reduces the effective stress and subsequently results in less mechanical compaction (Bjørlykke and Jahren 2010). Grain size and sorting may also effect the variation in IGV values (Figure 6.11). One of the calculated IGV values is as high as 52% which shows significantly low mechanical compaction or indicating an inaccurate point count which may be related to badly prepared thin sections (Appendix C), as ripped out grains may have been mistaken for porosity.

After plotting the point count results in petrographic classification it is revealed that most of the samples fall in subfeldspathic and sublithic arenites (Figure 6.3). The samples from well 1/3-5 mainly fall in subfeldspathic arenites indicating relatively high feldspar content and have low IGV values, probably suggesting that high feldspar content increases mechanical compaction. Grain crushing has also been observed in some samples from this well (Figure 6.28, Appendix C). Samples from well 2/10-2 mainly fall in sublithic and quartz arenites. No significant mechanical compaction has been observed in these samples, and high amounts of carbonate cements possibly indicating that early carbonate cementation may have preserved high IGV values and prevented the severe mechanical compaction. On the basis of point count results, provenance studies have also been done using Dickinson plots (Figure 6.4 and Figure 6.5).

In relation to the depositional environment of the Rotliegend sandstone (2.3.2), point count results have shown that samples from well 2/10-2 contain more amounts of detrital matrix and authigenic clays (Table 6.7 and Table 6.3 respectively) than that of the samples from well 1/3-5. Detrital matrix and authigenic clay content are expected to be lower in aeolian dune facies of Rotliegend sandstone than fluvial wadi facies which have more detrital matrix and argillaceous material. IGV is plotted separately against both detrital matrix and authigenic clays (Figure 6.12 and Figure 6.14) in order to investigate the relationship between the two parameters. As both the wells contain totally different sandstone facies, so no trend could be drawn. But apparently it shows that samples from well 2/10-2 have high amounts of detrital matrix and authigenic clay content which may have helped in preserving high IGV values. One more parameter that is associated with fluvial wadi sandstone facies is early carbonate cement. The plot between IGV and carbonate cement (Figure 6.13) shows that high amount of carbonate cement in the samples from well 2/10-2 has also preserved high values of IGV.

Sorting

The calculated IGV values are plotted against the grain sorting (Figure 6.11a) to investigate the relationship between the two. No apparent trend is drawn and samples from both the wells are marked separately. Samples from well 2/10-2 are moderate to poorly sorted and contain high IGV values, while samples from well 1/3-5 are moderate to well sorted and contain relatively low IGV values (Appendix B).

Grain size

The calculated IGV values are plotted against the grain size (Figure 6.11b) to see if any relationship existed between the two. No apparent trend is drawn and samples from both the wells are marked separately. Samples from well 2/10-2 mainly are fine to medium grained and contain high IGV values, whereas, samples from well 1/3-5 are medium grained and contain relatively lower IGV values (Appendix B). This shows that highest IGV values are preserved in fine sands, which subsequently indicates that mechanical compaction is more significant in the coarse sands.

Grain shape

The calculated IGV values are plotted against the grain shape (Figure 6.11c) to investigate the relationship between the two. The grain shape in most of the samples is subangular to subrounded. The angular grains have been point counted with high IGV values (Appendix B). This gives an impression that angular grains help in preserving high IGV values. Ramm (1992) reported the resistance of angular grains during mechanical compaction.

Influence on reservoir quality

High IGV values show that porosity is well preserved in the samples from well 2/10-2 and no significant effect of mechanical compaction has been observed, whereas samples from well 1/3-5 were very much mechanically compacted. Grain size, shape and sorting may have favored the high IGV preservation. At approximately 2.5 km, mechanical compaction seizes. Quartz cementation and grain shape helped to end mechanical compaction in well 1/3-5, while early carbonate cement and authigenic clays stopped mechanical compaction in well 2/10-2 preserved high IGV values (Figure 6.10b).

8.2 Chemical compaction

8.2.1 Carbonate cement

During the SEM analysis, four types of carbonate cements are observed in all the samples; ankerite (Figure 6.16a, b), dolomite (Figure 6.29a), siderite (Figure 6.29 b) and calcite (Figure 6.29c). Mainly ankerite and dolomite are found, whereas siderite and calcite are present at places. The composition of ankerite is closely related to dolomite, but differs from this in having magnesium replaced by varying amounts of iron (II) and manganese. Dolomite is most of the time precipitated as secondary mineral, as a result between different forms of $CaCO_3$ and Mg^{2+} and the reaction is dependent on the Mg^{2+}/Ca^{2+} ratio (Hanken et al. 2010). Dolomite occurs in the samples as rhombic crystals rooted on grain surfaces and as cements. Much higher amounts of carbonate cement have been observed in the samples from well 2/10-2 as compared to well 1/3-5 due to early carbonate cementation (Table 6.4). According to Bjørlykke and Jahren (2010), carbonate cement is typically formed during shallow diagenesis. The SEM observations have revealed that carbonate cement predates the quartz overgrowth

and there is hardly any quartz cementation in the samples from well 2/10-2 having high amounts of carbonate cement (Figure 6.2b). Although carbonate cementation has prevented quartz overgrowth but it has also destroyed the porosity by filling of most of the pore system (Figure 6.9b).

8.2.2 Authigenic clays

Two types of authigenic clays; kaolin and illite are present in the samples. Illite is more frequently found in all the samples, whereas kaolin is only present in the samples from well 2/10-2. Kaolinite is found at shallow depths but as the burial depth increases from 2-3km, the kaolinite is altered into dickite, therefore at the depth deeper than 4.5km, dickite is the only kaolin mineral present (Lanson et al. 2002). Dickite occurs as somewhat little thicker crystals and can be distinguished from kaolinite only on XRD scans (Bjørlykke and Jahren 2010). Otherwise it is very difficult to differentiate between the two, so kaolin has been used in the following discussion stating kaolin group.

From the point count results it is evident that the samples from well 1/3-5 have less amounts of clay as compared to the samples from well 2/10-2 (Table 6.1). These results have also been confirmed by SEM observations indicating almost no pore filling kaolin in the samples from well 1/3-5. The dissolution of feldspar and mica results in kaolin formation during early diagenesis, which cannot take place in a closed system (Bjørlykke 1998).

$$2K(Na)AlSi_3O_8 + 2H^+ + 9H_2O \longrightarrow Al_2SiO_5(OH)_4 + 2H_4SiO_4 + 2K(Na^+)$$

Feldspar Kaolinite

The samples from well 2/10-2 have been characterized as fluvial wadi sandstones deposited as a result of ephemeral streams, typical of desert environments. In the areas between the active wadi fluvial channels, sedimentation mainly results from the channel overflow. Since the channel and flooded area is initially dry, water may percolate downwards (Glennie et al. 1978; Walker 1976). These fluvial channels could be the only place where kaolinite formation might have taken place. But due to high rates of evaporation, water is quickly evaporated, hardly giving any time for downward percolation. Furthermore, rates of evaporation are many times higher than precipitation. And these fluvial channels are not active for long

enough to favor the kaolinite forming conditions. For kaolinite formation, very frequent meteoric water flushing is needed, that dissolves k-feldspar and forms kaolinite. As result of this reaction K^+ and silica is formed, which has to be removed to continue the kaolinite formation reaction. But as the solubility of silica is very less in water, so high flux/amounts of water is continuously needed to remove this silica. This high flux of meteoric water is impossible in these climatic conditions. Another factor that could have influenced the kaolinite formation is Permo-Carboniferous glaciation period. But according to Roscher and Schneider (2006), that glaciation period finished in Early Permian and aridity was at its maximum in Roadian-Wordian. Whereas, the deposition of Upper Rotliegend 2 has taken place between Wordian and Early Wuchiapingian age (2.3.1), so this cannot be the case here either. The other reason of kaolinite formation could be the climatic fluctuations that may have occurred during Permian time. There may be any other mechanisms for kaolinite formation in the study area, so further research is required to find out the possible reason of the kaolinite formation.

According to Ziegler (2006), Rotliegend sandstones were deposited in arid desert climate. And the dominant weathering product in arid desert environments is smectite (Chamley 1989; Bjørlykke 1983). During intermediate burial digenesis at 2km to 3.5km depth (50^oC-120^oC), this smectite clay in the presence of k-feldspar becomes unstable and dissolves to form mixed layer minerals (I-S).

$$\text{Smectite} + K^+ \longrightarrow \text{Illite} + \text{Silica (via mixed-layer minerals)}$$

(Bjørlykke et al. 1995)

The smectite distribution in North Sea suggest that smectite dissolves at temperatures of 65^oC-75^oC to form mixed-layer minerals (I-S), and at temperatures of 80^oC-100^oC these mixed layer minerals contain more than 70% illite (Dypvik 1983). The reaction depends on several factors including supply of K^+ and the time factor (Bole and Franks 1979). The flaky to honey comb morphology from SEM analysis suggests smectite as precursor for illite coating in all the samples (Figure 6.18).

Kaolin formed during early diagenesis becomes unstable and forms illite in the presence of k-feldspar at deeper depths (Bjørlykke 1998).

$$Al_2SiO_5(OH)_4 + KAlSi_3O_8 \longrightarrow KAl_3Si_3O_{10}(OH)_2 + 2SiO_2 + H_2O$$
Kaolinite K-feldspar Illite Quartz

$$3Al_2Si_2O_5(OH)_4 + 2KAlSi_3O_8 + 2Na^+ \longrightarrow 2KAl_3Si_3O_{10}(OH)_2 + 2NaAlSi_3O_8 + 2H^+ + 3H_2O$$
Kaolinite K-feldspar Illite Albite

In North Sea basin, illitization mainly takes place at temperatures between 130°C-140°C (Bjørlykke 1998) and a strong increase in illite content at the expense of kaolin is commonly observed in the North Sea at depths greater than 3.7km and 4km (Bjørlykke and Aagaard 1992). All the samples containing pore-filling authigenic kaolin from well 2/10-2 are burried below 3.7km and considerable amounts of illitization can be observed. However, it has been demonstrated from point count and SEM analysis that samples buried as deep as 4.1km contain significant amounts unaltered authigenic kaolin (Figure 6.26b). Hence this contradicts the argument about the main phase of illitization at depth 4 km.

The formation of illite at the expense of kaolin mainly depends on temperature and supply of K^+ from the dissolution of k-feldspar. The temperature and burial depth data (Table 7.1) suggests that all the samples containing kaolin at the depth 4.1 km have temperature of about 142°C, which appears to be high enough to reach illitization phase. Some amounts of k-feldspar have also been observed with unaltered kaolin, which suggests that the process of illitization is still going on. The point count and SEM analysis have confirmed some amounts of k-feldspar in the samples from well 2/10-2 (Table 6.1).

Influence on reservoir quality

Significant amounts of pore-filling authigenic kaolin have been observed in samples from well 2/10-2, reducing the porosity in the sandstone. However, large amounts of kaolin are not believed to greatly influence the permeability of the reservoir as fluids can easily flow through the morphology of authigenic kaolin.

A large amount of illite has been found in all the samples with often pore bridging and fibrous morphology. The typical fibrous morphology has severely damaged the permeability of reservoir (Table 4.1).

8.2.3 Quartz cementation

Although not much but some amount of quartz cementation is present in samples from well 1/3-5. The amount of quartz cement varies from 1% to 3% (Figure 6.2b, Table 6.1). Samples are medium grained and moderate to well sorted (Appendix B). The quartz cementation requires clean surface area which was not available due to very frequent clay coatings. The backscattered electron identification of the quartz cement combined with CL (cathodeluminesence) for easier discrimination between detrital quartz and quartz overgrowth (e.g., Götze et al. 2001) has been used. Some quartz cementation was found by backscattered electron (Figure 6.23). The possible source of quartz cement could be dissolution along stylolites, illitization of smectite or dissolution on grain to grain contacts. Oelkers et al. (2000) adapted so called I-MID (Illite-Mica Induced Dissolution) model and described that source of silica cement is surface of quartz adjoining Mica and/or clay at stylolite interface with in sandstone (3.6.1). The clay coating before the onset of quartz cementation has not given enough clean grain surface area for the precipitation. The carbon coated thin section study in SEM analysis has confirmed that quartz cementation has taken place only at place where grains were not fully clay coated (Figure 6.20a).

Influence on reservoir quality

The quartz cementation has severe effect on the reservoir quality by destroying porosity due to precipitation on the grains and in the pore spaces. So any mechanism that may inhibit or retard the quartz cementation is vital regarding good porosity preservation. The minor amounts of quartz cement suggest that clay coating have effectively prevented the quartz cementation in the samples.

8.3 Porosity preserving mechanisms

Most of the studied samples contain high intergranular volume (IGV) values, and chemical cementation by authigenic clays, carbonate cement and to some extent quartz cementation have filled the pore spaces and acted as main porosity reducing mechanisms in the study area. Although much of the porosity is reduced by these three factors, considering this burial depth the overall porosity in the samples is still high. The SEM observations have confirmed that

authigenic clay coating has effectively hindered quartz cementation in most of the samples. The most commonly observed porosity preserving mechanisms will be discussed in the following section.

Illite coating

Illite coating has been frequently observed in all the samples during SEM observations. Under scanning electron microscope it appears from carbon coated thin sections and stub mounted samples that illite coating is thick enough to completely inhibit or retard the quartz cementation development (Figure 6.18). So illite coating must have been present before the onset of quartz cementation at 2.5-3 km depth (90^{o}C-100^{o}C). According to Ehrenberg (1990), in North Sea basin illite precipitation from kaolinite usually takes place at 3.5-4km depth (120^{o}C-140^{o}C). The illite coating is thus formed earlier, proposing that either illite is precipitated from some precursor or probably from a clay rim (Figure 7.20b) (Aagaard et al. 2000). The rim forming mechanically infiltrated clay has been reported in Rotliegend aeolian sandstone (Glennie et al., 1978; Purvis, 1992; Ziegler 2006). The Rotliegend sandstone deposited in arid desert climate (Ziegler 2006). The surface water drainage (ephemeral interdune, channels, or wadi floods) has strongly influenced the fine grained material into the sand. The dominant weathering product in arid desert environments is smectite (Chamley 1989; Bjørlykke 1983), which is previously reported precursor for illite precipitation (Ziegler 2006; Ziegler 1993; Robinson et al. 1993). Hoffman and Hower 1979 reported illite precipitation at the expense of smectite at temperatures between 60^{o}C-100^{o}C, suggesting that illite precipitation from smectite predates the quartz cementation. Kaolinite is also reported as precursor for illite precipitation only by Rossel (1982), but illite precipitation from kaolinite precursor at temperatures between 120^{o}C-140^{o}C is too late to hinder the quartz cementation. The flaky to honey comb morphology of illite coating under SEM suggests smectite as the precursor (Figure 6.18) (Pollastro 1985). More fibrous illite observed as pore filling illite in samples from well 2/10-2.

Iron oxide coating

Iron oxides coating has been observed during point count analysis in red samples from well 1/3-5 (Figure 6.2b). Although it is not present frequently but still it has helped in preserving good porosity. The sediments are not red when deposited, but they redden with time.

Reddening is probably an early diagenetic event that is more closely related to wetting and drying. The mechanism for creating hematite is in-situ alteration of hydrated iron oxides derived from the oxidation of ferrous iron in iron bearing minerals, in a hot and arid climate (Friedman and Sanders 1978). The iron oxide coating has been previously reported by many workers, e.g., Gaupp et al. 1993; Glennie 1998; Hancock 1978.

Influence on reservoir quality

The samples of the studied wells indicate very good preserved porosity even at the depths more than 4km. It is evident from SEM analysis that illite coating has inhibited quartz overgrowth preserving porosity in the studied samples.

The illite coating in samples from well 2/10-2 has more grain coverage, leaving almost no surface area for quartz overgrowth. Whereas some samples from well 1/3-5 contain quartz cementation, indicating lack of illite coating at places. The quartz overgrowth is negligible, so it has not significantly influenced the porosity. The point count and petrophysical analysis has confirmed that samples from well 1/3-5 have more preserved porosity.

The iron oxide coating in some red samples has helped in preserving very good porosity by inhibiting effectively quartz cementation. The aeolian red Rotliegend sandstones assumed to have very good permeabilities. But permeability is severely damaged by fibrous illite (Table 4.1).

9. CONCLUSION

- The intergranular volume (IGV) in the studied wells is very high (up to 48%). The reason for high IGV in most of the samples is the early carbonate cementation and relatively high amount of matrix.

- The variation in IGV reflects different amounts of mechanical compaction. Samples from well 1/3-5 are more mechanically compacted than well 2/10-2. IGV depends on many factors including grain sorting, grain size and grain shape.

- Grain size has a significant effect on porosity of the sandstones in the area, where coarse grains have lost porosity more readily than finer grains during mechanical compaction.

- Illite coating is very common in the study area. It is present in all the samples and most likely the only grain coating preserving significant amounts of porosity.

- Quartz cementation has no significant effect on porosity loss. Porosity is mainly reduced by pore-filling kaolin and carbonate cement.

- The presence of unaltered kaolin with some amounts of k-feldspar suggests that illitization process of kaolin is still going on.

- Although not much, but iron oxide coating has also helped in preserving good porosity.

10. REFERENCES

Aagaard, P., P. K. Egeberg, et al. (1990). Diagenetic albitization of detrital K-feldspars in Jurassic, Lower Cretaceous and Tertiary clastic reservoir rocks from offshore Norway; II, Formation water chemistry and kinetic considerations. **60:** 575-581.

Aagaard, P., J.S. Jahren, et al. (2000). Formation of grain-coating chlorite in sandstones; laboratory synthesized vs. natural occurrences. **35:** 261-269

Aase, N. E. and O. Walderhaug (2005). The effect of hydrocarbons on quartz cementation: Diagenesis in the Upper Jurassic sandstones of the Miller field, North Sea, revisited. **11:** 215–223.

Adams, A. E., W. S. MacKenzie, et al. (1986). "Atlas of sedimentary rocks in thin section." Ferdinand Enke Stuttgart,Germany: 103.

Ajdukiewicz, J. M. and R. H. Lander (2010). Sandstone reservoir quality prediction: The state of the art. **94:** 1083-1091.

Anjos, S. M. C., L. F. De Ros, et al. (2009). "Chlorite Authigenesis and Porosity Preservation in the Upper Cretaceous Marine Sandstones of the Santos Basin, Offshore Eastern Brazil: Clay Mineral Cements in Sandstones." Blackwell Publishing Ltd.

Barclay, S. A. and R. H. Worden (2009). Petrophysical and Petrographical Analysis of Quartz Cement Volumes across Oil–Water Contacts in the Magnus Field, Northern North Sea. Quartz cementation in sandstones, Blackwell Publishing Ltd: 147-161

Bjørkum, P. A. (1996). How important is pressure in causing dissolution of quartz in sandstones? **66:** 147-154

Bjørlykke, K. and J. Jahren, (2010). Sandstones and Sandstone Reservoirs. Petroleum Geoscience: From Sedimentary Environments to Rock Physics, Springer Berlin Heidelberg**:** 113-140.

Bjørlykke, K. (1998). “Clay mineral diagenesis in sedimentary basins - a key to the prediction of rock properties; examples from the North Sea Basin.” Clay Minerals **33**(1): 15-34.

Bjørlykke, K., P. Aagaard, et al. (1995). Geochemical constraints from formation water analyses from the North Sea and the Gulf Coast basins on quartz, feldspar and illite precipitation in reservoir rocks. **86**: 33-50.

Bjørlykke, K. (1994). "Pore water flow and mass transfer of solids in solution in sedimentary basins: Quantitative Diagenesis." Recent Developments and Applications to Reservoir Geology, Kluwer Dordrecht.

Bjørlykke, K., T. Nedkvitne, et al. (1992). Diagenetic processes in the Brent Group (Middle Jurassic) reservoirs of the North Sea: an overview. **61:** 263-287.

Bjørlykke, K., M. Ramm, et al. (1989). "Sandstone diagenesis and porosity modification during basin evolution." Geologische Rundschau **78**(1): 243-268.

Bjørlykke, K., P. Aagaard, et al. (1986). "Diagenesis and reservoir properties of Jurassic sandstones from the Haltenbanken area, offshore mid-Norway: Habitat of hydrocarbons on the Norwegian continental shelf." Graham and Trotman, London: 275–286.

Bjørlykke, K. (1983). "Diagenetic reactions in Sandstones: Sediment Diagenesis." Reidel Publishing, UK: 169-214

Blatt, H. (1979). "Diagenetic processes in sandstones." SEPM Special Publication **26**: 141-157.

Bloch, S., H. Ler Robert, et al. (2002). "Anomalously high porosity and permeability in deeply buried sandstone reservoirs; origin and predictability." AAPG Bulletin **86**: 301-328.

Bloch, S., J. H. McGowen, et al. (1990). "Porosity prediction, prior to drilling, in sandstones of the Kekiktuk Formation (Mississippian), North Slope of Alaska." AAPG Bulletin **74**: 1371–1385.

Boles J.R. and S.G. Franks (1979). Clay diagenesis in Wilcox sandstones. **49:** 55 - 70.

Brekke, H., H. I. Sjulstad, et al. (2001). "Sedimentary environments offshore norway - an overview." Norwegian Petroleum Society Special Publications. J. M. Ole and D. Tom, Elsevier.**10**: 7-37.

Byrnes, A. P. and M. D. Wilson (1994). "Case history-St. Peter and Mt. Simon sandstones, Illinois basin: Reservoir quality assessment and prediction." SEPM Short Course **30**: 385-394.

Chamley, H. (1989). "Clay Sedimentology." Springer Verlag, New York: 623.

Chuhan, F. A., A. Kjeldstad, et al. (2003). "Experimental compression of loose sands: relevance to porosity reduction during burial in sedimentary basins." Canadian Geotechnical Journal **40**(5): 995-1011.

Chuhan, F. A., K. Bjørlykke, et al. (2000). "The role of provenance in illitization of deeply buried reservoir sandstones from Haltenbanken and north Viking Graben, offshore Norway." Marine and Petroleum Geology **17**(6): 673-689.

Deegan, C., E. and B. J. Scull (1977). "A standard lithostratigraphic nomenclature for the Central and Northern North Sea." UK Institute of Geological Sciences, Report 77/25: 1-36.

Dickinson, W. R. (1985). "Interpreting provenance relations from detrital modes of sandstones, Provenance of Arenites." D. Reidel Publishing Company, USA: 333–361.

Dypvik, H. (1983). "Clay mineral transformations in Tertiary and Mesozoic Sediments from the North Sea." AAPG Bulletin **67**: 160-165.

Ehrenberg, S. N. (1993)."Preservation of anomalously high porosity in deeply buried sandstones by grain-coating chlorite; examples from the Norwegian continental shelf." AAPG Bulletin **77**: 1260-1286.

Ehrenberg, S. N. (1990)."Relationship between diagenesis and reservoir quality in sandstones of the Garn Formation, Haltenbanken, mid-Norwegian continental shelf." AAPG Bulletin **74**: 1538-1558.

Emery, D. and K.J. Myres (1996). Sequence Stratigraphy, Oxford:Blackwell Science.

Emery, D., P. C. Smalley, et al. (1993). "Synchronous Oil Migration and Cementation in Sandstone Reservoirs Demonstrated by Quantitative Description of Diagenesis [and Discussion]. Philosophical Transactions." Physical Sciences and Engineering **344**: 115-125.

Erratt, D., G. Thomas, et al. (1999)."The evolution of the central North Sea Rift. Petroleum Geology of Northwest Europe." Proceedings of the Conference **5**: 63-82.

Fisher, Q., R. Knipe, et al. (2000). "The relationship between faulting, fractures, transport of silica and quartz cementation in North Sea oil fields." Blackwell Science, Oxford.

Friedman, G. M. and F. E. Sanders (1978)."Principles of sedimentology". Earth Surface Processes: 1-792.

Gaupp R., A. Matter, et al. (1993)."Diagenesis and fluid evolution of deeply buried Permian (Rotliegend) gas reservoirs, northwest Germany." AAPG Bulletin **77**: 1111-1128.

Giles, M. R., S. Stevenson, et al. (1992). "The reservoir properties and diagenesis of the Brent Group: a regional perspective." Geological Society, London, Special Publications **61**(1): 289-327.

Glennie, K. W. (2009). Lower Permian-Rotliegend. Petroleum Geology of the North Sea, Blackwell Science Ltd**:** 137-173.

Glennie, K., J. Higham, et al. (2003). Permian. The Millennium Atlas; Petroleum Geology of the Central and Northern North Sea, The Geological Society of London**:** 100-112.

Glennie, K. W. and R. R. Underhill (1998). Origin, Development and Evolution of Structural Styles. Petroleum Geology of the North Sea; Basic concepts and recent advances. Blackwell Science**:** 42-82.

Glennie, K. W., G. C. Mudd, et al. (1978). "Depositional environment and diagenesis of Permian Rotliegendes sandstones in Leman Bank and Sole Pit areas of the U.K. southern North Sea." Journal of the Geological Society of London **135**: 23-34.

Glennie, K. W. (1972). "Permian Rotliegendes of Northwest Europe Interpreted in Light of Modern Desert Sedimentation Studies." AAPG Bulletin **56**(6): 1048-1071.

Gluyas, J. G., S. M. Grant, et al. (1993)."Geochemical evidence for a temporal link control on sandstone cementation. Diagenesis and Basin Development."

Gowers, M., E. Holtar, et al. (1993)."The structure of the Norwegian Central trough (Central Graben area). Petroleum Geology of Northwest Europe." Proceedings of the Conference **4**: 1245-1254.

Götze, J., M. Plötze, et al. (2001)."Origin, spectral characteristics and practical applications of the cathodeluminesence (CL) of quartz – a review." Mineralogy and Petrology **71**(3): 225-250.

Hancock, N. J. (1978). "Possible causes of Rotliegend sandstone diagenesis in northern West Germany." Journal of the Geological Society **135**(1): 35-40.

Hanken, N. M., K. Bjorlykke, et al. (2010). Carbonate sediments. Petroleum Geoscience: From Sedimentary Environments to Rock Physics, Springer Berlin Heidelberg**:** 141-200.

Heald, M. T. and R. E. Larese (1974). "Influence of coatings on quartz cementation." Journal of Sedimentary Research **44**(4): 1269-1274.

Heald, M. T. and J. J. Renton (1966). "Experimental study of sandstone cementation." Journal of Sedimentary Research **36**(4): 977-991.

Heeremans, M., J. I. Faleide, (2004). "Late Carboniferous-Permian of NW Europe: an introduction to a new regional map." Geological Society, London, Special Publications **223**(1): 75-88.

Jahren, J. and M. Ramm (2009). The Porosity-Preserving Effects of Microcrystalline Quartz Coatings in Arenitic Sandstones: Examples from the Norwegian Continental Shelf. Quartz Cementation in Sandstones, Blackwell Publishing Ltd.**:** 271-280.

Johnson, R. H. (1920). "The cementation process in sandstones." AAPG Bulletin **4**: 33-35.

Lander, R. H., R. E. Larese, et al. (2008). "Toward more accurate quartz cement models: The importance of euhedral versus noneuhedral growth rates." AAPG Bulletin **92**(11): 1537-1563.

Land, L. S. and R. S. Fisher (1987). "Wilcox sandstone diagenesis, Texas Gulf Coast: a regional isotopic comparison with the Frio Formation." Geological Society, London, Special Publications **36**(1): 219-235.

Lanson, B., D. Beaufort, et al. (2002). "Authigenic kaolin and illitic minerals during burial diagenesis of sandstones: a review." Clay Minerals **37**(1): 1-22.

Lasaga, A. C. (1984)."Chemical kinetics of water-rock interactions." Journal of Geophysical Research **89**: 4009–4025.

McBride, E. F. (1989). "Quartz cement in sandstones: a review." Earth-Science Reviews **26**(1–3): 69-112.

Mial, A. D. (2000). "Principles of sedimentary basin analysis." Springer Berlin Heidelberg: 1-616.

Morad, S., H. N. B. Ismail, et al. (1994)."Diagenesis and formation water chemistry of Triassic reservoir sandstones from southern Tunisia." Sedimentology **41**(6): 1253-1272.

Oelkers, E. H., P. A. Bjørkum, et al. (2000)."Making diagenesis obey thermodynamics and kinetics: the case of quartz cementation in sandstones from offshore mid-Norway." Applied Geochemistry **15**(3): 295-309.

Paxton, S. T., J. O. Szabo, et al. (2002)."Construction of an Intergranular Volume Compaction Curve for Evaluating and Predicting Compaction and Porosity Loss in Rigid-Grain Sandstone Reservoirs." AAPG Bulletin **86**(12): 2047-2067.

Pittman, E. D., R. E. Larese, et al. (1992). "Clay coats: occurrence and relevance to preservation of porosity in sandstones."

Pollastro, R. M. (1985). "Mineralogical and morphological evidence for the formation of illite at the expense of illite/smectite." Clays and Clay Minerals **33**(4): 265-274.

Purvis, K. (1992). "Lower Permian Rotliegendes Sandstones, Southern North Sea: a case study of sandstone diagenesis in evaporate-associated sequences." Sedimentary Geology **77**: 155-171.

Ramm, M. and K. Bjørlykke (1994). "Porosity/depth trends in reservoir sandstones; assessing the quantitative effects of varying pore-pressure, temperature history and mineralogy, Norwegian Shelf data." Clay Minerals **29**(4): 475-490.

Ravnås, R., A. Nøttvedt, et al. (2000). "Syn-rift sedimentary architectures in the Northern North Sea: Dynamics of the Norwegian Margin." Geological Society of London, Special Publication **167**: 133-177.

Rimstidt, J. D. and H. L. Barnes (1980). "The kinetics of silica-water reactions." Geochimica et Cosmochimica Acta **44**(11): 1683-1699.

Roberts, A. M., G. Yielding, et al. (1990). "Tectonic evolution of the North Sea Rifts. A kinematic model for the orthogonal opening of the late Jurassic North Sea rift system, Denmark-Mid Norway." 181-199.

Robinson A.G., M.L.Coleman, et al. (1993). "The age of illite cement growth, Village Fields Area, Southern North Sea: Evidence from K-Ar ages and $^{18}O/^{16}O$ ratios." AAPG Bulletin **77**: 68-80.

Roscher, M. and J. W. Schneider (2006). "Permo-Carboniferous climate: Early Pennsylvanian to Late Permian climate development of central Europe in a regional and global context." Geological Society, London, Special Publications **265**(1): 95-136.

Rossel, N. C. (1982). "Clay mineral diagenesis in Rotliegend aeolian sandstones of the southern North Sea." Clay Minerals **17**(1): 69-77.

Rønnevik, H., W. Van Den Bosch, et al. (1975). "A proposed nomenclature for the main structural features in the Norwegian North Sea." 28-30.

Rutter, E. H. and D. Elliott (1976). "The Kinetics of Rock Deformation by Pressure Solution [and Discussion]." Philosophical Transactions of the Royal Society of London. Series A, Mathematical and Physical Sciences **283**(1312): 203-219.

Saigal, G. C. and K. Bjørlykke (1987). "Carbonate cements in clastic reservoir rocks from offshore Norway-relationships between isotopic composition, textural development and burial depth." Geological Society, London, Special Publications **36**(1): 313-324.

Saigal, G. C., S. Morad, et al. (1988). "Diagenetic albitization of detrital K-feldspar in Jurassic, Lower Cretaceous, and Tertiary clastic reservoir rocks from offshore Norway." Journal of Sedimentary Research **58**: 1003-1013.

Schmoker, J. W. and D. K. Higley (1991). "Porosity trends of the Lower Cretaceous Sandstone, Denver Basin, Colorado." Journal of Sedimentary Research **61**(6): 909-920.

Schmoker, J. W. and D. L. Gautier (1988). "Sandstone porosity as a function of thermal maturity." Geology **16**(11): 1007-1010.

Stemmerik, L., J. R. Ineson, et al. (2000). "Stratigraphy of the Rotliegend Group in the Danish part of the Northern Permian Basin, North Sea." Journal of the Geological Society **157**(6): 1127-1136.

Storvoll, V., K. Bjorlykke, et al. (2002). "Porosity preservation in reservoir sandstones due to grain-coating illite; a study of the Jurassic Garn Formation from the Kristin and Lavrans fields, offshore mid-Norway." Marine and Petroleum Geology **19**: 767-781.

Taylor, T. R., M. R. Giles, et al. (2010). "Sandstone diagenesis and reservoir quality prediction: Models, myths, and reality." AAPG Bulletin **94**(8): 1093-1132.

Taylor, T., R. Stancliffe, et al. (2004). "High temperature quartz cementation and the timing of hydrocarbon accumulation in the Jurassic Norphlet sandstone, offshore Gulf of Mexico, USA." Geological Society, London, Special Publications **237**(1): 257-278.

Thomson, A. (1979). "Preservation of porosity in the deep Woodbine/Tuscaloosa trend, Louisiana." Gulf Coast Association of Geological Societies Transactions **30**: 396–403.

Walderhaug, O. (1996). "Kinetic modeling of quartz cementation and porosity loss in deeply buried sandstone reservoirs." AAPG Bulletin **80**: 731-745.

Walderhaug, O. (1994). "Precipitation rates for quartz cement in sandstones determined by fluid-inclusion microthermometry and temperature-history modeling." Journal of Sedimentary Research **64**(2a): 324-333.

Walderhaug, O. (1994). "Temperatures of quartz cementation in Jurassic sandstones from the Norwegian continental shelf; evidence from fluid inclusions." Journal of Sedimentary Research **64**(2a): 311-323.

Walderhaug, O. (1990). "A fluid inclusion study of quartz-cemented sandstones from offshore mid-Norway; possible evidence for continued quartz cementation during oil emplacement." Journal of Sedimentary Research **60**(2): 203-210.

Worden, R. H. and S. Morad (2009). Quartz Cementation in Oil Field Sandstones: A Review of the Key Controversies. Quartz Cementation in Sandstones, Blackwell Publishing Ltd.**:** 1-20.

Zanella, E. and M. Coward (2003). "Structural framework. The Millennium Atlas: Petroleum Geology of the Central and Northern North Sea." Geological Society of London, Special Publications: 45–59.

Ziegler, K. (2006). "Clay minerals of the Permian Rotliegend Group in the North Sea and adjacent areas." Clay Minerals **41**(1): 355-393.

Ziegler, K. (1993). Diagenetic and geochemical history of the Rotliegend of the southern North Sea (UK sector): a comparative study. Thesis (Ph. D.)-University of Reading, 1993.

http://factpages.npd.no/factpages/Default.aspx?culture=en. Last accessed 20th May, 2012.

11. Appendix

Appendix A: Cross plots

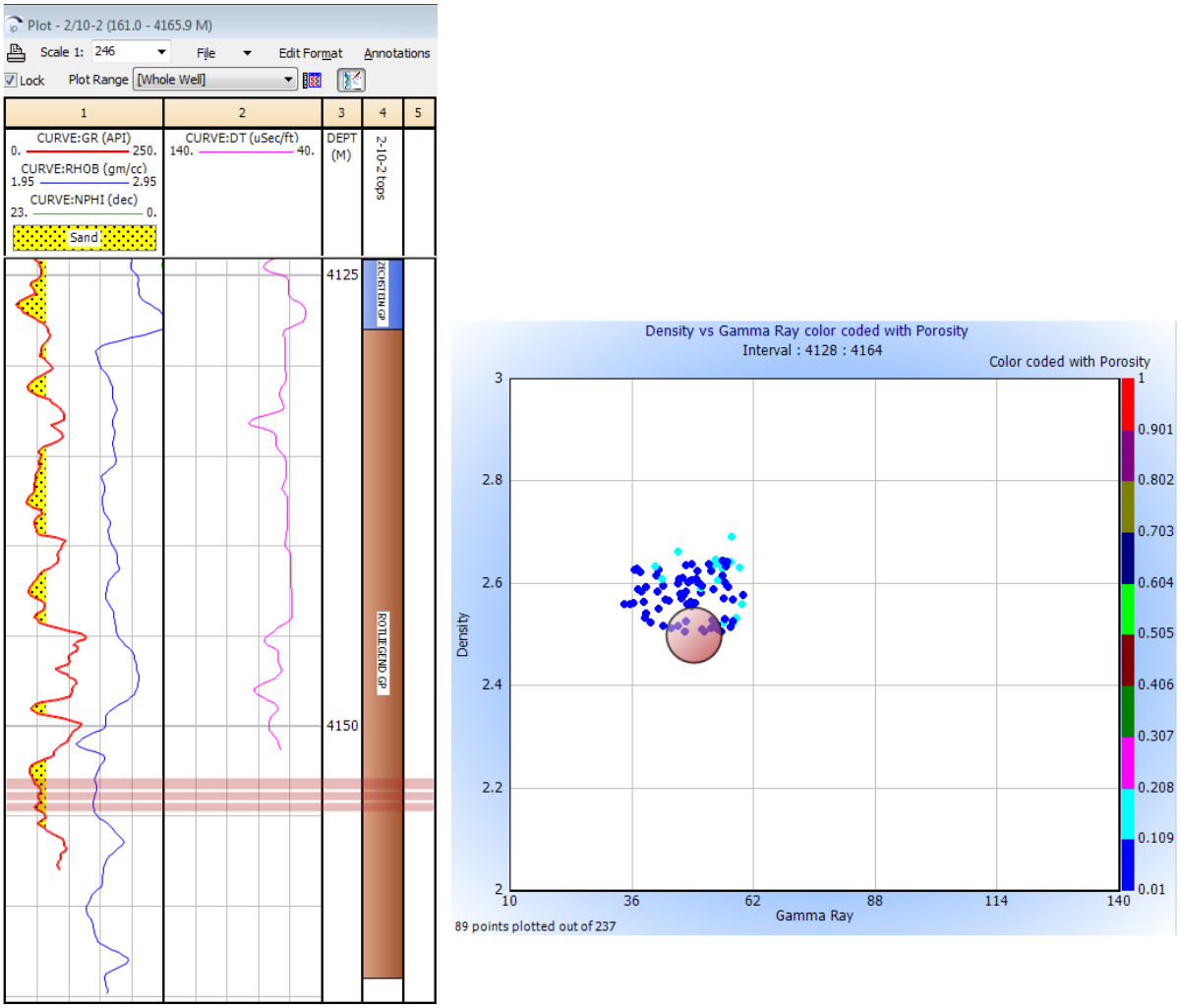

A1. The shaded area in both well 2/10-2 and crossplot represents porosity of cored interval.

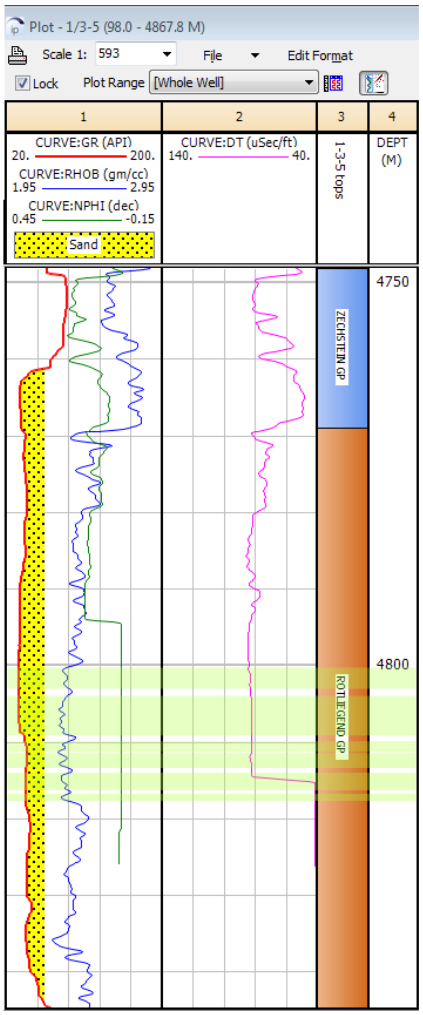

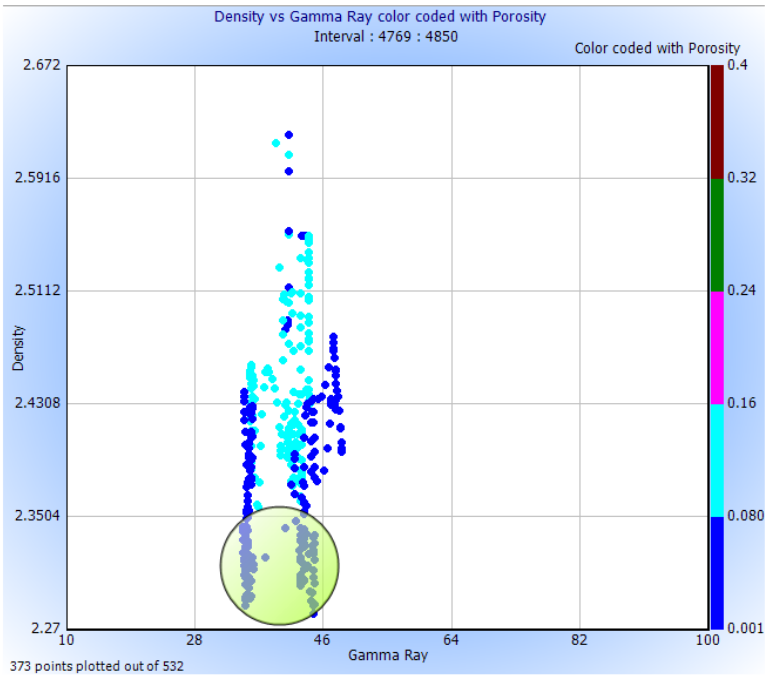

A2. The shaded area in both well 1/3-5 and crossplot represents porosity of cored interval.

Appendix B: Grain Textural Data

Well	Depth (m)	Grain size	Average grain shape	Sorting	IGV (%)
2/10-2	4152.6	medium	subrounded	poorly	43.7
	4157.6	coarse	subangular	moderate	44.6
	4159.7	fine	subrounded	poorly	46.1
	4159.2	medium	subangular	poorly	48.3
	4160.2	fine	subrounded	poorly	43.1
	4163.2	fine	subangular	moderate	52.1
1/3-5	4807.5	medium	subrounded	well	32.1
	4809.5	medium	subrounded	moderate	29.1
	4812.6	medium	subrounded	well	30.2
	4813.6	medium	subrounded	well	31.2

Appendix C: Thin-sections

C1 Grain crushing (4809.50 m, well 1/3-5)

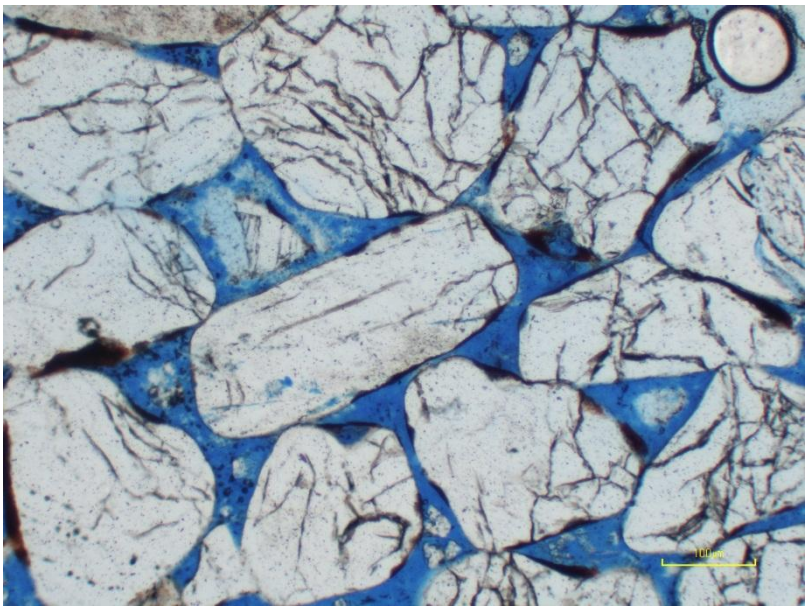

C2 Badly prepared thin section (4163.20 m, well 2/10-2)